OXYGEN ACTIVITY MEASUREMENTS IN SIMULATED CONVERTED MATTE

By

TSHILOMBO KABAMBA GHISLAIN

Submitted in fulfilment of the requirements for the degree of

Master of Engineering (Metallurgical Engineering)

in the Department of Materials Science and Metallurgical Engineering,
Faculty of Engineering, Built Environment and Information Technology,
University of Pretoria.

May 2006

OXYGEN ACTIVITY MEASUREMENTS IN SIMULATED CONVERTED MATTE

TSHILOMBO KABAMBA G.
Supervisor: **Professor Chris PISTORIUS**
Department of Materials Science and Metallurgical Engineering
Master of Engineering (Metallurgical Engineering)

ABSTRACT

Measurements of oxygen activities in a matte at high-temperature could be useful to determine and control the repartition of different elements, such as iron, copper, and nickel between the oxidised phase, (the slag) and the sulphide phase, (the matte). Electrochemical measurement of oxygen partial pressure in equilibrium with the melt can be performed by using solid electrolytes such as the zirconia solid electrolyte.

The oxygen measurements in Cu-Ni-Fe-S matte were studied experimentally by measuring the partial pressure of oxygen through the EMF, using a silica-saturated slag and either a CO-CO_2-SO_2 gas mixture or Ar gas, at 1250^{o}C. The calculated equilibrium oxygen partial pressure varied from $1.53x10^{-8}$ to $2.64x10^{-7}$atm. Oxygen measurements were conducted by using fully stabilized zirconia as solid electrolyte. Two different solid reference electrodes were used: Cr/Cr_2O_3 and Fe/FeO. EMF measurements obtained with Cr/Cr_2O_3 solid reference electrode were less stable and accurate compared to those with Fe/FeO solid reference electrode. Therefore, EMF measurements on oxygen concentration point out that the Fe/FeO is more suitable solid reference electrode for this application than Cr/Cr_2O_3.

Analyses were obtained using the SEM, (scanning electron microscope) and the electron probe microanalyser.

The measured oxygen concentration was found to be sensitive to the iron content in the matte.

KEYWORDS: Activity, matte, slag, solid electrolyte.

ACKNOLEDGEMENTS

The author would like to express his sincere appreciation to the following:

- His supervisor, Professor P.C. Pistorius, for the opportunity to work under him, his guidance and for the advice, constructive criticism, and encouragement during his supervision of this research project. The education received under him will be cherished forever.

-The University of Pretoria especially the department of Metallurgy for funding and laboratory facilities available for the completion of this research work.

- Mr. Peter Gräser for the help provided, in the sample analyses with the electron probe microanalyser CAMECA SX 100 at the department of Geology.

-Mr. Carel Coetzee for his assistance with the SEM analyses of all the samples at the Industrial Metals and Minerals Research Institute (IMMRI).

-All the staff of the department of Materials Science and Metallurgical Engineering for their support.

-Finally, to his family for all their love and understanding, for being a source of constant encouragement and inspiration.

TABLE OF CONTENT

TABLES OF FIGURES AND ILLUSTRATIONS

LISTS OF TABLES

CHAPTER I
INTRODUCTION

South Africa has more than 80% of the world's platinum reserves, and is the largest producer of platinum-group metals (PGMs) from ores containing copper, nickel and iron sulphide [JONES, 1999:42].

During treatment for metal recovery, sulphide ores are concentrated by flotation and smelted to a nickel or nickel-copper matte, which is further processed to nickel or nickel oxide by hydrometallurgical, pyrometallurgical, or vapometallurgical methods.

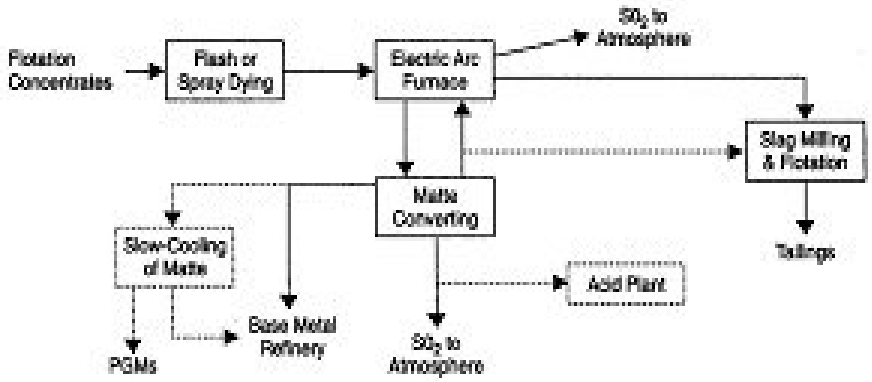

Figure 1-1. Simplified diagram showing the route to recover PGMs from sulphide flotation concentrates[CRAMER,2001:7]

The main chemical reactions and aim each processing step are summarised below:

Smelting: A metallurgical thermal processing operation used to separate the gangue (oxide or silicate) minerals from the sulphide minerals associated with the noble metals in a furnace at high temperature, with little chemical reaction.

Converting: consists of eliminating most iron and much sulphur by injecting oxygen in the form of air, oxygen enriched air or pure oxygen. The endpoint is crucial to be determined to avoid oxidation of valuable metals from the matte causing loss of metals in slag.

Main reactions

$$Cu(Ni)\text{-}Fe\text{-}S + O_2 + SiO_2 \rightarrow Cu(Ni)\text{-}S + 2FeO.SiO_2\ (+Fe_3O_4) + SO_2 \qquad [1]$$

$$FeS + 1.5\ O_2 \rightarrow FeO + SO_2 \qquad \Delta G^\circ = -349899.6\ J/mol \qquad [2]$$

$3\ FeS + 5O_2 \rightarrow Fe_3O_4 + 3\ SO_2$ [3]

$Cu_2S + 3/2\ O_2 = Cu_2O + SO_2$ $\Delta G° = -223369.1$ J/mol at 1250°C [4]

Refining: Hydrometallurgical refining is applied in the base metal refinery to dissolve and separate the iron, copper and nickel; the relevant reactions are given by equations (5) to (9). Its objective is to produce high-purity metal with a minimum consumption of energy.

Main reactions

Ni: $Ni_3S_2 + 0.5\ O_2 + 2\ H^+ \rightarrow Ni^{2+} + 2NiS + H_2O$ [5]

Cu: $2\ Cu^{2+} + Ni_3S_2 \rightarrow Cu_2S + NiS + 2\ Ni^{2+}$ [6]

$3\ Cu^{2+} + SO_4^{2-} + 4\ H_2O \rightarrow Cu(OH)_4SO_4 + 4H^+$ [7]

Fe: $Fe^{3+} + SO_4^{2-} + H_2O \rightarrow Fe(OH)SO_4 + H^+$ [8]

$2Fe^{3+} + 3\ SO_4^{2-} + 3H_2O \rightarrow Fe_2O_3 + 3H_2SO_4$ [9]

In industry, the iron in the matte from the converting process must be controlled to a low level. An excess of Fe in the matte compared with the required level (average 0.5 to 3 wt% iron) affects hydrometallurgical refining.

In this study, the oxygen activity for decreasing iron content in a simulated converting matte has been investigated. Generally, the converting process decreases the amount of iron contained in the matte from approximately 37-wt% iron to approximately 1.4 wt% iron [JONES, 1999:41].

According to the Gibbs free energy calculated with FactSage at 1250°C, the driving force for reaction (2) is larger than reaction (4). During oxidation, reaction (2) will take place first until the equilibrium is reached and thereafter oxidation of copper by reaction (4) may start only if the minimum value of Fe in the matte is reached.
The Ellingham diagram shows that between these two reactions, the formation of NiO is possible and can therefore take place before reaction (4). The presence of NiO can be used as an indicator in the slag-matte system. If NiO concentration increases in the slag, reaction (2) is close to completion.

The introduction of probes as measurement elements could perhaps be used as an alternative to measure and accurately determine the endpoint of oxygen blowing.

Electrochemical oxygen probes are used extensively in the steel industry to measure the oxygen potential in liquid steel [GELDENHUIS, 2004:24]. The application of this type of sensor contributes to the optimisation of the deoxidation process of steel.
The commercial oxygen probes give signals of thermoelectric voltage (for the temperature measurement) and cell potential (for oxygen activity measurements).
When these signals attain stability, they are processed to provide a graph displaying the cell potential (emf).
The following are of particular interest in this study:

- the relationship between iron content in the matte and the electromotive force (emf);
- the effect of slag composition on the emf.

In the present study, the experimental method consisted of the use of different matte grades (FeS contents) in contact with a constant slag composition under a continuous gas flow at 1250°C (average temperature in industry). A fayalitic slag saturated in silica was obtained by mixing pure FeO and SiO_2, or pure FeO, Fe_2O_3 and SiO_2. Slag with a composition of 62mass% FeO_x-38 mass% SiO_2 was used in both cases.

A CO-CO_2-SO_2 gas mixture with controlled partial pressure of oxygen was used (pO_2 from 1.53×10^{-8} atm to 2.65×10^{-7} atm) at 1250°C; pure Ar was also used. The gas composition was varied to test whether the gas has any affect on the presumed local matte-slag equilibrium.
To determine the influence of iron in the Cu-Ni-Fe-S system, experiments were performed from 8.8 % Fe to 1.0 % Fe, in the matte. The Ni-Cu ratio was kept constant, and the matte was made up as a mixture of Ni_3S_2, Cu_2S and FeS.

CHAPTER II
LITTERATURE SURVEY.

One of the objectives of this work was to understand the thermodynamic principles of the Fe-Cu-Ni-S system at 1250°C and the links between this system and recovery of Platinum Group Metals (PGM).
The first section reviews the treatment of ore in order to obtain PGM as product. Section two reviews the phase and stability diagrams of the relevant binary, ternary and quaternary systems.

II.1.PGM in South Africa

Generally, the ore is treated by crushing, grinding and flotation to produce a concentrate, which is molten in a furnace to produce two immiscible melts: a denser sulphide melt (matte) and a less dense silicate melt (slag).
The slag and matte phases are tapped through separate furnace tap holes; the slag is discarded or processed further to recover valuable metals; the matte is treated further. The matte is converted by blowing air or air-oxygen mixtures into the system, oxidising most of the Fe to FeO, which reacts with added SiO_2 to form fayalite slag (Fe_2SiO_4). The converted matte contains Cu, Ni, S principally, Fe and Co as secondary elements, and small amounts of PGMs, gold and silver.

In South Africa, three broad ore types are exploited: the Merensky Reef, the Upper Group Chromitite Reef No.2 (UG2) and the Platreef [CRAMER, 2001:7].
According to Jones [1999:41], ore from the Merensky Reef contains up to 3% base-metal sulphide minerals, distributed as follows: pyrrhotite (45%), pentlandite (32%), chalcopyrite (16%) and pyrite (2-4%). The majority of the PGMs are associated with pentlandite, Pt-Pd sulphides such as braggite-coopertite, laurite or ferroplatinum.
The UG2 consists primarily of chromite (60-90%), interstitial orthopyroxene and plagioclase, together with secondary minerals such as talc, chlorite and phlogopite. The major base metal sulphide minerals are pentlandite, chalcopyrite, pyrrhotite and minor amounts of pyrite and millerite [JONES, 1999:41].

Table 2-1. Average grades of the individual precious metals in Merensky, UG2 and platreef ores [JONES: 1999:42].

	Merensky ore		**UG2 ore**		**Platreef ore**	
	g/t	Mass%*	g/t	Mass%*	g/t	Mass%*
Pt	3.25	59	2.46	41	1.26	42
Pd	1.38	25	2.04	34	1.38	46
Rh	0.17	3	0.54	9	0.09	3
Ru	0.44	8	0.72	12	0.12	4
Ir	0.06	1	0.11	1.9	0.02	0.8
Os	0.04	0.8	0.1	1.7	0.02	0.6
Au	0.18	3.2	0.02	0.4	0.1	3.4
Total PGM+Au	**5.5**	**100**	**6.0**	**100**	**3.0**	**100**

Mass%*: relative mass%

Each type of ore requires different approaches to metallurgical processing. UG2 ore has a much lower content of nickel and copper sulphides, and contains much more chromite than Merensky ore. The lower based-metal sulphide content of the UG2 indicates that a more sophisticated procedure is required for PGM recovery from UG2 ore. Nevertheless, UG2 ore is by far the richest source of rhodium, and the high demand for palladium makes processing of this ore very attractive [JONES, 1999:42].

II.1.1. General flow sheet

The general process consists of the classic operations which include milling, flotation, drying, smelting, converting, refining.

II.1.1.1.Concentrate preparation and drying

The ore is crushed and milled to reduce the size of the rock particles and to expose the minerals that contain the PGM. The particles are mixed with water and special reagents and air is

pumped through the liquid, creating bubbles to which the PGM-containing particles adhere. These float to the surface and are removed as a soapy froth. The PGM content of this flotation concentrate varies between 100 and 1000 grams per tonne [MATTHEY, 2005:52].

The concentrate is dried in a flash drier. The dry concentrate is transferred pneumatically from the drier into the furnace.

Table 2-2. Typical concentrate compositions [CRAMER, 2001:7]

	Al_2O_3 Mass%	CaO Mass%	Co Mass%	Cr_2O_3 Mass%	Cu Mass%	FeO Mass%	MgO Mass%	Ni Mass%	S Mass%	SiO_2 Mass%	PGM g/ton
Amplats	3.2	4.7	0.08	0.80	2.1	20	15	3.6	9	34	143
Impala	4.1	2.9	0.06	1.1	1.3	18	18	2.1	5.6	42	138
Lonmin	1.8	2.8	0.08	0.4	2.0	23	18	3.0	9	41	130
Northam	2.6	3.0	0.05	0.87	1.3	17	18	2.5	5.4	47	132

II.1.1.2.Smelting

Smelting is used to separate the gangue (oxide or silicate) minerals from the sulphide minerals and the associated noble metals. Smelting uses an electric furnace at temperatures that can exceed 1500°C. Because of the low concentration of valuable minerals in the concentrate, the furnace is operated with a slag to matte production ratio of between 4 and 9.

The sulphide minerals form a denser molten matte with a relative density of about 4.8-5.3 g/cm^3 containing the valuable metals. This separates from the unwanted minerals which form a lighter silicate and iron-rich slag with a relative density around 2.7-3.3 g/cm^3; the slag is discarded [JONES, 1999:42].

Because of the low sulphur content of the UG2, it is not possible to matte smelt the UG2 on its own as an immiscible sulphide matte will not form. Therefore, UG2 concentrate is blended with Merensky concentrate prior to matte smelting. Matte temperature exceeds 1300°C for Merensky Reef concentrates and is in excess of 1500°C for UG2 concentrates [MERKLE, 2002:53].

The chromium, which is present as chromite in the furnace feed, can be a problem. Depending on the chromium content of the feed and the operating conditions of the furnace, it frequently happens that the slag becomes saturated with a chromium-rich spinel phase [NELL, 2004:63]. Usually a rough value of 3% by mass is used as the maximum allowable chromium content,

but studies have shown that the solubility of chromium in slag may be as low as 1% to 1.5% by mass chromium. The maximum chromium level that can be accommodated during smelting depends on: the smelting temperature, the proportion and type of fluxes used, and the exact concentrate blend being smelted [MERKLE, 2002:53].

Table 2-3. Furnace matte compositions [JONES, 1999:42]

	% Co	**% Cr**	**% Cu**	**% Fe**	**% Ni**	**% S**	**PGM(g/t)**
Amplats	0.5	0.5	9	41	17	27	640
Impala	0.4		16	34	20	28	1050
Lonmin	0.5	0.23	9.7	37	17	28	1000
Northam	0.4		7.9	41	16	27	724

Table 2-4. Furnace slag compositions [JONES, 1999:42]

	Al_2O_3 Mass%	CaO Mass%	Co Mass%	Cr_2O_3 Mass%	Cu Mass%	FeO Mass%	MgO Mass%	Ni Mass%	S Mass%	SiO_2 Mass%
Amplats	3.3	6.4	0.05	0.80	0.11	31	15	0.19	0.5	46
Impala	6	8	0.03	1.2	0.11	21	18	0.11	0.25	47
Lonmin	2	9.8	0.05	1.2	0.09	28	19	0.15		44
Northam	1.5	10	0.03	0.8	0.1	21	20	0.2		44

During smelting, oxidising conditions can lead to a high ferric ion content in the slag, causing magnetite (Fe_3O_4) to form as a separate phase. Some operational problems can emerge like false bottom between slag and matte with reduced operational furnace volume, and increase base metal loss in the slag. Carbon additions can reduce magnetite in the slag to liquid FeO:

$$C + Fe_3O_{4(s)} \rightarrow CO + 3\ FeO_{(l)}$$

This reaction decreases slag viscosity and improves settling rates [DAVENPORT, 2002:9].

As said, during smelting the matte phase accumulates on the furnace floor, while the slag forms a layer on top of the matte. From a production point of view, it is important to know where the interface between matte and slag is, in order to optimise the tapping schedules for matte and slag. This slag/matte interface level changes continuously between tapping events and the rate is determined by different factors:

- the smelting rate,
- 'matte fall' of the concentrate feed
- the power input
- and the concentrate feed rate into the furnace.

[GELDENHUIS, 2004:24].

Some slag characteristics, which are important for the melting of PGM concentrates, are as follows:

- a low viscosity to allow clean slag-matte separation
- a low liquidus temperature to avoid excessive superheating of the matte
- the ability to dissolve all the chromium which is present in the concentrate to avoid the formation of refractory chromium-bearing spinel and to avoid the transfer of chromium to the matte
- a limited solubility of nickel, copper and cobalt as oxides
- chemical compatibility with the refractory lining in the furnace.

However, the slag composition is determined by the composition of the concentrate charged to the furnace, and there is a very little freedom to manipulate the slag composition [NELL, 2004:63].

II.1.1.3.Converting

Converting consists of eliminating some sulphur and most iron from the matte by injecting oxygen in form of air, air enriched with oxygen or pure oxygen. This increases the PGM grade. The main raw materials for converting are sulphide matte, silica flux, air and/or industrial oxygen.

In the copper matte converting, the process is mostly done in the Peirce-Smith converter, which blows the blast into molten matte through submerged tuyeres. Several other processes are also used or are under development like Hoboken or siphon converter, Mistubishi top-blown converter, Outokumpu flash converting and Noranda continuous converting [DAVENPORT, 2002:9].

Converting of platinum-bearing Fe-Cu-Ni-S follows the same principle as for Cu-Fe-S mattes. Air (or oxygen) is blown into the matte, which originates from the matte-smelting furnace (often termed 'green matte'); this leads to removal of iron and sulphur from the matte by oxidation according to the main reactions:

$Cu\text{-}Fe\text{-}S + O_2 + SiO_2 \rightarrow Cu_2S + 2\ FeO.SiO_2(+Fe_3O_4) + SO_2$

The oxidation reaction is sufficiently exothermic to maintain a temperature around 1250°C in the converter and no external energy is required. The temperature is controlled by adding cold feed or revert materials (such as spillages) to the converter if it becomes too hot [JONES, 1999:42].

The melting point of FeO and Fe_3O_4 are 1385°C and 1597°C respectively, and silica flux is added during this stage by means of a flux gun to combine with the FeO and part of the Fe_3O_4 as liquid fayalitic slag; the sulphur leaving the system as SO_2 is captured to form sulphuric acid. The slag-forming stage is finished when the FeS in the matte has been almost completely oxidised i.e. to a point when the matte contains less than 5% Fe. Liquid fayalite ($2FeO.SiO_2$) slag, saturated with magnetite, is poured off at various times during slag forming but cannot be discarded due to its high base metal content. The oxygen partial pressure in converter slag is stated to be close to that of the quartz-fayalite-magnetite (QFM) redox buffer, which defines an oxygen partial pressure of $10^{-8.4}$ bar at 1200°C [NELL, 2004:63].

$3\ Fe_2SiO_4 + O_2 = 2\ Fe_3O_4 + 3\ SiO_2$

At 1200°C, $NiFe_2O_4$ coexists with a nickel-rich monoxide phase at oxygen partial pressures that are more oxidizing than $10^{-10.5}$bar. The oxidizing nature of the converting conditions means that high losses of cobalt, nickel and copper as oxides might be encountered unless blowing conditions are carefully controlled and monitored [NELL, 2004:63].

The converter matte (known as the 'white matte') consists of copper and nickel sulphide and copper–nickel alloy and smaller amounts of iron sulphide, cobalt and PGE [MERKLE, 2002:53]. Impurities such as chromium, selenium, tellurium, arsenic, lead, tin, antimony and bismuth may concentrate in the white matte. Generally, the white matte is cast into ingots or granulated prior to treatment in the base metal refinery except at Anglo Platinum where it is cast into large ingots and slow-cooled [MERKLE, 2002:53].

To improve the SO_2 emission and air pollution which are associated with Peirce-Smith converters, many projects have been directed to develop new and competitive technology for Cu matte smelting, with lower capital and operational costs compared with conventional technology, while achieving virtually total capture of the sulphur as SO_2 for acid production. Examples include:

- The Kennecott-Outokumpu flash converting process uses advanced technology of continuously converting copper matte and permits the capture of virtually 100% of the SO_2 generated for acid production [Internet, 2005].

- The innovative DON (Direct Outokumpu Nickel) process eliminates the need for Peirce-Smith converting and the ladle transfer of molten matte [Internet, 2005].
- The Anglo Platinum Converting Process (ACP) aims to improve the control of sulphur dioxide emissions while increasing the available converter capacity. The converter, developed in conjunction with Ausmelt and others, utilises a Sirosmelt process adapted to the requirements of nickel-copper matte smelting. The Ausmelt converter is a totally contained vessel, which makes it possible to contain all the gas generated in the converting process. The off-gas from the Ausmelt converter is then fed to a new acid plant, consisting of two sections, specifically selected for its ability to treat both the high strength Ausmelt converter gas and the low-strength gas from the existing electric furnaces [Internet, 2005].
    - ❖ Difference between the Peirce-Smith Converter and Ausmelt Converter.
- Ausmelt converter can be much smaller than the Peirce-Smith converter due to the rapidity of furnace reactions and a short residence time required to process most materials.
- The electric furnace matte is hot charged to the Peirce-Smith converter while the Ausmelt converter is fed with granulated electric furnace matte.
- Improve sulphur fixation levels of converter gas from the present 55% to more than 95%.

The end-point iron content is important in this study because:

- an iron excess in the matte compared with the specification has an impact on hydrometallurgical refining of the matte.
- an iron deficit in the metal compared with the specification has an impact on refining as iron is needed to increase the exothermicity of the refining.
- alloy formation during solidification of matte in ingots (slow cooling) depends on the iron content.

Table 2-5. Converter matte analyses [JONES, 1999:42]

	% Co	% Cu	% Fe	% Ni	% S	PGM(g/t)
Amplats	0.5	26	2.9	47	21	2100
Impala	0.4	31	0.5	47	21	3430
Lonmin	0.6	29	1.4	48	20	6000
Northam	0.5	27	1.0	51	19	2570

Table 2-6. Converter slag analyses [JONES, 1999:42]

	$\%Al_2O_3$	%CaO	%Co	$\%Cr_2O_3$	%Cu
Amplats	0.7	0.4	0.45	0.4	1.17
	%FeO	**%MgO**	**%Ni**	**%S**	$\%SiO_2$
Amplats	63	1.1	2.25	2.4	27
	$\%Al_2O_3$	%CaO	%Co	$\%Cr_2O_3$	%Cu
Impala	1.8	0.3	0.43	1.4	1.06
	%FeO	**%MgO**	**%Ni**	**%S**	$\%SiO_2$
Impala	64	0.71	1.9	1.0	27
	$\%Al_2O_3$	%CaO	%Co	$\%Cr_2O_3$	%Cu
Lonmin	0.7	0.5	0.39	1.4	0.94
	%FeO	**%MgO**	**%Ni**	**%S**	$\%SiO_2$
Lonmin	65	0.78	1.43	1.7	28
	$\%Al_2O_3$	%CaO	%Co	$\%Cr_2O_3$	%Cu
Northam	1.3	0.7	0.4	0.36	1.37
	%FeO	**%MgO**	**%Ni**	**%S**	$\%SiO_2$
Northam	64	0.82	2.18		27

II.1.1.4.Off-gas handling

Some of the sulphur leaves the system in the gas phase as sulphur dioxide (SO_2). Of the sulphur entering the smelter, 60% leaves in the converter gases, 20% in the smelter gases, 15% in the converter matte, and 5% in the furnace slag [JONES, 1999:42].

SO_2 from converting is almost always made into sulphuric acid, and occasionally liquid SO_2 or gypsum.

II.1.1.5.Refining

The objective of the refinery is to produce high-purity metals with a minimum consumption of energy.

According to Jones [1999:42], the converter matte is usually milled prior to treatment in the base-metal refinery, where the copper and nickel are extracted by sulphuric-acid leaching. The leach residue makes up the high-grade PGM concentrate that is supplied to the precious metals refinery for the final separation of the pure precious metals.

There are mainly two processes used in the base-metals refinery: The Outokumpu and Sherritt-Gordon processes. Both processes have the same rationale and operate in several steps of increasingly aggressive conditions:

- the initial stage operates under mild conditions to leach some Ni and Co, and uses fresh matte to remove Cu from nickel sulphate solution
- the middle stage operates under harsher conditions and aims at dissolving all the remaining nickel and cobalt, as well as some copper from the matte
- the final stage aims at dissolving all the remaining copper and some iron from the matte.

A simplified process flowsheet for both processes is illustrated below.

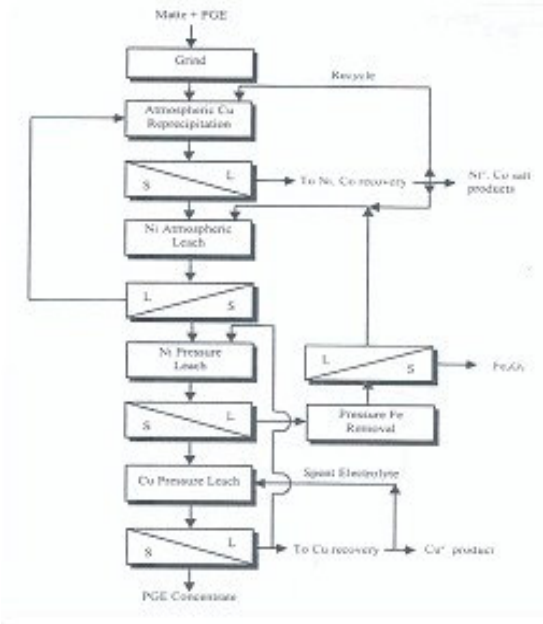

Figure 2.1. The Outokumpu process (Hartley platinum refinery)[COLE, 2002:6]

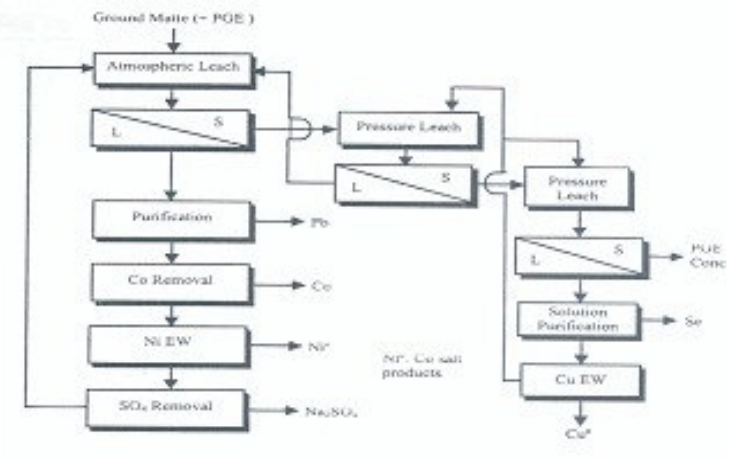

Figure 2.2. The Sherritt-Gordon process (Rustenburg base metals refinery) [COLE, 2002:6]

The precious-metal refining process consists of transforming the high-grade PGM concentrate (30% to 60% PGM) into high-purity (>99%) individual elements such as platinum, palladium, iridium, osmium, ruthenium, rhodium as well as recovering the gold and silver usually accompanying the PGM, see figure 2.3. [COLE, 2002:6].

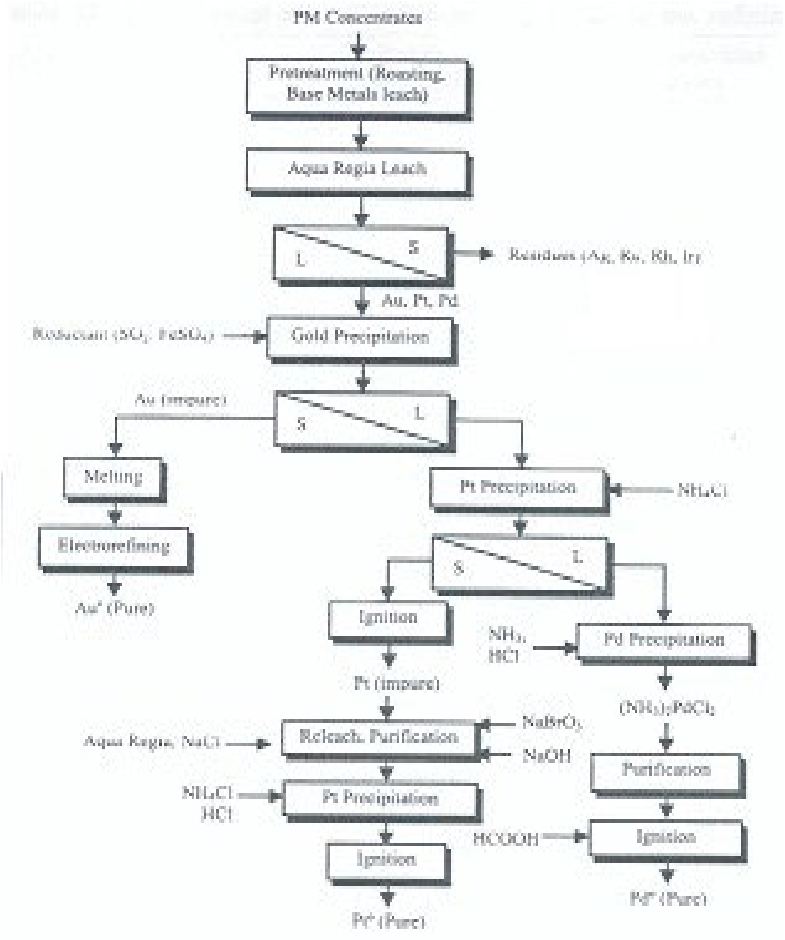

Figure 2.3. Refining process for Au, Pt, Pd (Inco Acton refinery)[COLE, 2002:6]

The refined PGMs have a purity of over 99.95 per cent, and can be produced in a number of forms: ingot, grain or a fine powder known as “sponge” [MERKLE, 2002:53].

The time between mining of the ore and production of pure metal typically ranges from around 6 weeks for palladium to up 20 weeks for rhodium [MATTHEY, 2005:52].

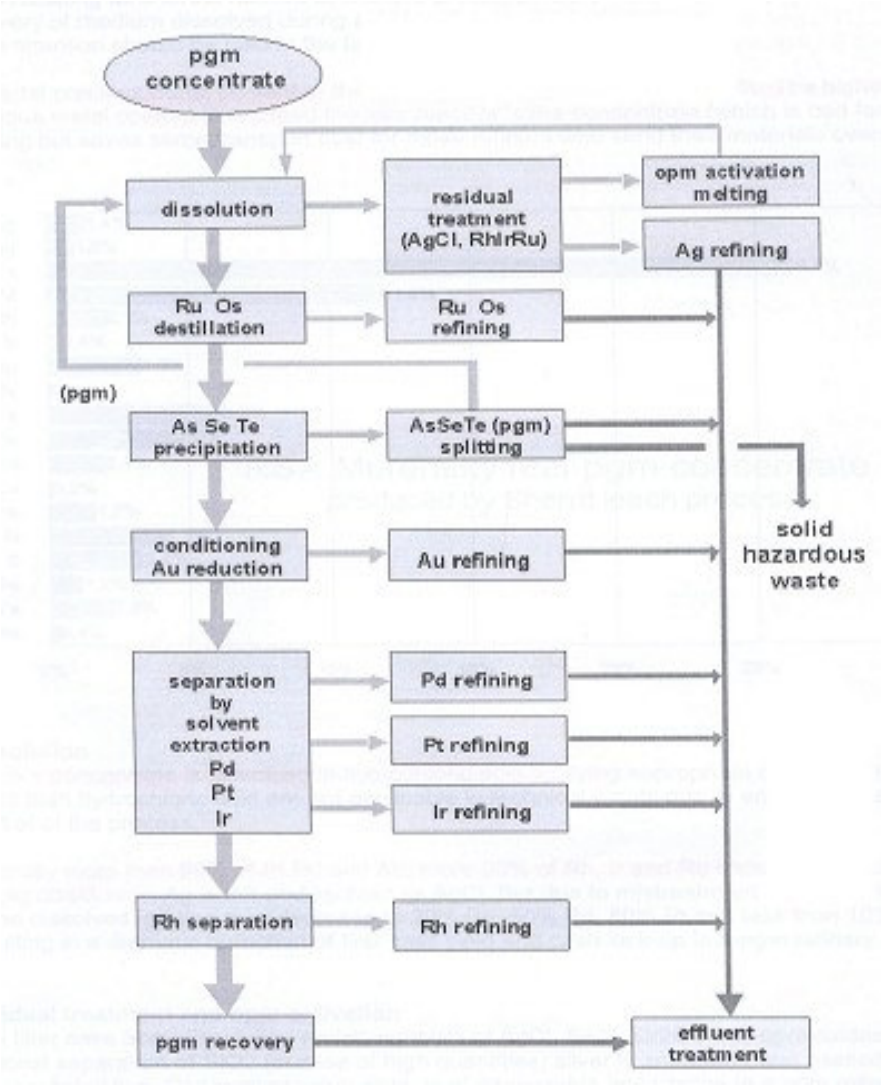

Figure 2-4. Refining of PGM converter matte [Internet, 2005]

General flow sheet

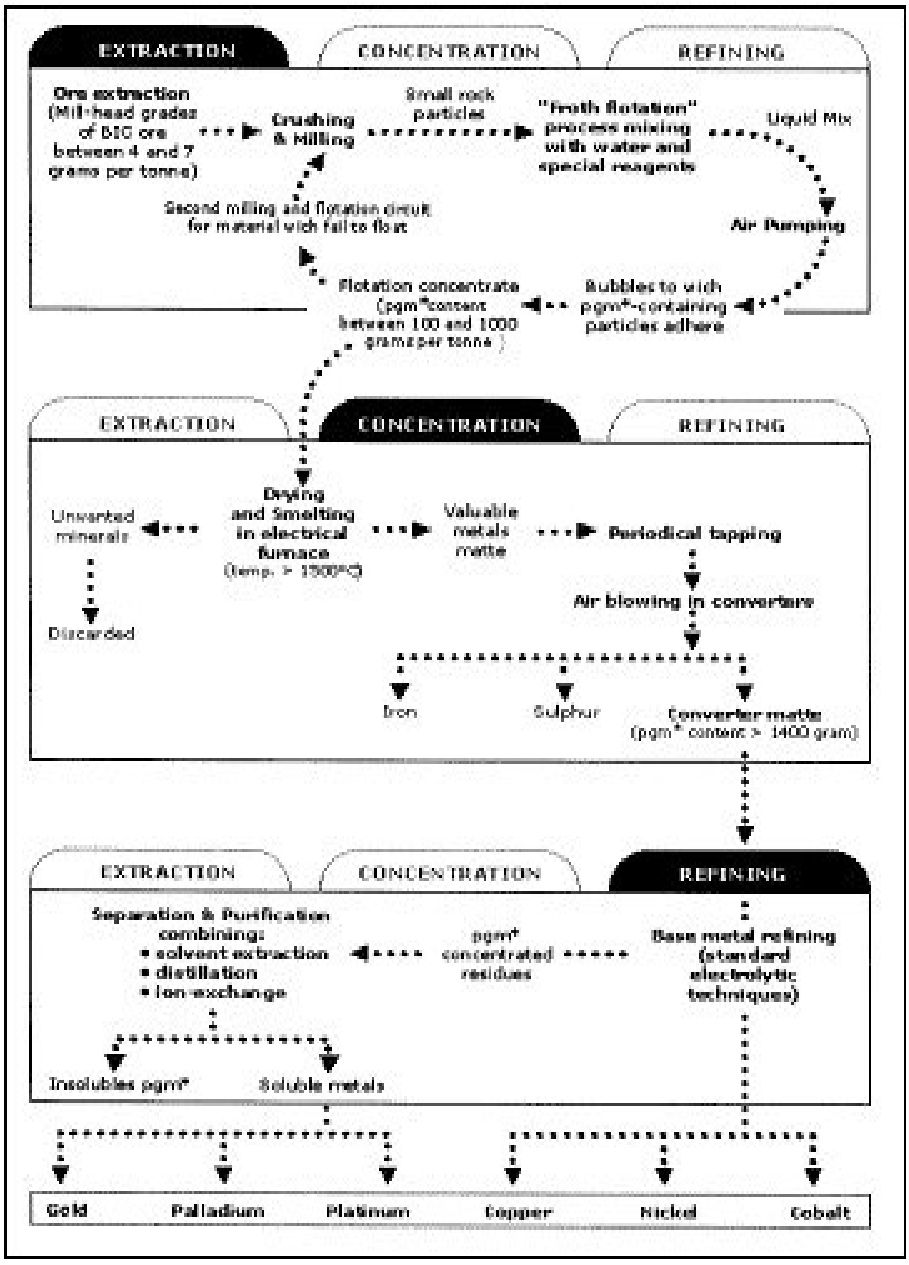

Figure 2-5. General flow sheet of PGMs [Internet, 2005]

II.2.Binary, ternary and quaternary systems

The understanding of the Cu-Ni-Fe-S system is discussed below to estimate converter matte and slag composition as functions of temperature and oxygen potential. Stability diagrams of the relevant binary and ternary systems are reviewed, and are presented to describe ores and natural mineral assemblages.

II.2.1. The binary system

II.2.1.1. The binary system FeO-Fe_2O_3

The FeO-Fe_2O_3 system is shown in figure 2.6. At 1250°C, the FeO-Fe_2O_3 system contains five phase fields appearing with the increase of FeO oxidation:

γ-Iron+wustite , wustite , wustite+magnetite , magnetite and magnetite+hematite .

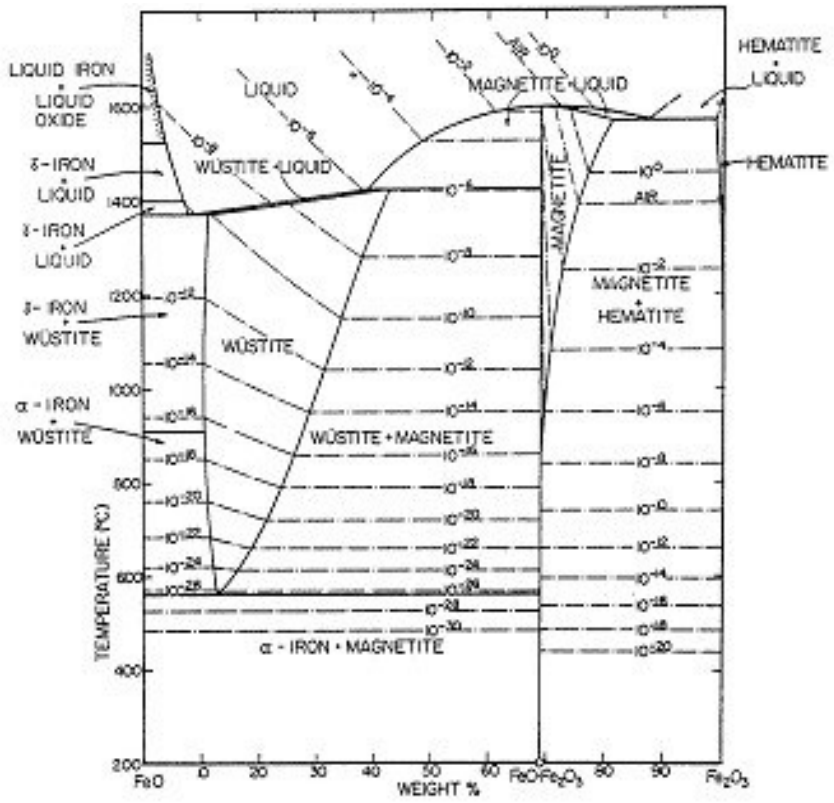

Figure 2-6. Diagram of the Fe-O system [ELLIOT, 1976:12]*

*: FeO is a simplified formula of wüstite. Its formula is more accurately written Fe_xO where the average value of *x* is 0.95 if the oxide is in contact with Fe metal.

II.2.1.2. The binary system FeO-SiO_2

All laboratory tests in this thesis were done with slag composed of 62 mass% FeO-38 mass%SiO_2. To assure a condition of silica saturation, SiO_2 was added in excess of saturation level. On the figure below, the range in which fayalite is liquid at 1250°C is approximately between 62 and 82 mass% FeO.

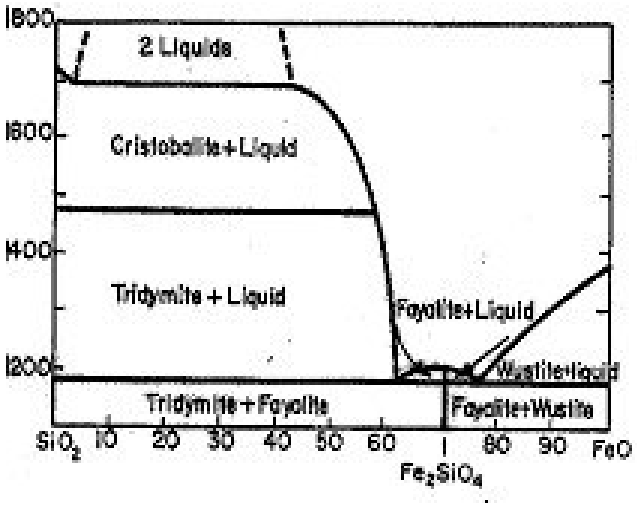

Figure 2-7. FeO-SiO_2 binary diagram [LEVIN, 1964:46]*

*: The phase diagram is based on equilibrium with metallic iron.

- Yazawa diagram

The stability of a metal relative to its oxide or sulphide depends on two reactions:

$M_{(s,l)} + ½\ S_2 = MS_{(s,l)}$ (1)

$M_{(s,l)} + ½\ O_2 = MO_{(s,l)}$ (2)

By knowing the log K_1 and log K_2 at a given temperature, by assuming a_M=a_{MS}= a_{MO}, figure 2-8 was constructed [Yazawa, 1974:93].

The sulphides of iron, copper and nickel tend to change into oxide during the converting process. For example, iron sulphide can changes to iron oxide at 1300°C for pO_2 values higher than the line between the FeS and FeO fields, starting at values of log (pS_2/atm) = -4.8 and log(pO_2/atm) = -10.8

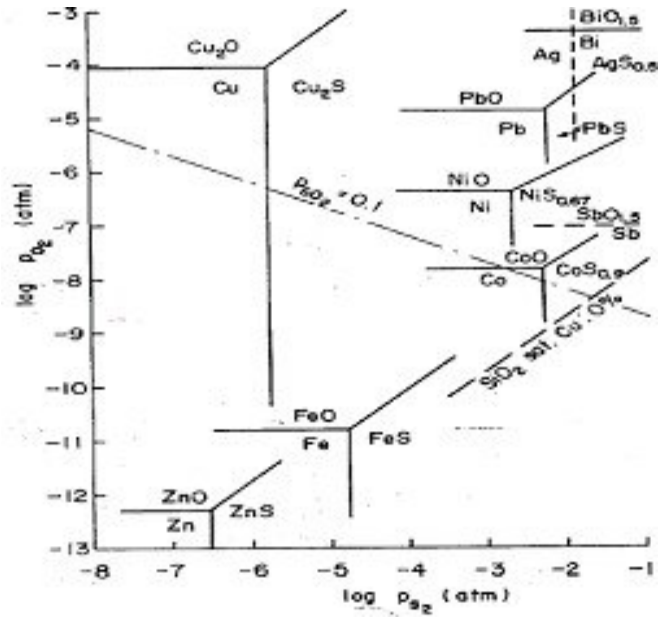

Figure 2-8. Sulphur-oxygen potential diagram for various metal-sulphur-oxygen systems at 1300°C [Yazawa, 1974]

II.2.2. Ternary systems

II.2.2.1. The ternary system FeO-FeS-SiO_2

This ternary system is the simplest to show the effect of silica on matte/slag separation.

The miscibility gap between the silicate and sulphide liquids is a prerequisite for matte-slag separation. The figure below shows that liquid FeO and FeS alone are miscible. In silica-free melts with FeS concentrations above approximately 31mass%, a single oxysulphide liquid is formed. However, the presence of SiO_2 introduces a miscibility gap causing the separation into two immiscible liquid phases. The gap becomes larger as more silica is added. The tie lines, a, b, c, d on the curve ACB showed below represent the equilibrium compositions of the two liquids, the sulphide-rich melt (matte) and the oxide-rich melt (slag)[DAVENPORT, 2002:9].

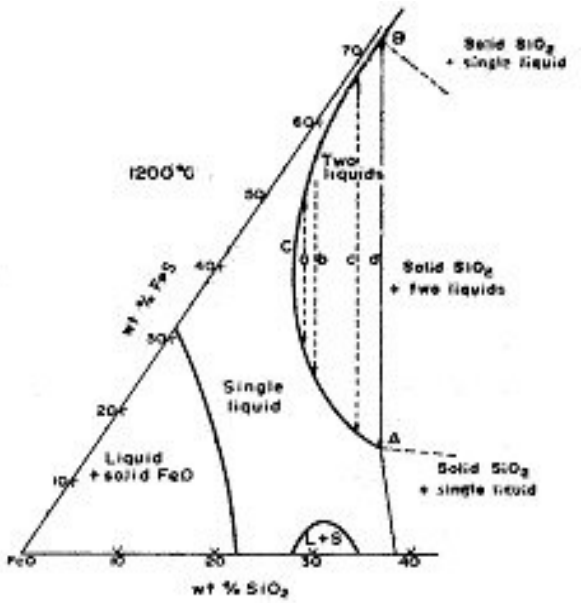

Figure 2-9. Phase diagram (1200°C) for the FeO-FeS-SiO_2 system showing the liquid-liquid immiscibility region created by the presence of silica [DAVENPORT, 2002:9]. *

*: The phase diagram is based on equilibrium with metallic iron.

An increased SiO_2 content induces liquid immiscibility between the sulphide and oxide-silicate phases, an effect that is maximal at SiO_2 saturation. This silica saturation condition forms a convenient boundary position used for the experimental investigation of this study.

II.2.2.2. The ternary system FeO-Fe_2O_3-SiO_2

As figure 2-10 shows, the SiO_2 content at saturation is affected little by the Fe_2O_3 content of the slag.

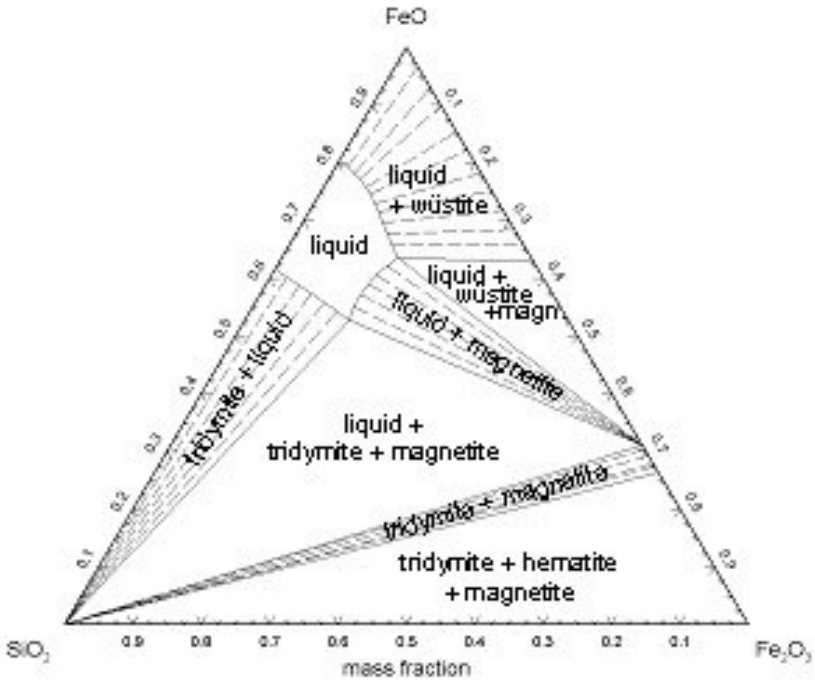

Figure 2-10. FeO-Fe_2O_3-SiO_2 diagram at 1250°C (FactSage).

II.2.3. The quaternary Fe-S-O-SiO_2 system

The stability diagram for the Fe-S-O-SiO_2 system for 1573K is shown below in terms of oxygen and sulphur potentials and the ratio $\frac{\%SiO_2}{(\%Fe+\%SiO_2)}$.

The volume, which represents the region of stability for iron silicate slags, is bounded at its surfaces by Fe_3O_4 (top), Fe (bottom), and SiO_2 (far face). At the left of the diagram, at low p_{S2}, there is an alternative representation of the well-known FeO-Fe_2O_3-SiO_2 ternary. Muan and Osborn gave oxygen potentials and liquidus boundaries, and Nagamori estimated activities of FeO and Fe_3O_4 at 1473 and 1573K. The surface of liquid oxysulfide stability is defined by points NOPQRN [CELMER, 1987:3].

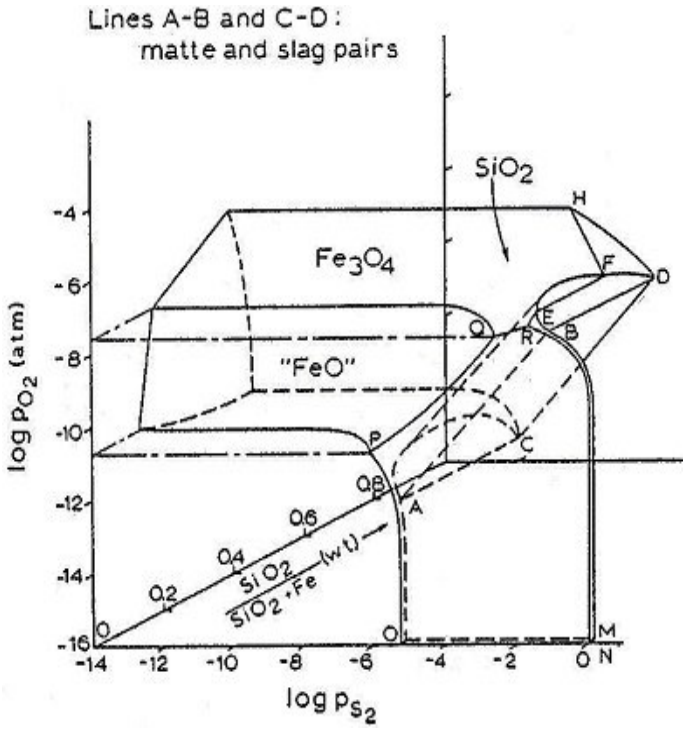

Figure 2-11. Stability diagram for the Fe-S-O-SiO_2 system at 1573K[CELMER, 1987:3].

II.3. Components and phase systems obtained with the Gibbs phase rule.

The selection of different variables is important in this study to determine the variance of the system. A variable is a component, which may be independently altered in value without disturbing the equilibrium of the system.

The variables that must be measured or controlled to define the equilibrium in the system are imposed by the degrees of freedom obtained with the Gibbs phase rule:

$$F = C + 2 - P$$

where F is the variance of the system or number of degrees of freedom,

C is the number of components and P is the number of phases. The number of degrees of freedom, F, is defined as the maximum number of variables, which may be independently altered in value without disturbing the equilibrium in the system.

If the system contains N species among which there are R independent reaction equilibria, then

$$F = (N-R) + 2 - P.$$ [GASKELL, 1981:21]

The phase rule gives

F = (12 - 6) – 3 + 2 = 5 (see appendix C)

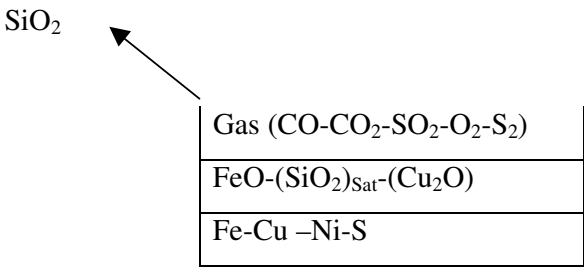

According to Celmer[1987:3], matte is not a rigorous thermodynamic variable because the activities of individual components ($a_{Fe,}$ a_{Ni}, p_{O2}, p_{S2}) are not necessarily constant at any value of matte grade. In practice, matte grade does closely define the matte composition in a smelting system, such that the activities of the constituent sulphides (FeS, $CuS_{0.5}$) are fixed [CELMER, 1987:3].

Some studies have been done on the phase equilibrium between the Ni_3S_2-FeS or Ni_3S_2-Cu_2S-FeS matte and the iron-silicate-based slag with the composition of 64 mass% FeO_x-36 mass% SiO_2 [FONT, 1999:16].

By applying the same principle in the Font experiments, the degree of freedom is found to be three: N = 10 (all species used in the experiment)

R = 6 (obtained with the rank of the echelon matrix)

P = 3 (solid, liquid and gas phase)

Thus, all the thermodynamic parameters can be defined by three variables chosen as: temperature, matte grade, the slag composition and the SO_2 partial pressure.

CHAPTER III
EXPERIMENTAL APPARATUS AND PRELIMINARY TESTWORK

III.1. Furnace assembly

Experiments were performed in a sealed vertical furnace tube. The furnace shell is of dimensions of 600 mm length, 600 mm width and 550 mm height. Silicon carbide (SiC) heating elements were used to provide external heat to the work tube. The hotrods (heating elements) of SiC can operate in the furnace up to 1550^{o}C.

The heating elements were concentrically arranged in the centre of the furnace and connected in series providing a zone of high temperature about 100 mm in length. Kaowool stuffing was used at the top of the furnace and around the thermocouple protection to prevent heat losses.

A mullite tube with a closed end was used as work tube with an inner diameter of 64 mm, an outer diameter of 73 mm and 520 mm length.

The system was closed gas tight by water-cooled brass end caps joined to the tube by compression 'O'-ring.

- Temperature profile

The objective of preliminary tests was to check and find the operating conditions required for accurate tests. These runs were used to check the gas flows, the gas tightness, and whether the temperature in the furnace remains constant over periods of time.

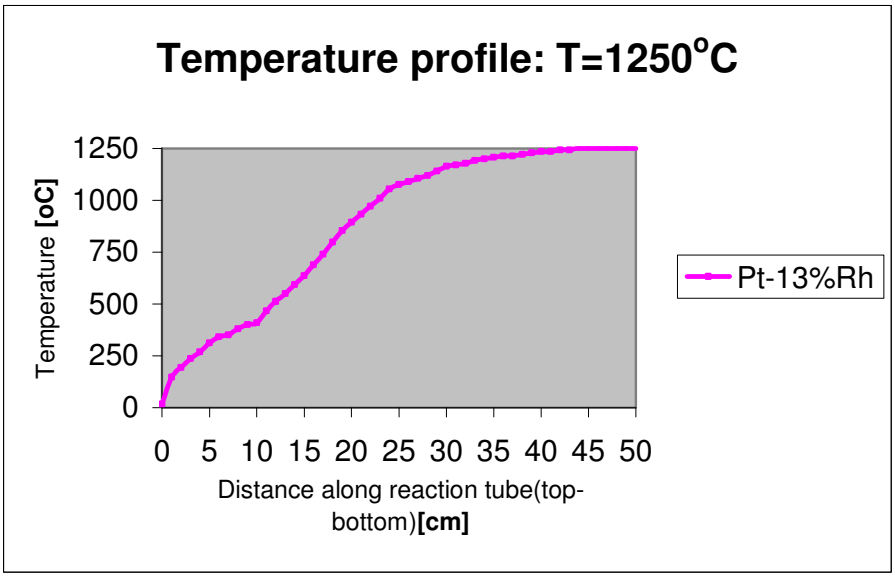

Figure 3-1 Temperature profile in the furnace

The temperature profile of the furnace showed a plateau region measuring 1523 K over a length of 6 cm. This was satisfactory for a depth of 10-20 mm of molten charge contained in the sample crucibles.

III.2. Apparatus

Experimental apparatus used in this study consisted of

- Zirconia electrolyte (4mm I.D., 6mm O.D., and 50mm in length) containing a mixture of Cr and Cr_2O_3 for the first experiments and Fe and FeO for the last experiments (as oxygen reference).
- An iron rod (2mm O.D and 75 mm in height) used as an electrical lead to the reference electrode, cemented onto the zirconia tube with alumina cement.

  The probe protection tube was a silica tube to minimise reaction of iron rod with the furnace content.
- Platinum wire (0.5mm diameter) to complete the electrical circuit of the cell, shielded with a mullite tube, immersed in the matte.
- A thermocouple (Pt-13%Rh) used to measure the temperature.

  The thermocouple protection tube was a mullite tube, 6 mm O.D., 2 mm I.D for each holes; the tip of the thermocouple was positioned approximately 1 cm from the crucible.

- The $CO/CO_2/SO_2$ inlet gas mixture was supplied through a 6 mm O.D., 4 mm I.D., silica tube . The gas left the furnace via a copper exit tube in the end cap. The tip of the gas inlet tube was approximately 2 cm from the top of the crucible.

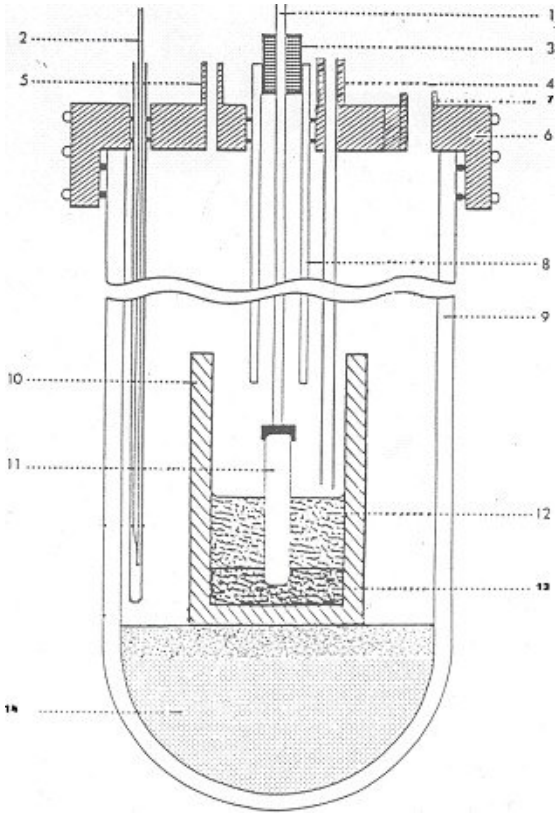

Figure 3-2. Reaction tube and crucible assembly used in the thesis.

1. Iron rod
2. Pt13Rh thermocouple
3. Rubber stopper
4. Platinum wire guide tube
5. Gas inlet
6. Water-cooled brass fitting
7. Gas outlet
8. Alumina guide tube
9. Mullite reaction tube
10. Silica crucible
11. Zirconia oxygen probe
12. Liquid slag
13. Liquid matte
14. Alumina beads

Samples were removed from the furnace and carefully separated from the silica crucible. The samples were ground in a mortar to obtain small pieces and then mounted for further analysis with SEM and the electron probe microanalyser. The matte composition was determined by an average value of the solidified matte.

Samples were analysed by scanning electron microscope (SEM) and also with an electron probe microanalyser (WDS). SEM measurements were performed with the following parameters: acceleration voltage of 25 kV, working distance of 20 mm, Norvar window and silica-lithium detector.

Samples were also analysed with an electron probe microanalyser (CAMECA SX-100), with four WDS spectrometers and a Röntek Xflash SDD detector. The beam conditions were 20 kV and 20 µA with measurement times (real time) of 120 s.

III.3.Zirconia solid electrolyte

According to Iwase [IWASE, 1992:34], the solid electrolyte is a diagnostic sensor that permits rapid determination of various elements dissolved in hot metal and liquid steel. Pure zirconia has a monoclinic crystal structure at room temperature and transforms to tetragonal and cubic forms at increasing temperatures. The volume expansion caused by the cubic to tetragonal to monoclinic transformations induces very large stresses, and causes pure zirconia to crack upon cooling from high temperatures. Several different oxides can be added to zirconia to stabilize the tetragonal and/or cubic phases such as magnesium oxide (MgO), yttrium oxide, (Y_2O_3), calcium oxide (CaO), and cerium oxide (CeO) [Internet,2005].

- Properties of ZrO_2 [JANKE, 1977:38]

ZrO_2	
Structure	Monoclinic
Transformation mono.↔ tetra.,^oC	800 to 1200
Transformation tetra.↔ cub.,^oC	≈ 2300
Melting point, ^oC	2680
Density at 20^oC, g.cm^{-3}	6.1
Free energy of formation ΔG^o, kJ.mol^{-1}	-1082.74 + 0.17806T
Log p_{O2}(1600^oC), atm	-20.88

Stabilized zirconia is predominantly an oxygen anion conductor because of the presence of a large amount of oxygen anion vacancies. Stabilized zirconia is used because the unstabilized zirconia has electronic conduction causing polarization of the electrolyte and incorrect readings [NAUDE, 2003:62]. Therefore, the addition of magnesia in the zirconia probe composition is important to ensure proper readings due to ionic conduction.

The accurate measurement of oxygen activity can be ensured only if the e.m.f. response has a stable e.m.f. plateau, a short response time, and good reproducibility. [VAN WIJNGAARDEN, 1987:86]

Solid zirconia electrolytes are used in high-temperature thermodynamic studies of slag-metal systems such as the production of iron, ferrochromium, and steel. The construction of the solid electrolyte oxygen cell is different depending on the practical conditions and the component to be measured: iron, matte, slag or steel. The use of zirconia electrolytes at high temperature and low oxygen potentials introduces a mixed ionic and *n*-type electronic conduction.

According to Schmalzried's analysis [GELDENHUIS, 2004:24], the cell EMF for a mixed ionic and electronic conduction of the oxide electrolyte at low oxygen partial pressures follows the equation:

$$E = \frac{RT}{F} \ln \left[\frac{\left(P''_{O_2}\right)^{\frac{1}{4}} + \left(P_e\right)^{\frac{1}{4}}}{\left(P'_{O_2}\right)^{\frac{1}{4}} + \left(P_e\right)^{\frac{1}{4}}} \right]$$

Where P'_{O_2} and P''_{O_2} are the respective partial pressures of oxygen at the two electrolyte-electrode interfaces, P_e is the oxygen partial pressure at which the *n*-type and ionic conductivities are equal, R is the gas constant, F the Faraday constant, and T the absolute temperature.

According to Van Wijngaarden[1988:84], the electrical properties of solid electrolytes are influenced by the type and concentration of the stabilizing oxide, the phase composition, the impurities in the electrolyte, and the microstructure of the electrolyte and can therefore be influenced by the chemical and physical properties of the original raw materials, as well as by the heat treatment to which the electrolyte is exposed during fabrication.

Two different reference electrodes have been used in this thesis to see their behaviour in the melt at a given temperature.

a. Electrochemical oxygen probe with Cr/Cr_2O_3 reference.

A mixture of $Cr\text{-}Cr_2O_3$ was used as reference electrolyte.

The principal reaction is

$$2\ Cr + \tfrac{3}{2} O_2 = Cr_2O_3$$

Chromium and chromium oxides used were laboratory chemicals (see Appendix –E).

The equilibrium constant $K = \dfrac{a_{Cr_2O_3}}{a_{Cr}^2 . p_{O_2}^{1.5}}$, therefore $p_{O_2} = \left(\dfrac{a_{Cr_2O_3}}{K} \right)^{\frac{2}{3}} . \dfrac{1}{a_{Cr}^3}$

Oxygen partial pressure depends on temperature, activities of chromium and chromium oxide.

If Cr_2O_3 and Cr are pure, $pO_2 = 6.48 \times 10^{-18}$ atm (FactSage, 1250°C)

The $Cr\text{-}Cr_2O_3$ mixture was placed in a zirconia electrolyte tube stabilized with MgO (see appendix-I) of 50 mm length, 5 mm I.D and 6 mm O.D. An iron wire served as the electrical lead to the reference electrode used for electrical contact and was cemented into the zirconia tube with alumina cement. No alloying between Fe and Cr was observed after use of the probe at 1250°C.

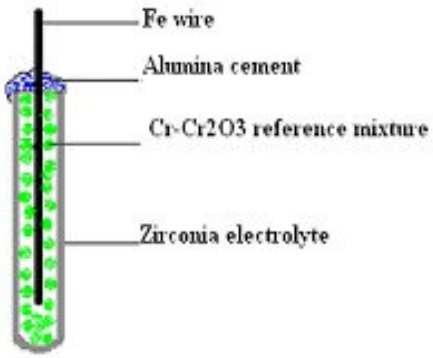

The electrolyte was heated at 300°C in a resistance furnace for about a day to dry and harden the alumina cement.

b. Electrochemical oxygen probe with Fe/FeO reference.

The reaction for this reference electrode is

$Fe + ½\ O_2 = FeO$

Fe was a laboratory chemical (see Appendix-E) while FeO was prepared from $FeC_2O_4.2H_2O$ by using a muffle furnace at 1000°C according to the reaction:

$FeC_2O_4.2H_2O_{[S]} \xrightarrow{Ar} FeO_{[S]} + CO_{[g]} + CO_{2\,[g]} + 2H_2O_{[g]}$. Details are presented in Appendix-F.

The equilibrium constant $K_T = \frac{a_{FeO}}{a_{Fe} x \left(p_{O_2}\right)^{0.5}} \quad \Rightarrow \quad p_{O_2} = \left[\frac{a_{FeO}}{K_T . a_{Fe}}\right]^2$

$a_{Fe} = a_{FeO} = 1$ (solid reference)

$K_T = 591720$ (1523K)

$P_{O2} = 2.86x10^{-12}$atm

- ❖ Fe/FeO reference with added silver.

The iron –iron oxide reference electrode was improved in terms of conductivity by adding silver in the reference electrode. Silver was used in the electrode to enhance the electronic conductivity of the electrodes [XIA, 2002:91] and served as stabiliser for the EMF measurements and reading.

The cross section of the zirconia probe after the test did not show any reaction between zirconia, iron oxide and silver. SEM pictures of the cross section are presented below

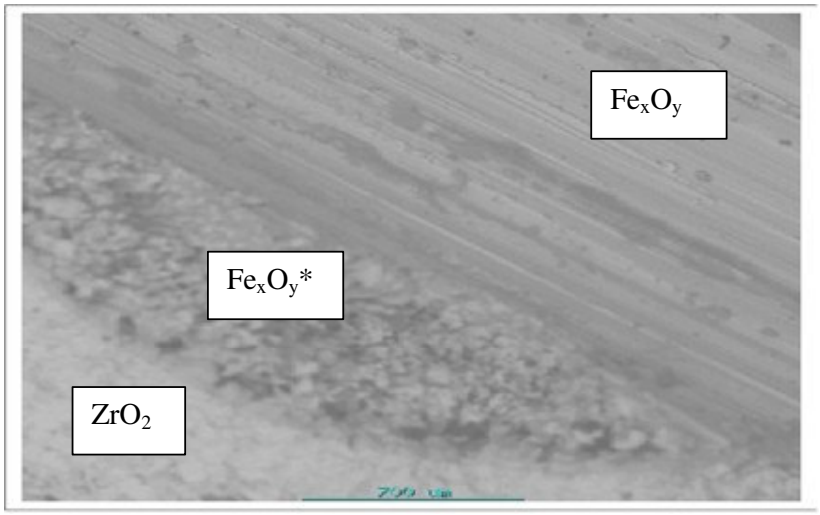

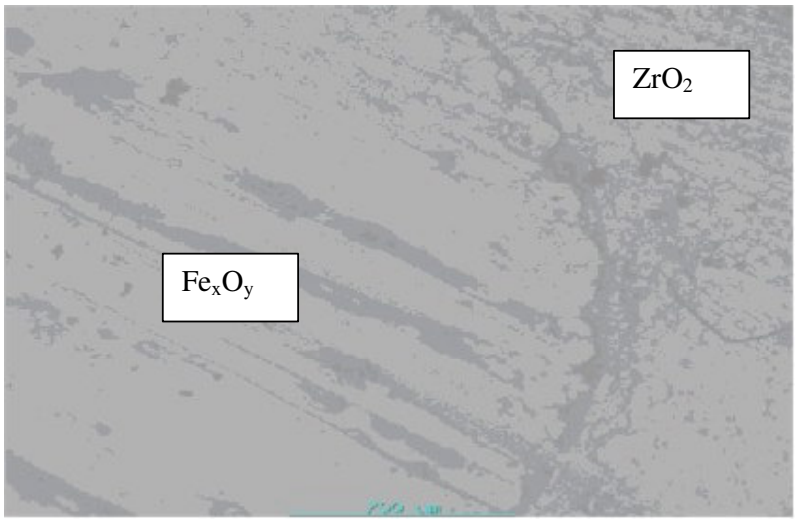
ZrO_2
Fe_xO_y

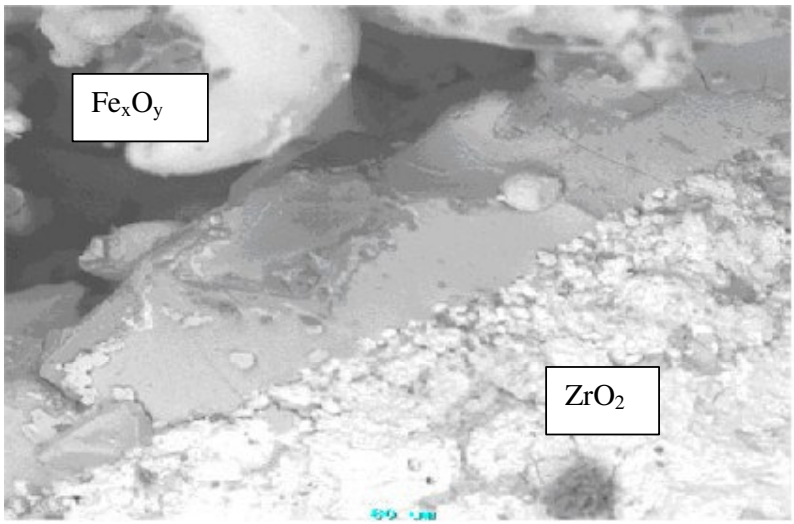
Fe_xO_y
ZrO_2

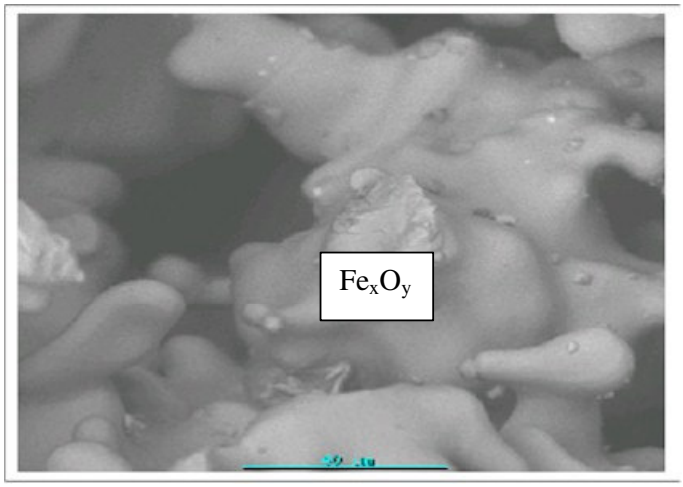

Figure 3-3. SEM micrograph of zirconia cross-section showing the boundary between zirconia probe and iron oxide solid reference electrolyte.

The cross section of zirconia probe shows a net separation between zirconia and iron oxide. No reactions take place between the two compounds. Fe_xO_y differ from $Fe_xO_y^*$ in terms of microstructure probably because of a temperature gradient.

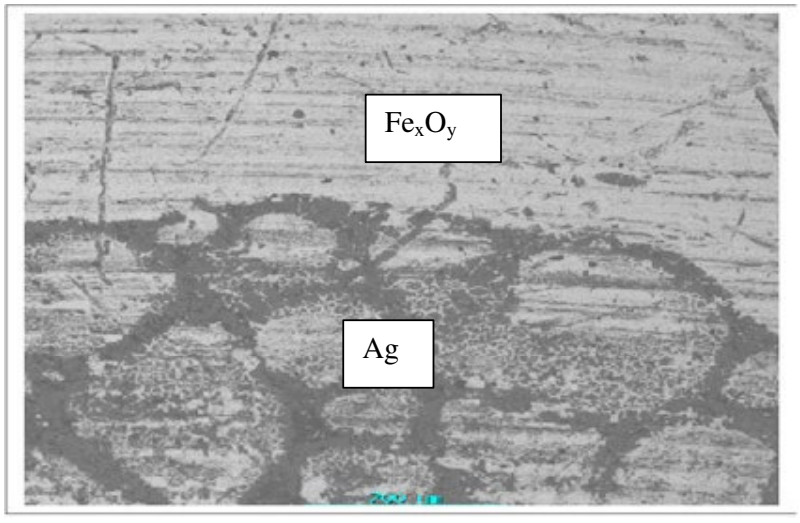

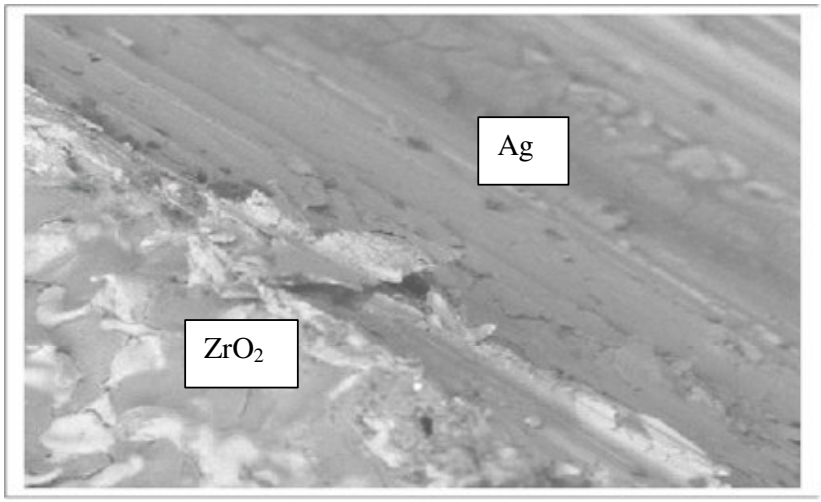

Figure 3-4. SEM micrograph of zirconia cross-section showing the boundary between zirconia probe and silver used as stabiliser.

C. Preliminary tests

The purpose of these tests was firstly to compare the two different reference electrodes at 1250°C and secondly to see the impact of different gas composition on the results.

Table 3-1 shown below presents the EMF results for Cr/Cr_2O_3 and Fe/FeO solid electrolytes obtained at 1250°C using Cu and Cu_2O as melts (fig. 3-5). The expected oxygen activity using the Ellingham diagram was about $6x10^{-4}$ atm; the value obtained with FactSage was $1x10^{-4}$ atm.

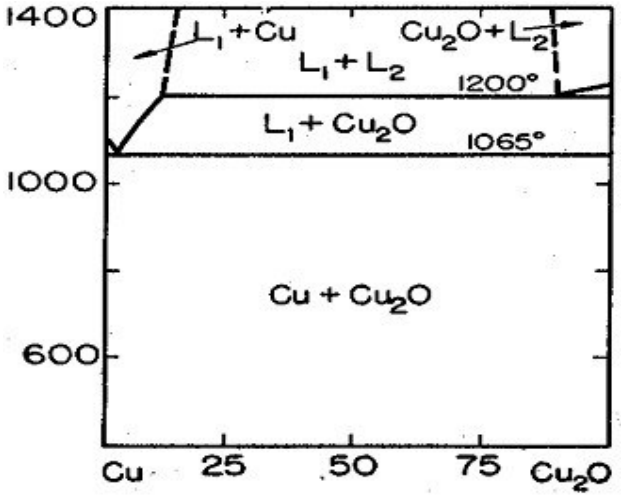

Figure 3-5. Phase diagram of Cu-Cu_2O

Details of calculation (for 1523 K):

<u>Cr/Cr_2O_3 reference</u>

$2Cr + 3/2\ O_2 = Cr_2O_3$; $K = 1.97\times10^{25}$, $pO_2^{ref} = 1.37\times10^{-17}$ atm

<u>Fe/FeO reference</u>

$Fe + ½\ O_2 = FeO$; $K = 4.64\times10^{5}$; $pO_2^{ref} = 4.65\times10^{-12}$ atm

Cr/Cr_2O_3 reference		**Fe/FeO reference**	
E [mV]	**log (pO_2/atm)**	**E [mV]**	**log (pO_2/atm)**
-124	-15.22	-621	-3.11
-116	-15.33	-603	-3.35
-111	-15.39	-589	-3.53
-108	-15.43	-567	-3.82

Table 3-1. EMF results when testing oxygen probes with Cr/Cr_2O_3 and Fe/FeO references in a Cu melt in contact with Cu_2O, at 1523 K. Different values are for repeat tests.

The oxygen partial pressure for both reference electrodes are completely different, values obtained with Fe/FeO reference electrodes are close to the expected results.

A second test was performed with the experimental matte and slag in a $CO\text{-}CO_2\text{-}SO_2$ gas mixture. The results obtained with the Cr/Cr_2O_3 solid electrolyte are presented in this chapter while the results obtained with Fe/FeO solid electrolyte are presented in the next chapter.

- Tests run using Cr/Cr_2O_3 reference electrode.

EMF results obtained using Cr/Cr_2O_3 as reference in different tests, the iron content varying from 8.8 % to 4 % in the matte, with $CO/CO_2/SO_2$ gas mixture are given below.

Test 1	8.4wt%Fe	Test 2	4.2wt%Fe	Test 3	2.2wt%Fe	Test 4	1.3wt%Fe
EMF (mV)	log pO2(atm)	EMF (mV)	log pO2(atm)	EMF (mV)	log pO2(atm)	EMF (mV)	log pO2(atm)
-297	-12.87	-286	-13.02	-129	-15.10	-124	-15.16
-268	-13.26	-231	-13.75	-128	-15.11	-116	-15.27
-201	-14.14	-176	-14.47	-119	-15.23	-111	-15.33
-186	-14.34	-129	-15.10	-112	-15.32	-108	-15.37

Table 3-2. Results of pO_2 measurements in different experimental runs with different Fe contents in the matte in contact with silica-saturated slag, using a Cr/Cr_2O_3 reference. Different values at each matte composition are from repeat tests. The values are erroneous because the unreliability of this reference under the experimental conditions used here.

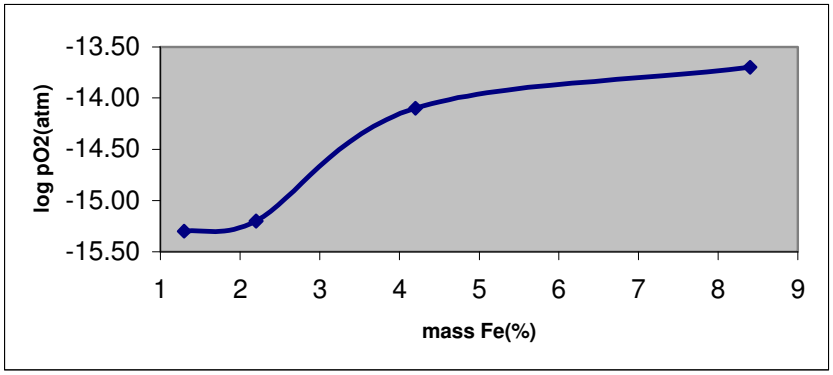

Figure 3-6. Apparent (erroneous) relationship between matte Fe content and measured oxygen activity, for a Cr/Cr_2O_3 reference.

Results presented on table 3.2 shows a trend of increasing pO_2 with a decrease of iron content in matte. The expectation was a decrease of pO_2 with a decrease of $(\%Fe)_{matte}$. Measurements on different rows show results as a function of (%Fe) decrease in the matte.

The oxygen partial pressure obtained was very low compare with the expected value, which was about 10^{-9} atm (see next chapter for predicted values). Analysis of the zirconia probe after the test revealed that:

- There was possible poor contact between the chrome-chrome oxide (oxygen reference) and the iron wire.
- The surface of the iron wire in the zirconia tube discoloured, more so close to the point of entry into the probe.
- The oxygen partial pressure in the reference electrode is unstable due to gas leakage through the alumina cement on top of the zirconia tube.

It is essential for all the experiments to obtain a stable e.m.f. plateau in order to classify the reading as successful in terms of the exact oxygen potential of the melt. A typical signal trace from Cr/Cr_2O_3 and Fe/FeO probes is given in figure 3-7. The $Cr\text{-}Cr_2O_3$ reference electrode used in the first part of this project was not successful. Several factors could strongly affect oxygen potential measurements when electrochemical oxygen probes were applied in slag-matte melts, such as polarization effects on the electrodes. In the case of polarization effects, the e.m.f. signal declines as a function of time.

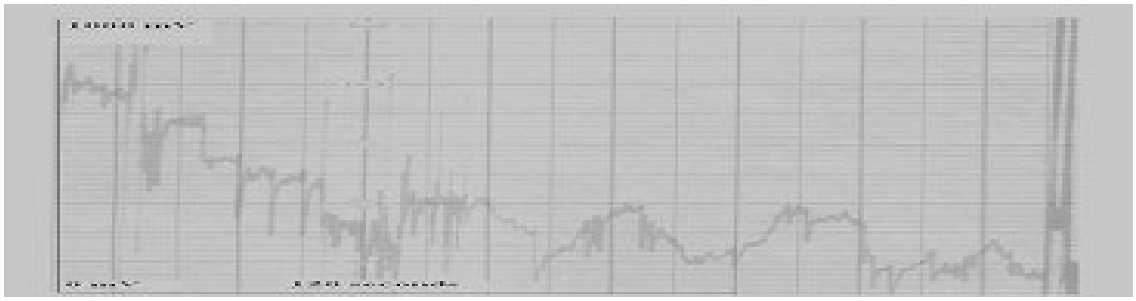

Cr/Cr_2O_3 reference probe in a $CO\text{-}CO_2\text{-}SO_2$ environment

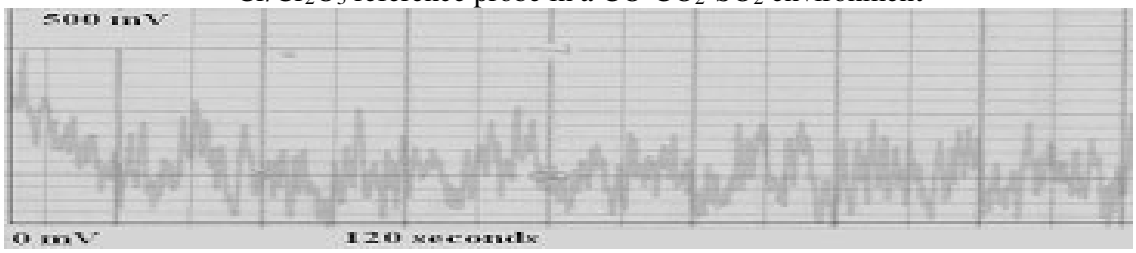

Fe/FeO reference probe in a $CO\text{-}CO_2\text{-}SO_2$ environment

Figure 3-7. Potential vs. time produced by the Cr/Cr_2O_3 and Fe/FeO reference probes.

For these reasons, it was imperative to find an alternative to the chrome-chrome oxide reference electrode utilized in the first phase of experiments.

As the wire used is iron, a mixture of iron-iron oxide was used as reference electrode. The advantage of the use of iron-iron oxide is:

- Oxygen concentration should be constant in all the zirconia tube, avoiding the different colour in the zirconia tube.
- Any excess of iron does not affect the measurement of oxygen activity according to the relation $Fe_{powder,\ wire} + ½\ O_2 = FeO_{powder}$

Figure 3-8 shows SEM micrographs of different samples of Cr/Cr_2O_3 before (room temperature) and after the test (1250°C).

For the Cr/Cr_2O_3 grains are not uniform in size and shape before and after, although there is a slight growth of grain after the test observed with an image magnification of 8000. Some researchers [MARTIN, 2003:51] have shown that a much more open pore structure is observed after sintering at 1250°C, which can have an implication for a reduction of the electrode surface area.

Although the colour is different: Bright green before the test and dark green after the test.

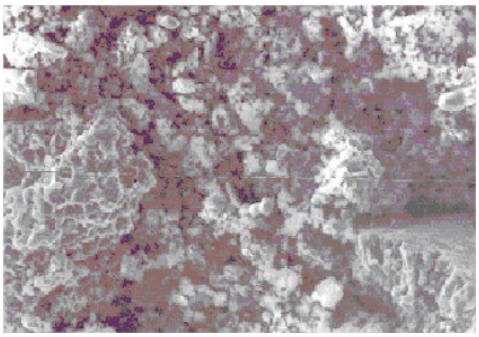

Before Cr/Cr_2O_3 1.25µm

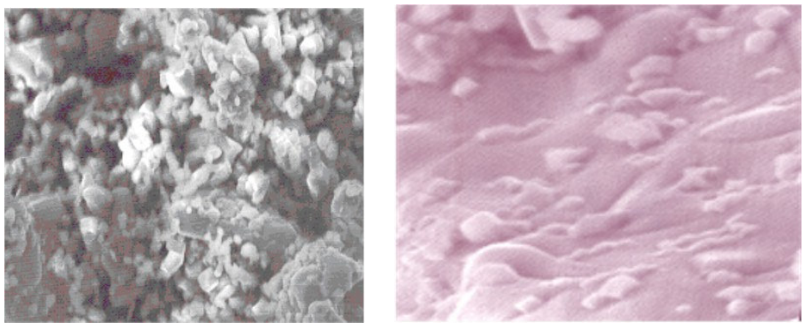

After Cr/Cr_2O_3

Figure 3-8. SEM micrograph of Cr/Cr_2O_3 solid reference before and after use.

For Fe/FeO, the situation is completely different. Figure 3-9 shows SEM micrographs of Fe/FeO before (room temperature) and after the test (1250°C). At room temperature, the microstructure reveals a non-uniform distribution of grains with small and large grains, and formation of small rods. However a uniform size distribution is observed after the test with a

low porosity. The change in grain size of the FeO is because of sintering at 1250°C as the temperature is not far below the melting point of wustite.

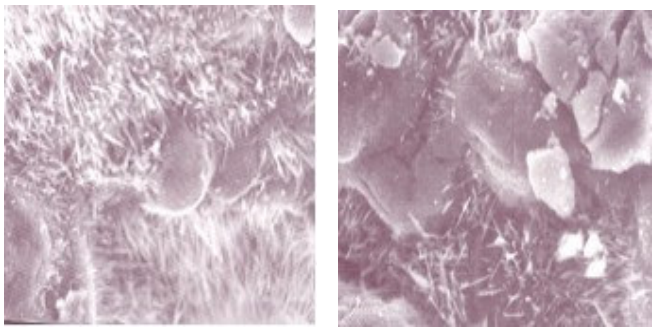

Fe/FeO before

1.25µm

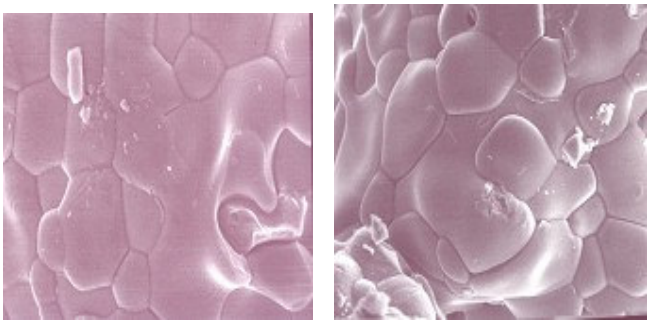

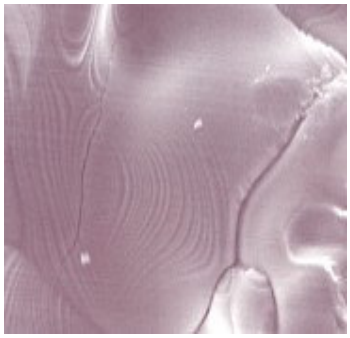

Fe/FeO after

1.25µm

Figure 3-9. SEM micrograph of Fe/FeO solid reference before and after use.

On the basis of these differences between chromium and iron references, the iron reference was preferred to chromium reference as it gave more accurate and stable reading measurements compared to the chromium reference.

- Effect of gas mixture in the furnace on the results

Different gas compositions have been used to see their effect on the melt results. Same matte were used for all tests performed at 1250°C: 6.4 wt%Fe, 22.8 wt%Cu, 48.9 wt%Ni and 21.8 wt%S; 6.0 wt%Fe, 22.5 wt%Cu, 50.7 wt%Ni and 21.5 wt%S; 3.7 wt%Fe, 21.5 wt%Cu, 52.8 wt%Ni and 21.9 wt%S. The average slag composition was 54.8 wt%Fe, 16.3 wt%Si and 28.9 wt%O. The iron reference was slowly introduced from the top of the furnace until it reached the liquid melt in a silica crucible. The gas composition used was: 0.44 atm SO_2, 0.45 atm CO_2 and 0.02 atm CO. The expected pO_2 and EMF if equilibrium with the gas was achieved were $3.6x10^{-8}$atm and –294 mV respectively; with a total pressure of 0.91 atm. The gas mixture of $CO/CO_2/SO_2$ was flown through the gas inlet tube for the whole tests. After a determined time (five minutes for each test), the iron reference was slowly removed from the crucible. EMF values obtained were compared to those obtained in the same conditions but with Ar gas as furnace atmosphere.

Results obtained with $Cr\text{-}Cr_2O_3$ reference electrode showed pO_2 values far too low and unstable compare to Fe-FeO reference electrode in the same conditions.

$(\%Fe)_{matte}$	**Measured EMF (mV)**	
	$CO\text{-}CO_2\text{-}SO_2$	**Ar**
6.4	- 194	- 196
6.0	- 229	- 230
3.7	- 232	- 234

Table 3.3. EMF measurements corrected for the thermal EMF between the Pt and the Fe with the Fe/FeO reference, for different gas atmospheres and for matte compositions, in contact with silica-saturated fayalite slag.

Results of oxygen measurements obtained with $CO\text{-}CO_2\text{-}SO_2$ gas mixture and Ar gas using Fe-FeO reference electrode present similar tendency of EMF stability for both cases. The oxygen activity was similar independently on the gas mixture. As the oxygen partial pressure did not affect the values of the results, Ar was chosen as inlet gas for all the subsequent tests.

III.4. Thermal EMF of Pt-Fe

The thermal EMF of a Pt/Fe thermocouple was measured at 1250°C. This was necessary to determine the correct value of the final emf by subtracting the thermal emf from cell voltage measured during oxygen probe measurements.

The Pt/Fe thermocouple was made of reference grade platinum of 99.999% purity and iron of 99+% purity wires (0.5-mm diameter for platinum and 1.8mm diameter for iron) and 55-cm length. The wires were cleaned with alcohol, and inserted in twin bore alumina tube of 2 mm inside diameter. Pt was the negative pole while the Fe was the positive pole during the potential measurements. All of the EMF measurements were made with a calibrated digital voltmeter.

The average EMF of the thermocouple at 1250°C was +17.7 mV.

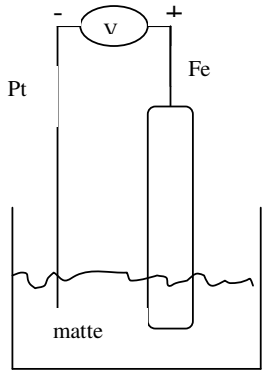

Figure 3-10. Schematic representation of Fe-Pt

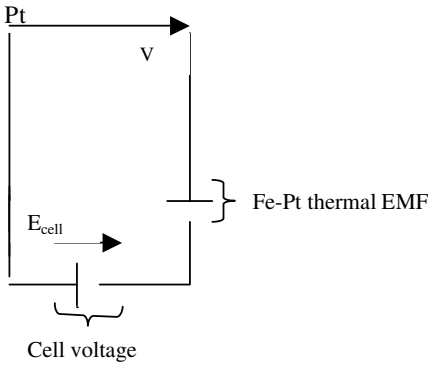

Figure 3-11. Fe-Pt circuit

Ecell = E_{meas} – Thermal $EMF_{Fe\text{-}Pt}$

= E_{meas} – 0.017 V

The following graph on figure 3-12 was calculated for values between 0°C and 1000°C and was extrapolated beyond that temperature to estimate the EMF value at 1250°C. The following formula was used in that purpose:

$$S_{AB}(T) = \lim_{\Delta T \to 0}\left(\frac{\Delta U}{\Delta T}\right) = S_B(T) - S_A(T)$$ [HELLWEGE, 1985:27]

where S is the absolute thermopower of a material, T is absolute temperature, ΔU is the voltage and A,B are the materials forming the thermocouple.

Extrapolation to 1250°C was necessary since the source that was used contained Seebeck coefficients for iron up to 1000°C only.

The graph was extrapolated from two different assumptions:

- the absolute thermopower was kept constant

-the trend of the slope was kept constant

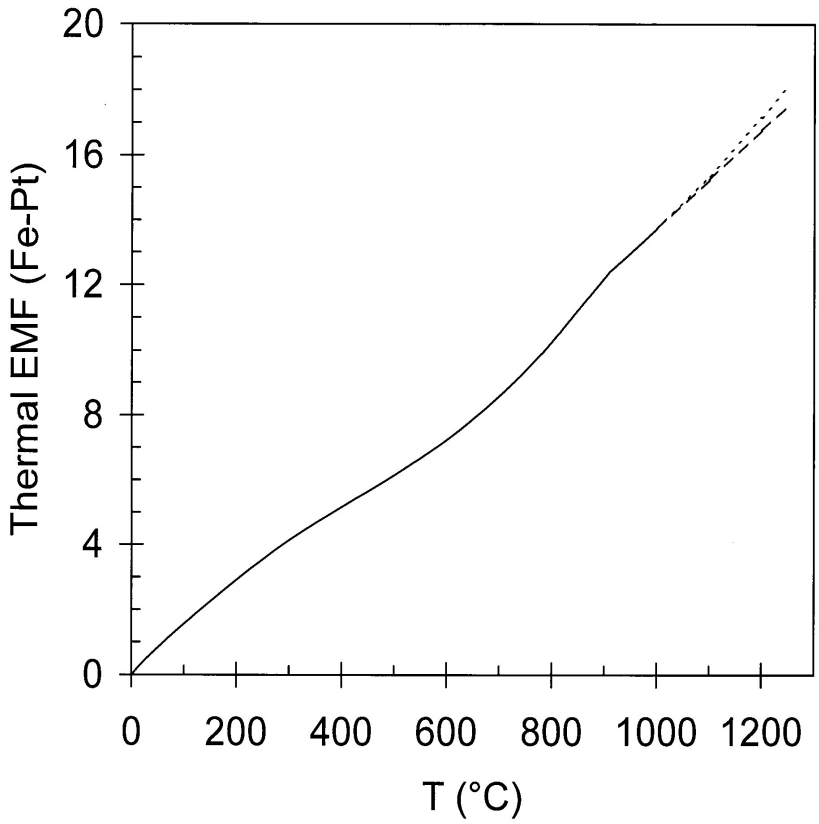

Figure 3-12. Thermal EMF vs temperature for Fe-Pt system

The predicted thermal EMF can be seen to agree with the measured value.

III.5. Experimental apparatus and procedure

III.5.1.Gas system

The choice of CO-CO_2-SO_2 gas mixture was made to provide oxygen and sulphur partial pressure in the furnace environment which may affect the equilibrium with the matte-slag system under conditions of constant temperature.

The gas system supplied high purity CO, CO_2 and SO_2 inlet gas at constant flowrates controlled by means of a digital readout and control system E-7000 supplied by BRONKHORST HIGH-TECH B.V. The oxygen potential in the gas at equilibrium with iron sulphide at 1250^{o}C was calculated (details in Appendix-A) and was in the range of 1.53×10^{-8} to 2.78×10^{-7} atm. The CO/CO_2 ratio for all tests was of the order of 5.85×10^{-2} to 4.34×10^{-2}.

III.5.2.Experimental procedure.

The matte and slag were prepared in the laboratory from chemically pure or high quality commercial materials. Ni_3S_2, Cu_2S and FeS for the matte components were premelted in a silica crucible. The slag with the composition of 62 mass% FeO-38 mass% SiO_2 was premelted by fusing FeO powder and SiO_2 powder under argon atmosphere in an iron crucible. SiO_2 was added in excess of saturation (62mass% FeO-38mass%SiO_2) to assure a condition of silica saturation.

Slag was premelted in a furnace at 1400^{o}C in an argon atmosphere to form fayalite. The cooled slag melt was milled and charged to the furnace as powder form. 5g of slag were used for each test. The matte was also preheated in the same furnace and milled before use in experiments.

Slag and matte powders were mixed intimately. 5g of matte and 5g of slag were put in a SiO_2 crucible with an inner diameter of 33 mm and a height of 37mm.

The charged silica crucible was carefully introduced into the furnace, which was then preflushed with Ar for 30 min to expel all the air. The gas mixture of $CO/CO_2/SO_2$ (or Ar) flowed through the gas inlet tube. The furnace was heated to 1250°C at 100^{o}C per hour.

After a determined time (1h, 2h, 3h and 4h), samples were sucked into a silica tube by using a syringe at the end of the tube, which is introduced through the sampling hole. Some samples

withdrawn before the end of the complete experiment were quenched in water. The sampling procedure was not easy to apply because of the small melt quantity.

At the end of the experiment the gas mixture was replaced with Ar, and the crucible cooled with the furnace. Each measurement was performed twice.

- Behaviour of iron

A test of experimental accuracy was performed to study the behaviour of iron content in matte as shown on figure 3.13 and 3.14.

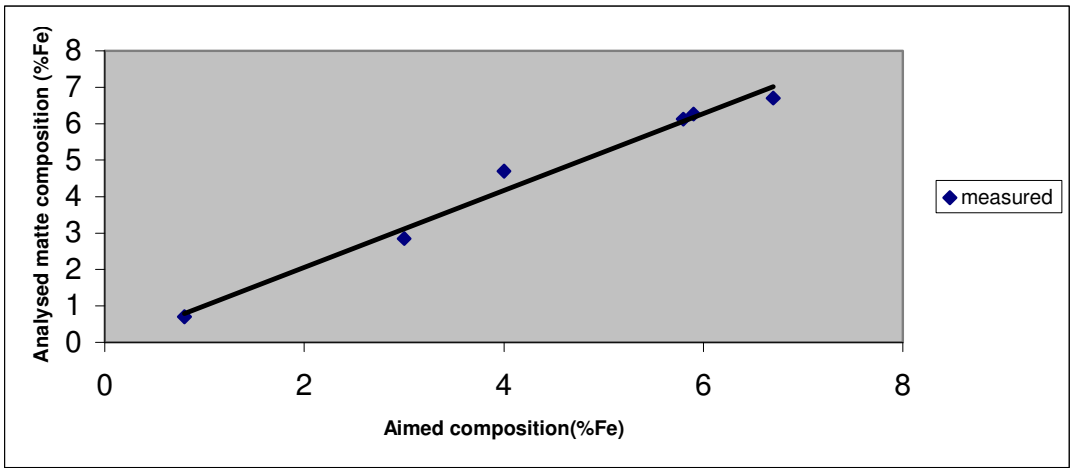

Figure 3-13. Tendency of iron for aimed composition matte vs. analysed matte (FeO slag)

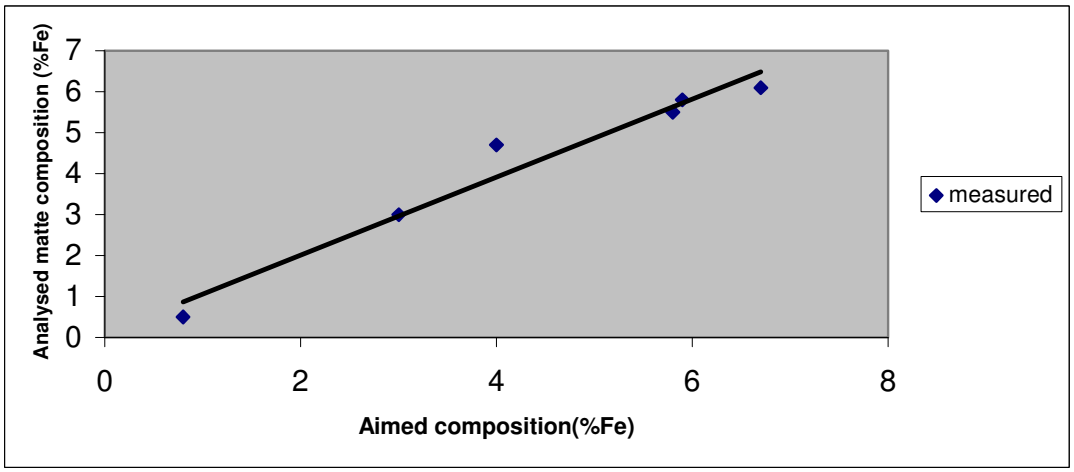

Figure 3-14. Tendency of iron for aimed composition matte vs. analysed matte matte (FeO/Fe_2O_3 slag)

Figure 3-13 and figure 3-14 show the aimed composition and analysed iron of the matte. Good agreement is shown between the expected values and the measured values.

III.6. Error analysis

The error involved in the different measurements after sampling the melt, cooling the crucible were significant and could change values of the matte-slag composition. These errors were due to

- the delicate manipulation of the probe according to the short height of the melt.
- the disturbance of gas composition in the furnace due to the opening on the top of the furnace for each experiment and sampling.

Confidence intervals (95%) on the potential measurements of all tests were calculated by using the t distribution.

For microprobe measurements, the total amount of the four components in the matte (iron, nickel, copper, and sulphur) varied from 99.6% to 100.4% for analyses done with Fe-FeO reference electrode.

CHAPTER IV
EXPERIMENTAL RESULTS

IV. 1. Results overview

This chapter presents the experimental results of the present investigation. The main variable in the investigation was the oxygen partial pressure. The temperature was maintained constant during all the experiments at 1250°C, and the total pressure was 0.86 atm, average pressure in Pretoria.

The initial oxygen activity was estimated from the data using FACTSAGE.

The expected oxygen activity was obtained by using thermodynamic calculations for the reaction Fe + ½ O_2 = FeO with $k = \frac{a_{FeO}}{a_{Fe} p_{O_2}^{0.5}} = 498080$ (temperature = 1250°C, FACTSAGE).

The activity of FeO was found to be 0.35 (liquid reference state) for SiO_2 saturated FeO-SiO_2 at 1250°C. The activity of iron in matte was calculated using FactSage.

All the measurements reported in this chapter were performed with Ar as flushing gas.

IV.2.Results of different tests

The tests were performed with two different slags:

One set used slag containing SiO_2 and FeO, and in the other case Fe_2O_3 was added to the slag. Fe_2O_3 was added to yield a Fe^{2+}: Fe^{3+} ratio of 2:1. Thus corresponds to magnetite saturation.

The hematite was added to test the effect of ferric ions on the measured oxygen potential.

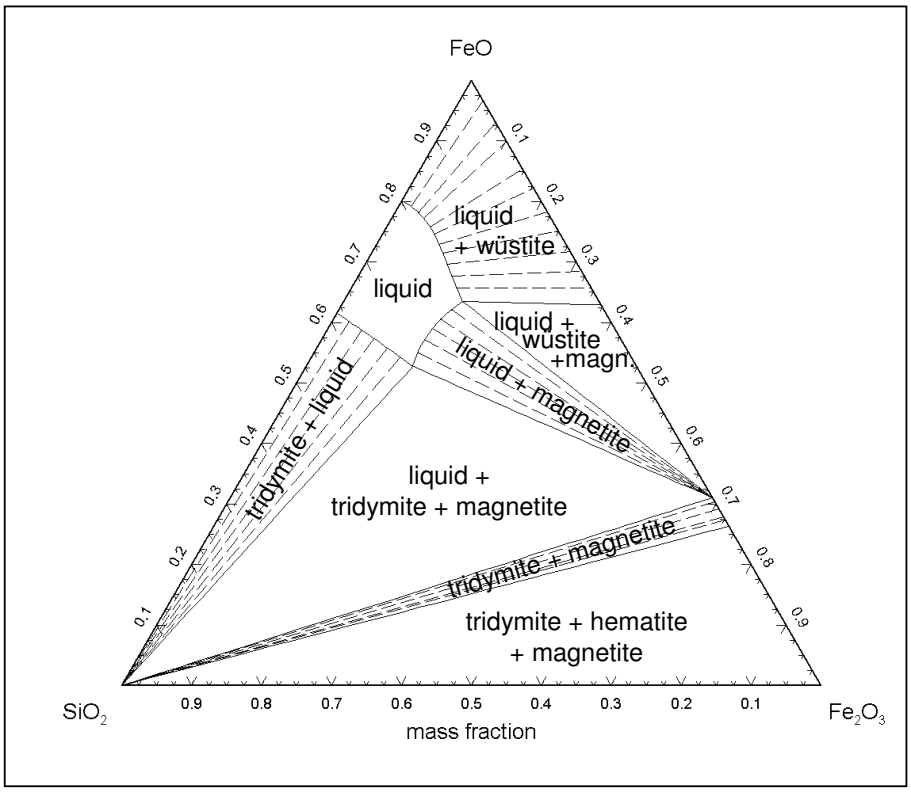

Figure 4-1. Phase diagram for FeO-SiO_2-Fe_2O_3 at 1250°C (FACTSAGE)

IV.2.1.FeO-SiO_2 slag

Results obtained with different matte composition varying between 8.8 wt% and 1 wt% iron content, a slag composition of 30 Wt% SiO_2 and 70Wt% FeO in argon at 1250°C are presented in Appendix- B.

In the figures in this chapter, 'oxygen calculated' expresses the theoretical calculations performed with FACTSAGE (matte was assumed to be in a liquid phase and the initial composition used was the matte weighed in the laboratory) to determine the expected oxygen activity. Meas A and B express the measurements performed with same matte composition with different sample weight: 5g and 10g respectively. The horizontal and vertical error bars on figure 4.2 show the range of analysed iron content and oxygen activity respectively.

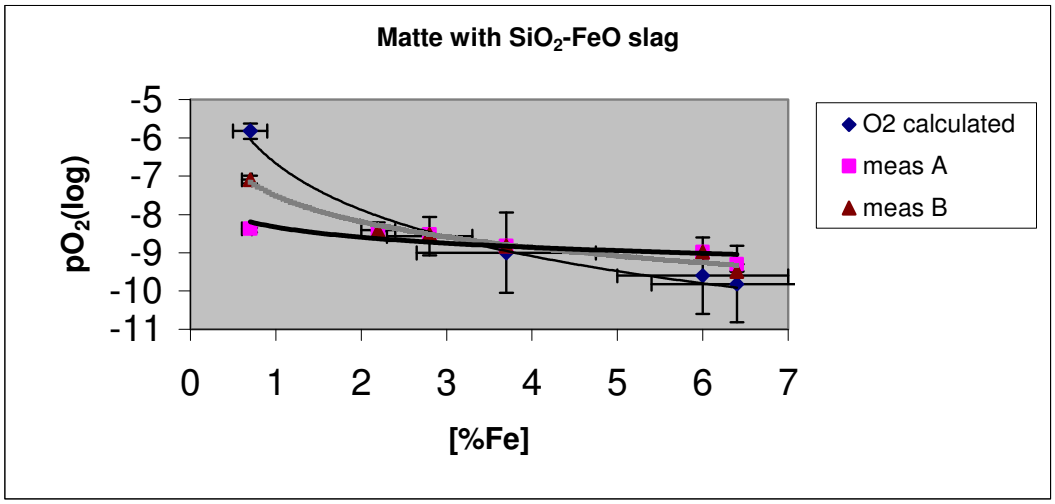

Figure 4-2. Evolution of iron content vs oxygen pressure (FeO slag)

IV.2.2. $FeO-Fe_2O_3-SiO_2$ slag

The EMF results shown below were obtained using Fe/FeO as reference in Ar atmosphere with $FeO-SiO_2-Fe_2O_3$ slag. In the figure, 'oxygen calculated' expresses the theoretical calculations (FACTSAGE) to determine the expected oxygen activity.

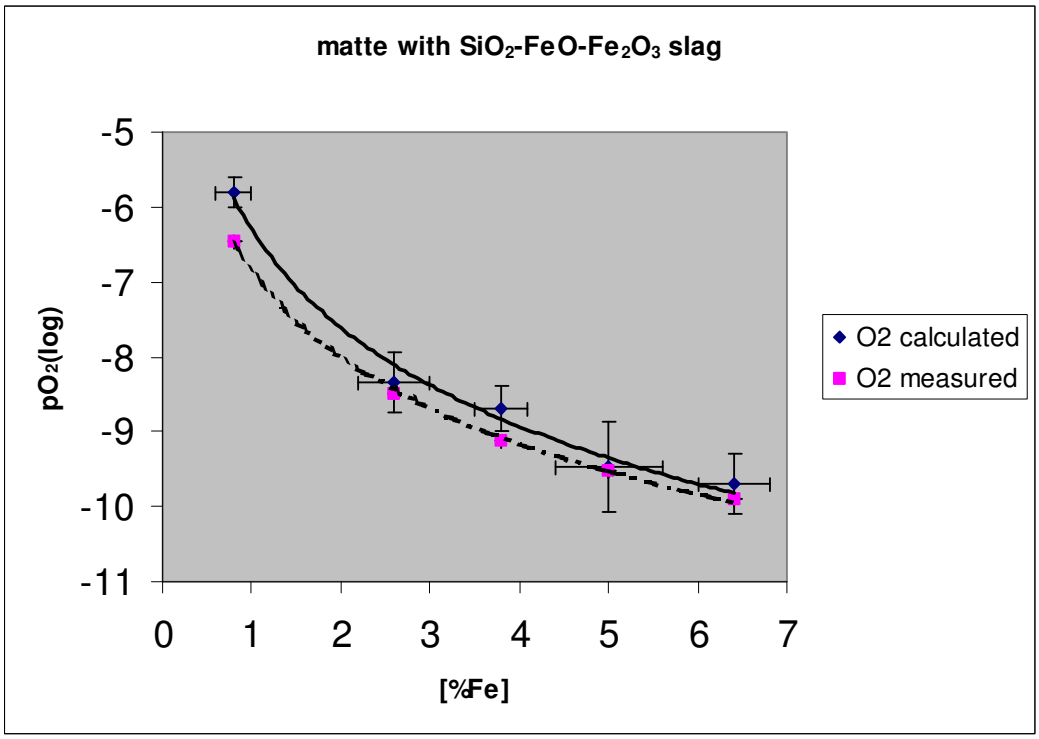

Figure 4-3. Evolution of iron content vs oxygen pressure (FeO/Fe_2O_3 slag)

CHAPTER V.

DISCUSSION OF RESULTS

In this chapter, the results obtained in the previous section (experimental tests) are discussed. The main focus is on the behaviour of oxygen and iron in Fe-Cu-Ni-S matte with two different slag compositions. The first part gives an overview of the results obtained with zirconia probes using Fe-FeO reference electrode. The second part presents the results obtained with the electron probe microanalyser CAMECA SX 100.

V.1. The behaviour of oxygen

The experimental study involved the investigation of the behaviour of oxygen activity for Fe-Cu-Ni-S matte in contact with fayalite slag, as a function of iron content in matte.

1. Figure 4-2 shows the results of the study (values are given in tables B-5 in appendix B). The results plotted on the diagram show the trend of decreasing oxygen activity with increasing matte iron for both results measured. Measurements A differ from measurements B by the sample mass analysed for each test. A high sensitivity is noticed in the average range between 3 and 1 % iron in the matte for both measurements. The different curve shapes are due to the different sample mass, which was larger for series B. The sample mass has an impact on the oxygen activity: with a larger matte volume the measured values approach the predicted values. In series A, the gap between the calculated and measured oxygen partial pressures was much wider. This likely reflects experimental difficulties when working with small samples, rather than any fundamental effect.

This might be due to the better circulation of oxygen between the matte and slag in a bigger volume than smaller one, or simply better contact with the probe by the two phases.
The results obtained with FeO-SiO_2 slag (fig. 4.2) and FeO-SiO_2-Fe_2O_3 slag (fig 4.3) show a similar trend of decreasing oxygen concentrations with increasing iron in the matte. Results for FeO-SiO_2-Fe_2O_3 slags were closer to the expected values compare with those for FeO-SiO_2 slags. This can be because the presence of trivalent iron oxide serves as a better buffer for the

oxygen content of the matte. The results for the FeO-SiO_2-Fe_2O_3 are expected to be more representative of actual practical measurements, since converter slags do contain ferric ions.

V.2. Matte analyses.

V.2.1. Tables

All results are tabulated in appendix-H.

V.2.2. Images

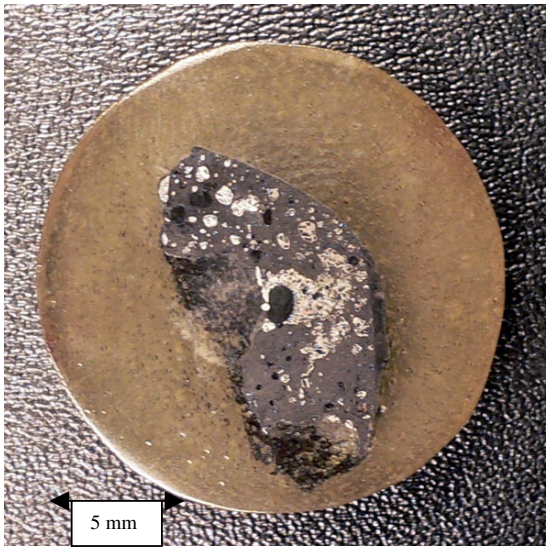

Figure 5-1. Picture of a solidified sample containing sulphide and oxide phases.

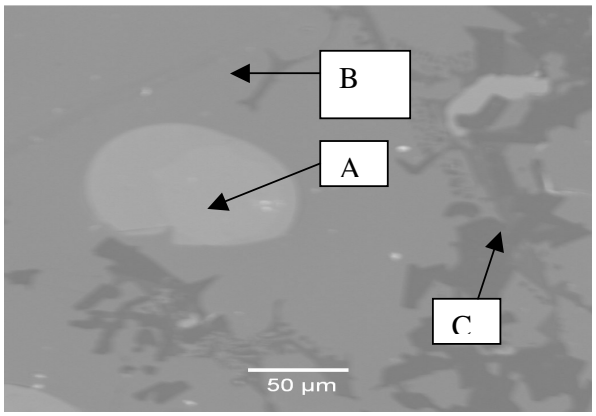

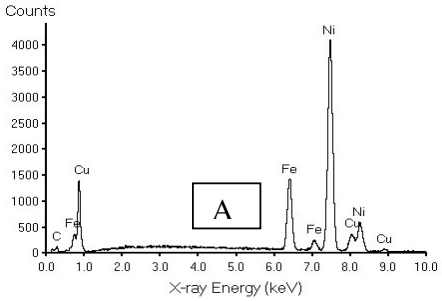

Element	k-ratio (calc.)	ZAF	Atom %	Element Wt %	Wt % Err. (3-Sigma)
Fe-K	0.698	0.97	68.8	67.5	+/- 3.0
Ni-K	0.263	1.04	26.5	27.3	+/- 3.7
Cu-L	0.012	4.38	4.7	5.2	+/- 1.8
S -K	0.000	1.17	0.0	0.0	+/- 0.0
Total			100.0	100.0	

FeNiCu alloy

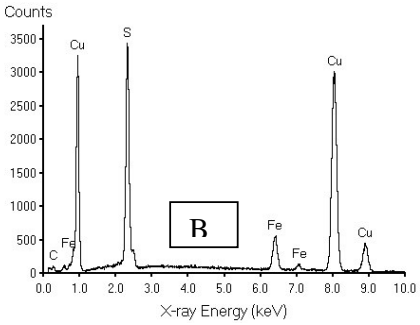

Element	k-ratio (calc.)	ZAF	Atom %	Element Wt %	Wt % Err. (3-Sigma)
Fe-K	0.007	0.91	0.6	0.6	+/- 0.5
Ni-K	0.005	1.01	0.4	0.5	+/- 0.8
Cu-L	0.630	1.17	59.2	73.8	+/- 3.3
S -K	0.212	1.19	39.9	25.1	+/- 0.6
Total			100.0	100.0	

Cu_2S

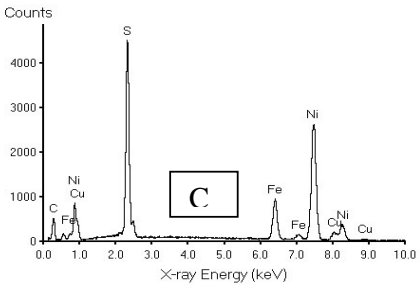

Element	k-ratio (calc.)	ZAF	Atom %	Element Wt %	Wt % Err. (3-Sigma)
Ni-K	0.670	1.05	57.3	70.0	+/- 1.9
Cu-K	0.021	1.09	1.7	2.3	+/- 0.6
S -K	0.159	1.69	40.3	26.9	+/- 0.7
Fe-K	0.009	0.89	0.7	0.8	+/- 0.3
Total			100.0	100.0	

Ni_3S_2

Figure 5.2. Microstructure, EDX and analyses of phases matte in 6.4wt% Fe, 22.8wt%Cu, 48.9wt%Ni and 21.8wt%S

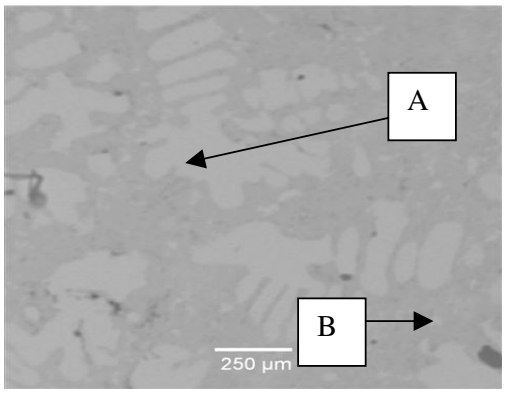

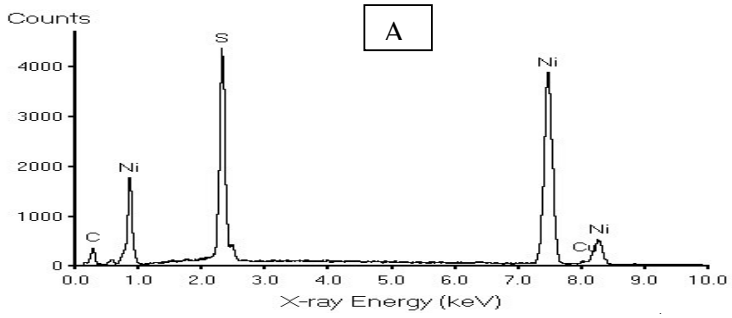

Fe-K	0.004	0.87	0.3	0.4	+/- 0.2
Ni-K	0.690	1.04	59.3	71.8	+/- 1.5
Cu-K	0.023	1.09	1.9	2.5	+/- 0.9
Total			100.0	100.0	

Ni_3S_2

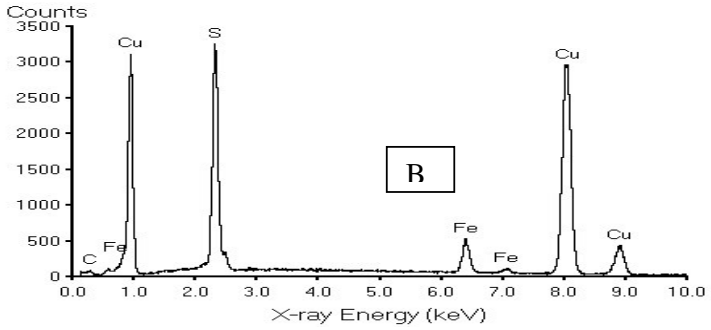

Element	k-ratio (calc.)	ZAF	Atom %	Element Wt %	Wt % Err. (3-Sigma)
S -K	0.129	1.68	35.3	21.7	+/- 0.5
Fe-K	0.058	0.89	4.8	5.2	+/- 0.5
Ni-K	0.001	1.00	0.1	0.1	+/- 0.2
Cu-K	0.691	1.06	59.8	73.0	+/- 1.7
Total			100.0	100.0	

Cu_2S

Figure 5.3. Microstructure, EDX and analyses of phases matte in 6.0wt% Fe, 22.5wt%Cu, 50.7wt%Ni and 21.5wt%S

V.5.3. Comments

As examples, micrographs of two mattes photographed with backscattered mode, EDX spectra and analyses are shown on figure 5-2 and figure 5-3. According to Viljoen[2001:88], the temperature and the bulk composition of a matte determine the path of crystallisation. For the matte represented on figure 5-2 and 5-3, FactSage 5.3.1 calculations between 1250°C and 400°C (temperature where all constituents are supposed solid) shows that the following phases occur depending on the temperature:

1. From 1250°C-750°C: matte
2. At 750°C: Beta_Ni_2S and alloy phases were formed + matte.
3. At 700°C: Cu_2S is formed + alloy stable phase + matte.
4. At 500°C: Ni_3S_2 is formed + Cu_2S + alloy stable phase + Beta_Ni_2S
5. At 450°C: pentlandite is formed + Ni_3S_2 +Cu_2S + alloy stable phase.

The matte (liquid) phase decreases and disappears at 600°C. The matte components split into different phases forming heterogeneous sulphide phases.

2. On figure 5-2 and 5-3, the presence of Cu_2S ,Ni_3S_2 and alloy phases is in line with FactSage predictions.

3. Pentlandite expected with FactSage was not present in figure 5-2 and 5-3, probably because cooling took place under non-equilibrium conditions.

However, in general, a good agreement was obtained between results measured and predicted with FactSage.

XRD results presented in Appendix-J show clearly the different major phases, which are in the matte and the slag after the cooling procedure. These major phases agree with those obtained using the SEM results. In the case of the matte, it is heazlewoodite (Ni_3S_2), digenite (Cu_2S) and for the slag, it is fayalite (Fe_2SiO_4) and tridymite (SiO_2).

V.3. Comparison with other investigators.

The relationship between pO_2 and mass% Fe in matte obtained in this thesis seems to be in agreement with the investigation done by Font and *al* [FONT, 1999:16]. They presented a contribution to understanding oxygen blowing of the nickel-copper-iron matte, the phase

equilibrium and the distribution of minor elements such as arsenic and bismuth between the iron-silicate base slag saturated with silica and the Ni_3S_2-Cu_2S-FeS matte with a Ni: Cu molar ratio of 1. While the initial conditions were different for the two studies, similar conclusions have been found:

Different matte grades were used in the two investigations, different temperatures (1573K with Font and *al* and 1523K in this thesis), different gas composition controlling the system (SO_2 with Font and *al*, SO_2, CO_2, CO or Ar with this thesis), different crucibles (magnesia crucible with Font and *al*, silica in this thesis). However, a common decrease of iron content with an increase of oxygen content has been noticed. In Font et *al* investigation, the iron range was from 70mass% Fe in matte to 0mass% Fe in matte, whereas in this thesis the iron range was from 8mass% Fe in matte to 1mass% Fe in matte.

Gisby and *al* [GISBY and al, 2002:26] found the same decreasing trend of iron content for increasing oxygen activity in a general slag-matte-gas system.

CHAPTER VI
SUMMARY AND CONCLUSIONS

The oxygen potential established by contact between Fe-Cu-Ni-S matte and FeO_x-SiO_2 (saturation) slag at 1250°C was investigated. The predicted partial pressure of oxygen varied from 1.53 x 10^{-8} atm to 2.65 x 10^{-7} atm for matte. The working temperature was 1250°C, the average temperature used in industry.

The gas composition did not affect the results, therefore the CO-CO_2-SO_2 gas mixture was replaced by Ar for most of the tests. Mattes were sampled using a silica tube, after flushing the furnace with argon. Iron analysis was obtained through the scanning electrode microscope SEM and the electron probe microanalyser. XRD results have been used to verify experiments results. The oxygen partial pressure was calculated and compared with the expected values and it was found to have the same trend for both values.

Two different reference electrodes had been tested. With a Cr/Cr_2O_3 reference, the electromotive force obtained was unstable. Therefore, as alternative a Fe/FeO reference electrode was used showing a stable plateau of EMF for all the results obtained in the laboratory.

Visual examination of the samples after test showed a mixture of different phases containing sulphides, oxides, and alloy.

The oxygen potential was found to increase with decreasing iron content in the matte.

It may be concluded that

- Oxygen is sensitive to iron content below 4% iron content in matte.
- the zirconia probes containing Fe/FeO reference electrode was the better device for oxygen measurements compare with a Cr/Cr_2O_3 reference electrode.
- Gas composition does not affect oxygen activity for measurements performed here.

Zirconia probes can be used to determine the oxygen partial pressure within the furnace at working temperature, to track the iron content in the matte.

REFERENCES

1. BISWAS, A.K. & DAVENPORT W.G. 1980. *Extractive metallurgy of copper*, second edition, Pergamon Press.

2. BRUWER J.S., 1996, *Experimental investigation of the phase relations in the system Cu-Ni-S in the temperature ranges 1200℃ to 1700℃*, MSc thesis, University of Pretoria.

3. CELMER, R.S. 1987. *The distribution of minor elements in the nickel matte smelting*, PhD thesis, University of Toronto.

4. CHEN X.J., KHOR K.A., CHAN S.H. and YU L.G. 2003. *Preparation yttria-stabilized zirconia electrolyte by spark-plasma sintering,* Materials Science and Engineering A341, pp 43-48.

5. COCOCCIONI M., CORSO A., and GIRONCOLI S. 2003. *Structural, electronic, and magnetic properties of Fe_2SiO_4 fayalite: comparison of LDA and GGA results,* Physical review B67, and pp 0941061-7.

6. COLE S. and FERRON C.J. 2002. *A review of the beneficiation and extractive metallurgy of the Platinum-Group Elements, highlighting recent process innovations*, Canadian Institute of Mining, Metallurgy and Petroleum, Montreal, L.J. Cabri(ed.), special volume 54, The Geology, Geochemistry, Mineralogy and Mineral Beneficiation of PGE, pp 811-844.

7. CRAMER, L.A., October 2001. *The extractive metallurgy of South Africa's platinum ores*, JOM, pp 14-18.

8. DARKEN, L.S. & GURRY R.W. 1946, *Iron-oxygen equilibria involving liquid oxide*, Contribution to the research laboratory, volume 68, pp 798-816.

9. DAVENPORT W.G, KING M., SCHEILESINGER M. & BISWAS A.K. 2002, *Extractive metallurgy of copper,* Pergamon, 4th edition.

10. DE VILLIERS, J.P.R. & KLEYENSTUBER A.S.E. 1984, *The partitioning of chromium between sulphide and silicate melts at controlled partial pressures of oxygen and sulphur*, Mintek report.

11. DEGTEROV, S.A. & PELTON A.D. 1998, *A thermodynamic database for copper smelting and converting*, Metallurgical and Materials Transactions B, volume 30B, pp 661-669.

12. ELLIOT J.F. 1976. *Phase relationships in the pyrometallurgy of copper,* Metallurgical Transactions B, volume 7B, pp 17-33.

13. FLOYD J.M. 2000. *Research and development of Ausmelt technology,* The Brimacombe Memorial Symposium*,* Metallurgical Society of CIM, pp 173-191.

14. FONT J.M., HINO M. & ITAGAKI K., 1998. *Minor elements distribution between iron-silicate base slag and Ni_3S_2-FeS matte under high partial pressures of SO_2,* Materials Transactions, JIM, volume 39, pp 834-840.

15. FONT J.M., HINO M. & ITAGAKI K., 2000. *Phase equilibrium and minor-element distribution between Ni_3S_2-FeS matte and calcium ferrite slag under high partial pressures of SO_2*, Metallurgical and Materials Transactions B, volume 31B, pp 1231-1239.

16. FONT M., HINO M.,& ITAGAKI K., 1999. *Phase equilibrium and minor elements distribution between iron-silicate base slag and nickel-copper-iron matte at 1573K under high partial pressures of SO_2*, Materials Transactions, JIM, volume 40, number 1, pp 20-26

17. FONT, M., TAKEDA, Y.& ITAGAKI, K. 1998. *Phase equilibrium between iron-silicate base slag and nickel-iron matte at 1573K under high partial pressures of SO_2* , Materials Transactions, JIM, volume 39, number 6, pp 652-657

18. FREDRIKSSON P. and SUNDMAN BO. 2001. *A thermodynamic assessment of the Fe-Pt system.* Calphad, volume 25, No 4, pp 535-548.

19. FUKUYAMA H., DONALD J.R., and TOGURI J. 1997. *Wetting behaviour between fayalite-type slags and solid magnesia,* Journal of the American Ceramic Society volume 80, pp 2229-2236.

20. FUSHEN LI, YUHUA TANG & LIFEN LI. 1996. *Distribution of oxygen potential in ZrO_2-based solid electrolyte and selection of reference electrode of oxygen sensor*, Solid State Ionics volume 86-88, pp 1027-1031.

21. GASKELL D.R. 1981. *Introduction to metallurgical thermodynamics.* McGraw-Hill, pp 433-459.

22. GEORGALLI G.A., EKSTEEN J.J., and REUTER M.A. 2002. *An integrated thermochemical-systems approach to the prediction of matte composition dynamics in an Ausmelt nickel-copper matte converter,* Minerals Engineering volume 15, pp 908-917.

23. GELDENHUIS J.M.A. 1991. *Development of electrochemical sensing techniques for the determination of activity-composition relations in liquid alloys and slags at 1873K,* PhD thesis, University of Pretoria.

24. GELDENHUIS J.M.A., D. MILLER, B. VAN BEEK, J. NDLOVU, and K.T. HARA. 2004. *Development of alternative techniques for matte level measurements in sulphide smelting furnaces*, International Platinum Conference 'Platinum Adding Value', The South African Institute of Mining and Metallurgy, pp 25-35.

25. GELDENHUIS J.M.A and DIPPENAAR R.J. 1991. *A reassessment of the activity of chromium in the Fe-Cr-O system at 1873K,* Metallurgical Transactions B, volume 22B, pp 915-918.

26. GISBY J.A., DINSDALE A.T., BARTON-JONES I., GIBBON A. & TASKINEN P.A., 2002. *Predicting phase equilibria in oxide and sulphide systems*, The Minerals, Metals & Materials Society Annual Meeting, Seattle, pp 533-545

27. HELLWEGE K.H., MADELUNG O., 1985. *Numerical Data and Functional Relationships in Science and Technology*, Springer Londolt-Bornstein, volume 15, Metals: electronic transport phenomena, pp 48-63

28. HINO M., PAGADOR R.U. & ITAGAKI K., 1999. *Distribution of minor elements between saturated FeO_x-MgO-SiO_2 or FeO_x-CaO-MgO-SiO_2 slag and nickel alloy,* materials transactions, JIM, volume 40, pp 225-232.

29. HINO M., ROGHANI G. & ITAGAKI K., 1997. *Phase equilibrium and minor elements distribution between SiO_2-CaO-FeO_x-MgO slag and copper matte at 1573K under high partial pressures of SO_2*, Material Transactions, JIM, volume 38, pp 707-713.

30. ILUNGA M., 1996. Cours de metallurgy des metaux non-ferreux. Universite de Lubumbashi.

31. International Platinum Association. 2002. *Mining and production*. [Online]. Available http://www.platinuminfo.net/minpro.html

32. Internet .2005: *Title of web page*.
http://www.outokumpu.com/pages/Page_8086.aspx. Visited on 15 March 2005
www.angloplatinum.com. Visited on 15 March 2005

1. http://www.halwachs.de/pgmref.html. Visited on 15 March 2005

2. http://www.nationmaster.com/encyclopedia/Zirconia. Visited on 28 July 2005

33. IMANAKA N., OGURA A., KAMIKAWA M. and ADACHI G. 2001. *CO_2 gas sensor with the combination of tetravalent zirconium cation and divalent oxide anion conducting solids with water-insoluble oxycarbonate electrode*, Electrochemistry Communications volume 3, pp 451-454.

34. IWASE M., 1992. *Developments in zirconia sensors during the 1980's-laboratory and in-plant applications in iron and steelmaking,* proceedings of the 1st International Chromium Steel and Alloys Congress, The South African Institute of Mining and Metallurgy, volume 2, pp 49-61.

35. IWASE M., MCLEAN A, KATOGI K., KIKUCHI Y. and WAKIMOTO K. 2004. *Evaluation and control of iron and steelmaking slags through electrochemical FeO sensors,* VII International Conference on Molten Slags Fluxes and Salts, The South African Institute of Mining and Metallurgy, pp 787-796

36. IWASE M., YAMANDA N, NISHIDA K and ICHISE E. 1984. *A thermodynamic study of $CaO+CaF_2+Fe_xO$ fluxes used for the external dephosphorisation of hot metal,* ISS Transactions, volume 4, pp 47-53.

37. IWASE M., YAMANDA N, NISHIDA K and ICHISE E. 1984. *A rapid determination of the activities in $CaO-Fe_xO$ liquid slags by disposable electrochemical oxygen probes,* ISS Transactions, volume 4, pp 69-75.

38. JANKE D. 1977a. *Physico-chemical properties of solid oxide electrolytes at steelmaking temperatures,* Arch. Eisenhüttenwes. Volume 48, pp 255-260.

39. JANKE D. 1977b. *Thermal and mechanical properties of solid oxide electrolytes at steelmaking temperatures,* Arch. Eisenhüttenwes. Volume 48, pp 467-474.

40. JANKE D. 1977c. *Electrical properties of solid oxide electrolytes at steelmaking temperatures,* Arch. Eisenhüttenwes. Volume 48, pp 311-318.

41. JANKE D. 1982. *Oxygen probes based on calcia-doped hafnia or calcium zirconate for use in metallic melts,* Metallurgical Transactions B, volume 13B, pp 227-235.

42. JONES, R.T. 1999. *Platinum smelting in South Africa*. South Africa Journal of Science volume 95, pp 525-534.

43. KONGOLI F., DESSUREAULT Y. and PELTON A.D. 1998. *Thermodynamic modelling of liquid Fe-Ni-Cu-Co-S mattes,* Metallurgical and Materials Transactions B, volume 29B, pp 591-601

44. KYLLO A.K. and RICHARDS G.G. 1990. *A mathematical model of the nickel converter: Part I. Model development and verification,* Metallurgical Transactions B, volume 22B, pp 153-161.

45. KURCHANIA R. and KALE M. 2001. *Measurement of oxygen potentials in Ag-Pb system employing oxygen sensor*, Metallurgical and Materials Transactions B, volume 32B, pp 417-421.

46. LAIURA G.H., WATANABE K., and YAZAWA A. 1980. *The behaviour of lead in silica-saturated, copper smelting systems,* Canadian Metallurgical Quarterly, volume 19, pp 191-200.

47. LEVIN E., ROBBINS C. and McMURDIE H. 1964. *Phase diagrams for ceramists*, The American Ceramic Society, Inc, p 59.

48. LIAO L. and FRUEHAN R.J. 1990. *Thermodynamics of Ti, Al and inclusion formation in stainless steel and nickel alloys,* ISS Transactions, volume 11, pp 105-111.

49. MACKEY P.J. 1982. *The physical chemistry of copper smelting slags-a review,* Canadian Metallurgical Quarterly, volume 21, No.3, pp 221-260.

50. MAJUMDAR R., SARKAR P., RAY U., and MUKHOPADHYAY. 1999. *Secondary catalytic reactions during thermal decomposition of oxalates of zinc, nickel and iron (II),* Thermochemica Acta 335, pp 43-53.

51. MARTIN P.L., PHAM A.Q. and GLASS R.S.2003. *Effect of Cr_2O_3 electrode morphology on the nitric oxide response of a stabilised zirconia sensor*, Sensor and Actuators B 96, pp 53-60.

52. MATTHEY J., 2005.[Online]. http://www.platinum.matthey.com/production/africa.php. Visited on 14 March 2005.

53. MERKLE R.K.W. and McKENZE A.D. 2002. *The mining and beneficiation of South African PGE ores-an overview,* The Geology, Geochemistry, Mineralogy and Mineral Beneficiation of Platinum-Group Elements, Edited by L.J. Cabri , Canadian Institute of Mining, Metallurgy and Petroleum, special volume 54, pp 793-809.

54. MERUVA R.K. and MEYERHOFF M.E. 1997. *Potentiometric oxygen sensor based on mixed potential of cobalt wire electrode,* Analytica Chemica Acta volume 341, pp 187-194.

55. MORTIMER A.G., and REED G.P. 1995. *Development of a robust electrochemical oxygen sensor,* Sensors and Actuators B volume 24-25, pp 328-335.

56. MOSTERT J.C. & ROBERTS P.N. 1973. *Electric smelting at Rustenberg Platinum Mines Limited of nickel-copper concentrates containing platinum-group metals.* Journal of the South African Institute of mining and Metallurgy, pp 290-299.

57. NAGAMORI M., 1974. *Sulfidic and oxidic dissolution of copper in fayalite slag from low-grade matte*, Metallurgical Transactions, volume 5, pp 531-538

58. NAGAMORI M. and MACKEY P.J. 1978. *Thermodynamics of copper matte converting: Part I. Fundamentals of the Noranda process.* Metallurgical Transactions B, volume 9B, pp 255-265.

59. NAGAMORI M., ERRINGTON W.J., MACKEY P.J. and POGGI D., 1994. *Thermodynamic simulation model of the Isasmelt process for copper matte*, Metallurgical and Materials Transactions B, vol 25B, pp 839-853.

60. NALDRETT A.J. 1969. *A portion of the system Fe-S-O between 900 and 1080°C and its application to sulfide ore magmas,* Journal of Petrology, volume 10, part 2, pp 171-201.

61. NALLICHERI, N.V. 1988. *Behaviour of oxygen and sulphur in mattes containing nickel*, MSc thesis, M.I.T.

62. NAUDE, N. 2003. Ferro-alloys technology IV. Course. Tshwane university of Technology.

63. NELL J. 2004. *Melting of platinum group metal concentrates in South Africa,* The Journal of the South African Institute of mining and Metallurgy, volume 104, pp 423-428

64. NELSON G.O. 1992. *Gas mixtures: preparation and control,* Lewis Publishers, pp 26-235

65. NEWMAN, M.A., 1972. *Platinum,* Transactions of the Institute of Mining and Metallurgy, pp A52-A68.

66. PENGFU TAN & NEUSCHUTZ D., 2001. *A thermodynamic model of nickel smelting and direct high-grade nickel matte smelting process: part I. Model development and validation*, Metallurgical and Materials Transactions B, volume 32, pp 341-351.

67. PERT E., CARMEL Y., BIONOMIC A., OLORUNYOLEMI T., GERSHON D., CALAME J., LLOYD I.K., and WILSON O.C. Jr. 1984. *Temperature measurements*

during microwave processing: the significance of thermocouple effects. Journal of the American Ceramic Society. Pp 1981-1986

68. PISTORIUS, PC. 2003. *Pyrometallurgical Process Analysis.* Pretoria: University of Pretoria.

69. PREIDEL W., RAO J.R., MUND K, SCHUNCK O., and DAVID E. 1995. *A new principle for an electrochemical oxygen sensor,* Sensors and Actuators B volume 28, pp 71-74.

70. RAO, YK.1985. *Stoichiometry and thermodynamics of metallurgical processes,* Cambridge University Press, pp 692-820.

71. REDDY R.G. and BLANDER M. 1987. *Modeling of sulfide capacities of silicate melts,* Metallurgical Transactions B, volume 18B, pp 591-596.

72. *Refining of platinum group metals / principle flow sheet.* [Online]. Available www.halwachs.de/pgm-**refining**.htm

73. ROSENQVIST T., 1978. *Phase equilibria in the pyrometallurgy of sulphide ores*, Metallurgical Transactions B, volume 9B, pp 337-351

74. RUPARD R.G. and GALLAGHER P.K. 1996. *The thermal decomposition of coprecipitates and physical mixtures of magnesium-iron oxalates,* Thermochimica Acta 272, pp 11-26.

75. SOLTANIEH M., TOGURI J.M., SRIDHAR R. & TAKASU T., 2000. *The thermodynamics of the Ni-Co-S ternary system,* Metallurgical and Materials Transactions B, volume 31B, pp 121-128.

76. SOMSIRI C. and GASKELL D.R.1995. *The activities of sulphide and oxide components and solubility of oxygen-iron-sulphur-oxygen mattes at 1300°C*, Metallurgical and Materials Transactions B, volume 26B, pp 1157-1164.

77. SOTIROPOULOS S. and WALLGREN K. 1999. *Solid-state microelectrode oxygen sensors.* Analytica Chemica Acta volume 388, pp 51-62

78. STOFKO M., SCHMIELD and ROSENQUIST T. 1974. *Thermodynamics of iron-sulphur-oxygen melts at 1200°C*, Scandinavian Journal of Metallurgy volume 3, pp 113-118.

79. TASKINEN P., 1984. *Thermodynamics of liquid copper alloys at 1065-1450°C*, Scandinavian Journal of Metallurgy, volume 13, pp 75-82.

80. TASKINEN P., SEPPALA K., LAULUMAA J. & POIJARVI J., 2001. *Oxygen pressure in the Outokumpu flash smelting furnace-part 1 and 2: copper flash smelting settler*, Transactions of the Institution of Mining and Metallurgy, volume 110, pp C94-C108.

81. TURKDOGAN E.T., 1980. *Physical chemistry of high temperature technology,* Academic Press, pp 5-24.

82. UECKERMANN, H. 2002. *Partitioning of platinum-group elements between metal and sulphide melt in the Cu-S and Ni-S systems*, MSc thesis, University of Pretoria.

83. ULMER, G.N. 1971. *Research techniques for high pressure and high temperature*. Springer-Verlag.

84. VAN WIJNGAARDEN M.J.U.T., GELDENHUIS J.M.A. & DIPPENAAR R.J., 1988, *Determination of the electrical characteristics of a commercially available yttria-stabilized zirconia electrolyte used in the high-temperature thermodynamic studies,* Journal of South African Institute of Mining and Metallurgy, volume 88, pp 265-271.

85. VAN WIJNGAARDEN, M.J.U.T. & DIPEENAAR, R.J. 1986. *The use of zirconia-based solid electrolytes for the rapid determination of iron oxide activities in iron and steel making slags*, journal of the South Africa institute of mining and metallurgy, November, volume 86, pp 443-453.

86. VAN WIJNGAARDEN, M.J.U.T., DIPPENAAR R.J. & VAN DEN HEEVER P.M.1987. *An evaluation of the electrochemical oxygen probes used in steelmaking*, journal of the South Africa institute of mining and metallurgy, September, volume 87, pp 269-278.

87. VAN WIJNGAARDEN, M.J.U.T. & DIPPENAAR, R.J. 1988. *The activity of iron oxide in (CaO+CaF_2+ SiO_2+ Fe_xO) slags,* Iron and Steelmaker, volume15, no. 2, pp 49-55.

88. VAN WIJNGAARDEN, M.J.U.T. & DIPPENAAR, R.J. 1988. *A thermodynamic study of lime-based slags used for the external refining of hot metal,* 71st Steelmaking Conference Proceedings, volume 71, pp 395-403.

89. VILJOEN, W.2001. *Phase relations in the system Cu-Fe-Ni-S and their application to the slow cooling of PGE matte*, PhD thesis, University of Pretoria.

90. WRIGHT S., JAHANSHAHI S. and SUN S.2004. *Activities of Cu, Fe and Ni in Cu-Fe-Ni-S mattes,* VII International Conference on Molten Slags Fluxes and Salts, The South African Institute of Mining and Metallurgy, pp 277-284.

91. XIA C. and *al.* 2003. *Composite cathode based on yttria stabilized bismuth oxide for low-temperature solid oxide fuel cells,* Applied Physics Letters, American Institute of Physics, volume 82, pp 901-903.

92. YANNOPOULOS, JC.1976. *Extractive metallurgy of copper*, The Metallurgical Society of AIME, volume 1.

93. YAZAWA A. 1974. *Thermodynamic considerations of copper smelting,* Canadian Metallurgical Quarterly, volume 13 number 3, pp 443-453.

APPENDIX - A

CALCULATION OF INLET GAS COMPOSITION

The inlet gas composition is a mixture of CO,CO_2 and SO_2 in different proportions to obtain the required oxygen and sulphur potentials a t 1523K .

The species considered are CO,CO_2 ,SO_2 , S_2 ,O_2. The reactions and equilibrium constants at 1523K are listed below:

$$CO_2 = CO + 0.5\ O_2$$

$$0.5S_2 + O_2 = SO_2$$

The equilibrium constants were calculated with FACTSAGE.

Another reaction considered in the calculation is

$$Fe + 0.5\ O_2 = FeO$$

due to the influence of iron in the system.

$$Fe_l + 0.5\ O_2 = FeO_l \qquad k_1 = 4.95\text{x}10^{5} \qquad (1)$$

$$CO_2 = CO + 0.5\ O_2 \qquad k_2 = 7.23\text{x}10^{-6} \qquad (2)$$

$$0.5\ S_2 + O_2 = SO_2 \qquad k_3 = 6.9\text{x}10^{9} \qquad (3)$$

From equations (1) to (3) written above, we write:

$$k_1 = \frac{a_{FeO}}{a_{Fe}.p_{O_2}^{0.5}} \qquad (4)$$

$$k_2 = \frac{p_{CO}.p_{O_2}^{0.5}}{p_{CO_2}} \qquad (5)$$

$$k_3 = \frac{p_{SO_2}}{p_{S_2}^{0.5}.p_{O_2}} \qquad (6)$$

$$p_T = p_{S2} + p_{CO} + p_{CO2} + p_{O2} + p_{SO2} \qquad (7)$$

$$\text{If} \quad x = \frac{p_{CO_2}}{p_{CO}} \tag{8}$$

Combining (5) and (8),

$$x = \frac{p_{O_2}^{0.5}}{k_2} \tag{9}$$

From equation (6),

$$p_{SO_2} = (k_3).p_{O_2}.(p_{S_2})^{0.5} \tag{10}$$

Results

a_{FeO}	a_{Fe}	p_{O2}	p_{CO}/p_{CO2}	a_s	$\mathbf{p_{SO2}}$	$\mathbf{p_{CO2}}$	$\mathbf{p_{CO}}$	Total gas	$\%SO_2$	$\%CO_2$	%CO
0.37	6.05E-03	1.53E-08	5.85E-02	<<0	0.44	0.45	0.02	0.91	48.07	49.24	2.68
0.37	5.55E-03	1.81E-08	5.37E-02	<<0	0.51	0.37	0.02	0.90	56.55	41.39	2.07
0.37	5.03E-03	2.21E-08	4.87E-02	<<0	0.61	0.27	0.01	0.90	68.21	30.42	1.37
0.37	4.49E-03	2.78E-08	4.34E-02	<<0	0.76	0.13	0.01	0.90	84.99	14.43	0.58

The total pressure used in the calculation is 0.86 atmospheres, average pressure in Pretoria and a_{Fe} was obtained with FactSage calculation.

APPENDIX-B.

MATTE, SLAG AND ALLOY COMPOSITION

B.1. Matte, slag and gas starting composition

A total of four series were conducted, comprising of 21 experiments in the following conditions:

T: 1523 K

Flowing gas: CO,CO_2,SO_2

Table B-1 presents the starting charge composition of the matte and slag used in the first series of experiments. A total of four sub-series were conducted comprising three experiments for each sub-series.

Matte	Wt%Fe	Wt%Cu	Wt%Ni	Wt%S
Test 1	8.8	19.9	49.7	21.2
Test 2	7.6	21.2	54.8	16.4
Test 3	5.3	27.3	50.4	17.0
Test 4	4.0	23.9	50.3	21.8

Slag	Wt%Fe	Wt%Si	Wt%O
All	54.8	16.3	28.9

Table B-1. Starting charge composition for different experimental series.

Table B-2 presents the expected oxygen pressures for the various experimental tests. The oxygen activity increases for each test while the sulphur activity decrease. These results have been obtained using the FACTSAGE and the quasichemical calculation [PISTORIUS]. The log P_{O2} varied from –7.82 to –7.56 and the log P_{S2} varied from –2.38 to –2.40.

Test	PS_2(atm)	PO_2(atm)
1	$4.15x10^{-3}$	$1.53x10^{-8}$
2	$4.09x10^{-3}$	$1.81x10^{-8}$
3	$4.04x10^{-3}$	$2.21x10^{-8}$
4	$3.98x10^{-3}$	$2.78x10^{-8}$

Table B-2.Oxygen and Sulphur pressures for the various experimental series.

Table B-3 shows the inlet gas composition required to yield the desired oxygen and sulphur pressures for different experiments at 1250°C.

Log pO_2	p SO_2	p CO_2	p CO
-7.82	0.44	0.45	0.02
-7.74	0.51	0.37	0.02
-7.66	0.51	0.27	0.01
-7.56	0.76	0.13	0.01

Table B-3. Inlet gas composition

Table B-3' below presents the matte composition obtained with two different gas mixture composition. Composition with * was obtained with Ar gas .

		*		*		*		*
	Wt% Fe		**Wt% Cu**		**Wt% Ni**		**Wt% S**	
	8.3	8.3	25.1	24.9	46.1	46.2	20.4	20.6
	8.2	8.7	29.4	24.9	42.6	44.8	20	21.5
	8.8	8.3	24.8	28.9	45.1	42.4	21.4	20.3
Average	8.4	8.4	26.4	26.2	44.6	44.5	20.6	20.8
Standard deviation	0.3	0.2	2.6	2.3	1.8	1.9	0.7	0.6
95% confidence interval	0.8	0.7	6.4	6.1	4.5	4.6	1.8	1.7

Table B-3'. Results of composition obtained with different gas composition

B.2.Tests run using Cr/Cr_2O_3 reference electrode.

Table B-4 presents the results of the composition before and after different tests. The samples were analysed especially for iron content in the different phases. The scanning electronic microscope was used in that purpose, in SE mode.

	Test 1			
	Wt%Fe	**Wt%Cu**	**Wt%Ni**	**Wt%S**
	8.3	25.1	46.1	20.4
	8.2	29.4	42.6	20
	8.8	24.8	45.1	21.4
average	8.4	26.4	44.6	20.6
Standard Deviation	0.3	2.6	1.8	0.7
95%confidence interval	0.8	6.4	4.5	1.8

	Test 2			
	Wt%Fe	**Wt%Cu**	**Wt%Ni**	**Wt%S**
	3.9	27.3	50.4	18.4
	4.2	24.1	51	20.2
	4.6	25.3	47.5	23.4
Average	4.2	25.6	49.6	20.7
Standard Deviation	0.4	1.6	1.9	2.5
95%confidence interval	0.9	4.0	4.6	6.3

	Test 3			
	Wt%Fe	**Wt%Cu**	**Wt%Ni**	**Wt%S**
	2.2	25.5	54.4	16.8
	2.2	28.5	52.5	16.8
	2.2	28.5	54.4	14.7
average	2.2	27.5	53.8	16.1
Standard Deviation	0.0	1.7	1.1	1.2
95%confidence interval	0.0	4.3	2.7	3.0

	Test 4			
	Wt%Fe	**Wt%Cu**	**Wt%Ni**	**Wt%S**
	1.3	26.7	51.7	20.4
	1.2	22.6	54.8	21.1
	1.3	24.7	53.2	20.8
average	1.3	24.7	53.2	20.8
Standard Deviation	0.1	2.1	1.6	0.4
95%confidence interval	0.1	5.1	3.9	0.9

Cr_2O_3 slag

	Test 1	
	Wt%Fe	**Wt%Si**
	77	23
	79.9	20.1
	78.3	21.7
average	78.4	21.6
Standard Deviation	1.5	1.5
95%confidence interval	3.6	3.6

	Test 2	
	Wt%Fe	**Wt%Si**
	78.6	21.4
	81.9	18.9
	80.5	19.5
average	80.3	19.9
Standard Deviation	1.7	1.3
95%confidence interval	4.1	3.2

	Test 3	
	Wt%Fe	**Wt%Si**
	84.9	15.1
	84.4	15.6
	83.3	16.7
average	84.2	15.8
Standard Deviation	0.8	0.8
95%confidence interval	2.0	2.0

	Test 4	
	Wt%Fe	**Wt%Si**
	80.9	19.1
	81.6	18.4
	79.6	20.4
average	80.7	19.3
standevia	1.0	1.0
confidence	2.5	2.5

Table B-4. Results of different experimental tests.

B.3. Tests run with Fe/FeO reference electrode

B.3.1. FeO-SiO_2 slag

The results show below has been proceed in an argon atmosphere in the following conditions:

T: 1523 K

Flowing gas: N_2

The table B-5 shows the results obtained

	Test 1			
	Wt% Fe	**Wt% Cu**	**Wt% Ni**	**Wt% S**
	7	21.2	48.5	22.9
	7.6	24.1	45.9	22.5
	5	25.1	47.4	22.1
	7.7	24	50.9	17.3
	5.5	20	52.1	22.4
	5.6	21.2	52.4	20.8
	6.3	24.1	44.9	24.7
average	6.4	22.8	48.9	21.8
Standard Deviation	1.1	2.0	3.0	2.3
95%confidence interval	1.0	1.8	2.8	2.1

	Test 2			
	Wt% Fe	**Wt% Cu**	**Wt% Ni**	**Wt% S**
	7	22.1	50.4	21.3
	6.1	22.5	50.8	21.3
	4.5	20	50.4	25.3
	8	19.6	49.6	22.9
	6.3	24.2	48.2	21.4
	5.4	25.8	50.3	18.5
	5.5	23.5	50.3	20.6
	4.9	18.6	55.2	20.3
average	6.0	22.5	50.7	21.5
Standard Deviation	1.1	2.5	2.0	2.0
95%confidence interval	1.0	2.1	1.7	1.7

	Test 3			
	Wt% Fe	**Wt% Cu**	**Wt% Ni**	**Wt% S**
	4.2	24.1	51	20.2
	2.1	19.9	54.6	23.3
	5.2	20.9	50.4	23.1
	4.8	22.9	53.1	19.2
	3	18.4	58.1	20.5
	3.8	23.3	53.1	19.8
	2.7	20.8	49.1	27.4
average	3.7	21.5	52.8	21.9
Standard Deviation	1.14	2.04	3.01	2.89
95%confidence interval	1.05	1.89	2.78	2.68

	Test 4			
	Wt% Fe	**Wt% Cu**	**Wt% Ni**	**Wt% S**
	2.4	22.6	54.8	20.3
	2.1	23.6	54.4	19.9
	3.5	25.3	50.1	21.1
	2.4	19	49.5	29.1
	3.6	23.3	52.1	20.9
	2.7	26.3	46.5	24.4
	2.8	19.5	56.6	21.1
average	2.8	22.8	52.0	22.4
Standard Deviation	0.6	2.7	3.5	3.3
95%confidence interval	0.5	2.5	3.3	3.0

	Test 5			
	Wt% Fe	**Wt% Cu**	**Wt% Ni**	**Wt% S**
	2.1	27.8	50.4	19.7
	2	27.2	50.8	20.1
	2.1	22.6	51.7	23.6
	2.4	23.2	51	23.4
	2.4	19.7	56.1	21.7
	2.3	20.4	53	24.3
average	2.2	23.5	52.2	22.1
Standard Deviation	0.2	3.4	2.1	1.9
95%confidence interval	0.2	3.5	2.2	2.0

	Test 6			
	Wt% Fe	**Wt% Cu**	**Wt% Ni**	**Wt% S**
	0.7	20.8	53	25.5
	0.9	23.7	50.7	24.7
	0.5	23.7	51.6	24.2
	0.9	23.1	49.5	26.5
	0.4	18.4	50.1	31.1
	0.7	27.7	51.5	20.1
average	0.7	22.9	51.1	25.4
Standard Deviation	0.2	3.1	1.2	3.6
95%confidence interval	0.2	3.3	1.3	3.7

	FeO slag *Test 1*	
	Wt%Fe	**Wt%Si**
	81.6	18.4
	82.1	17.9
	78.8	21.2
average	80.8	19.2
Standard Deviation	1.8	1.8
95%confidence interval	4.4	4.4

	Test 2	
	Wt%Fe	**Wt%Si**
	81.4	18.6
	79.3	20.7
	79.6	20.4
average	80.1	19.9
Standard Deviation	1.1	1.1
95%confidence interval	2.8	2.8

	Test 3	
	Wt%Fe	**Wt%Si**
	80.2	19.8
	80.4	19.6
	80.1	19.9
average	80.2	19.8
Standard Deviation	0.2	0.2
95%confidence interval	0.4	0.4

	Test 4	
	Wt%Fe	**Wt%Si**
	82	18
	80.6	19.4
	80.5	19.5
average	81.0	19.0
Standard Deviation	0.8	0.8
95%confidence interval	2.1	2.1

	Test 5	
	Wt%Fe	**Wt%Si**
	80.4	19.6
	82.5	17.5
	81.1	18.9
average	81.3	18.7
Standard Deviation	1.1	1.1
95%confidence interval	2.7	2.7

	Test 6	
	Wt%Fe	**Wt%Si**
	80.6	19.4
	81.2	18.8
	78.7	21.3
average	80.2	19.8
Standard Deviation	1.3	1.3
95%confidence interval	3.2	3.2

Table B-5. Composition of different experimental tests (FeO/SiO_2 slag).

All the EMF values shown below are EMF_{cell} .

$E_{cell} = E_{meas} - E_{Fe\text{-}Pt}$

$= E_{meas} - 0.017$ V

Test1		**Test 2**		**Test 3**	
EMF (mV)	**log pO2(atm)**	**EMF (mV)**	**log pO2(atm)**	**EMF (mV)**	**log pO2(atm)**
-161	-9.2	-181	-8.93	-184	-8.89
-154	-9.29	-177	-8.99	-187	-8.85
-151	-9.33	-176	-9.00	-189	-8.83
-148	-9.37	-174	-9.03	-194	-8.76

Test4		Test 5		Test 6	
EMF (mV)	log pO2(atm)	EMF (mV)	log pO2(atm)	EMF (mV)	log pO2(atm)
-218	-8.44	-226	-8.34	-229	-8.3
-212	-8.52	-220	-8.42	-226	-8.34
-211	-8.54	-216	-8.47	-221	-8.4
-208	-8.58	-214	-8.50	-218	-8.44

Table B-6. EMF results obtained with $FeO\text{-}SiO_2$ slag

B.3.2. $FeO\text{-}Fe_2O_3\text{-}SiO_2$ slag

The results show below has been proceed in an argon atmosphere in the following conditions:

T: 1523 K

Flowing gas: N_2

The table B-8 below shows the results of the experiments

	Test 1			
	Wt% Fe	Wt% Cu	Wt% Ni	Wt% S
	6.9	22.8	50.4	20
	5.6	25.1	50.4	18.9
	6.5	24.6	45.4	23.5
	5.6	25	45.4	24
	6.6	26.5	47.5	19.4
	6.8	22.6	51.5	19
	6.9	16.7	50.1	26.4
	6.6	26.5	47.9	19.1
Average	6.4	23.7	48.6	21.3
Standard Deviation	0.5	3.2	2.4	2.9
95%confidence interval	0.4	2.7	2.0	2.4

	Test 2			
	Wt% Fe	Wt% Cu	Wt% Ni	Wt% S
	5.4	28.3	45.7	20.7
	4.1	25.6	46.5	23.9
	5.5	26.6	47.6	20.6
	4.9	18.6	55.2	20.3
	4.9	23.1	50.6	21.3
	5.4	27.6	46.5	20.5
average	5.0	25.0	48.7	21.2
Standard Deviation	0.5	3.6	3.6	1.4
95%confidence interval	0.6	3.8	3.8	1.4

	Test 3			
	Wt% Fe	**Wt% Cu**	**Wt% Ni**	**Wt% S**
	3.8	18.2	55.1	22.9
	3.8	17.4	52.9	25.9
	4.2	18.6	52	25.2
	4.2	22.7	50.9	22.2
	4	27.3	47.2	21.5
	3.2	25.2	50.1	21.5
	3.5	27.6	47	21.9
average	3.8	22.4	50.7	23.0
Standard Deviation	0.4	4.4	3.0	1.8
95%confidence interval	0.3	4.1	2.7	1.7

	Test 4			
	Wt% Fe	**Wt% Cu**	**Wt% Ni**	**Wt% S**
	2.4	22.6	53.8	21.3
	2.9	22.6	51.8	22.7
	2.2	19.4	49.2	29.2
	2.4	19.9	56	21.7
	3.1	19.8	55.9	21.2
	2.6	25	50.8	21.8
average	2.6	21.6	52.9	23.0
Standard Deviation	0.3	2.2	2.8	3.1
95%confidence interval	0.4	2.3	2.9	3.2

	Test 5			
	Wt% Fe	**Wt% Cu**	**Wt% Ni**	**Wt% S**
	1.1	30.1	47	21.9
	0.5	26.7	46.1	26.7
	0.9	20	52.1	27
	0.5	16.3	52.8	30.4
	1	17.9	50.1	31
	0.7	31	48.2	20.1
	0.8	29.2	48.6	21.2
average	0.8	24.5	49.3	25.5
Standard Deviation	0.2	6.2	2.5	4.4
95%confidence interval	0.2	5.7	2.3	4.1

	Test 1	
	Wt%Fe	**Wt%Si**
	67.8	32.2
	64.8	35.2
	68.1	31.9
average	66.9	33.1
Standard Deviation	1.8	1.8
95%confidence interval	4.5	4.5

	Test 2	
	Wt%Fe	**Wt%Si**
	69.6	30.4
	68	32
	67.2	32.8
average	68.3	31.7
Standard Deviation	1.2	1.2
95%confidence interval	3.0	3.0

	Test 3	
	Wt%Fe	**Wt%Si**
	67	33
	66.2	33.8
	67.8	32.2
average	67.0	33.0
Standard Deviation	0.8	0.8
95%confidence interval	2.0	2.0

	Test 4	
	Wt%Fe	**Wt%Si**
	67.4	32.6
	66.9	33.1
	66.2	33.8
average	66.8	33.2
Standard Deviation	0.6	0.6
95%confidence interval	1.5	1.5

	Test 5	
	Wt%Fe	**Wt%Si**
	67.8	32.2
	67.9	32.1
	67	33
average	67.6	32.4
Standard Deviation	0.5	0.5
95%confidence interval	1.2	1.2

Table B-7. Composition of different experimental tests ($FeO/Fe_2O_3/SiO_2$ slag).

Test1		**Test 2**		**Test 3**	
EMF (mV)	**log pO2(atm)**	**EMF (mV)**	**log pO2(atm)**	**EMF (mV)**	**log pO2(atm)**
-161	-9.2	-215	-8.48	-230	-8.28
-162	-9.18	-207	-8.59	-229	-8.30
-169	-9.09	-206	-8.60	-213	-8.51
-186	-8.87	-196	-8.73	-201	-8.67

Test4		**Test 5**	
EMF (mV)	**log pO2(atm)**	**EMF (mV)**	**log pO2(atm)**
-204	-8.63	-233	-8.24
-210	-8.55	-232	-8.26
-232	-8.26	-216	-8.47
-234	-8.23	-212	-8.52

Table B-8. EMF results obtained with $FeO\text{-}Fe_2O_3\text{-}SiO_2$ slag

B.4. Alloy composition

Tests with FeO slag

Test 1

Platinum	40.3	2.9
Nickel	25.6	75.6
Copper	4.1	11.0
Iron	13.2	10.5

Test 2

iron	13.5	13.7	4.2	9.6	1.5
nickel	72.2	78.5	80	82.3	75.8
copper	14.2	7.8	15.8	8.1	22.7

Test 3 ***Test 3***

Iron	38.3	56.8	**nickel**	64.2
copper	29.1	43.2	**Copper**	35.8

Test 4

iron	94.7	98.3
nickel	5.3	1.7

Tests with FeO+ Fe_2O_3 slag

Test 1

Platinum	45.6	34.1
Nickel	34.4	46.6
Copper	9.6	7.4
Iron	10.4	11.9

Test 2

iron	1.6	11.2	11.7	12
nickel	78.9	80.7	80.5	80.5
copper	19.5	8	7.8	7.5

Test 3

nickel	58	15
Copper	42	85

APPENDIX-C.

DISCUSSION ON EQUILIBRIUM IN COMPLEX SYSTEMS

C.1. The phase rule for reactive component [RAO, 1985:69]

Consider a heterogeneous system composed of N chemical species or constituents. Except in simple systems, the number of species is different from the number of components. For simplicity, assume that only three of the N species are chemically active and participate in the following reaction:

$$AB_{(s)} = A_{(g)} + B_{(g)}.$$

The number of variables is found in the same manner as with no reactive species.

Thus, total number of variables = $p(N-1) + 2$ (1)

Where p: number of phases and N: number of species

Phase-equilibrium considerations provide a total of n (p-1) equations. These enable us to fix n(p-1) variables.

The fact that the independent reaction equilibrium $AB_{(s)} \rightarrow A_{(g)} + B_{(g)}$ exists provides the following additional equation. For the reaction at equilibrium,

$\Delta G = 0 = \mu_A + \mu_B - \mu_{AB}$ (2)

Additionally, in the absence of $A_{(g)}$ and $B_{(g)}$ in the starting reacting mixture, stoichiometric considerations require that $p_A = p_B$ (3)

Sometimes special restrictions are placed on the system. For instance, suppose that in the system under consideration the partial pressure of A is fixed at, say, λ atm. This gives the following additional equation:

$$P_A = \lambda$$

We found by summation that

Total number of equations = $n(p-1) +1+1+1$ (4)

The variance or the number of degrees of freedom is found by subtracting equation (4) from (1).

Thus, $F= p(N-1) +2 – N(p-1) –3 = (N-2) –p+1 = c-p+1$

Where c is the number of components.

Generalizing, for a system in which there are r independent chemical equilibria, s stoechiometric relations (or constraints), and t special constraints, we have

$F = (N-r-s-t) - p + 2 = c-p+2-t$

Where, in complex systems, the number of components is given by $C = N- r- s$

Atom matrix is a numerical schemes used in computational mathematics to determine the elemental (or atom) coefficient of an element or species and the minimum number of independent reactions describing the chemical system.

In a closed system, suppose that there are N species that in principle can be synthesized from M elements. Let A_i denote the *i*th species and e_j represent the *j*th element (or atoms of the *j*th kind). Then in matrix notation, we can write

$$A_i = \sum_{j=1}^{M} a_{ij} e_j \quad (i = 1,2\ldots N)$$

Where a_{ij} is the elemental (or atom) coefficient that denotes the number of atoms of the *j*th element present in one molecule of the *i*th species. The rank of an atom matrix is a useful quantity for determining the minimum number of independent reactions required to describe the chemical system.

Applying the above theory to the complex system Fe-Ni-Cu-S-Si-O-C of synthetic matte and slag used in this thesis mentioning that the advantage of using synthetic matte and slag avoid to affect the quality of the final products with minor elements between matte, slag and gas.

A matte: Cu-Fe-Ni-S

A slag: Fe-O-Si; excess of SiO_2

The inlet gas composed of CO-CO_2-SO_2 mixed to obtain the required oxygen and sulphur partial pressure at 1250^{o}C.

At equilibrium, the system has twelve species: $Cu_2S_{(s)}$, $Cu_2O_{(s)}$, $FeS_{(s)}$, $FeO_{(s)}$, $Ni_3S_{2(s)}$, $NiO_{(s)}$, $SiO_{2(s)}$, CO, CO_2, SO_2, S_2, O_2.

C.1.1.Atom matrix

The matrix of atom coefficients is deduced as follows:

I	Species	C(j=1)	O(j=2)	S(j=3)	Fe(j=4)	Cu(j=5)	Ni(j=6)	Si(j=7)
1	CO	1	1	0	0	0	0	0
2	CO_2	1	2	0	0	0	0	0
3	SO_2	0	2	1	0	0	0	0
4	S_2	0	0	2	0	0	0	0
5	O_2	0	2	0	0	0	0	0
6	FeS	0	0	1	1	0	0	0
7	FeO	0	1	0	1	0	0	0
8	Ni_3S_2	0	0	2	0	0	3	0
9	NiO	0	1	0	0	0	1	0
10	Cu_2S	0	0	1	0	2	0	0
11	Cu_2O	0	1	0	0	2	0	0
12	SiO_2	0	2	0	0	0	0	1

Atom matrix can be used to determine the minimum number of independent reactions describing the chemical system.

$$\begin{bmatrix} 1 & 1 & 0 & 0 & 0 & 0 & 0 \\ 1 & 2 & 0 & 0 & 0 & 0 & 0 \\ 0 & 2 & 1 & 0 & 0 & 0 & 0 \\ 0 & 0 & 2 & 0 & 0 & 0 & 0 \\ 0 & 2 & 0 & 0 & 0 & 0 & 0 \\ 0 & 0 & 1 & 1 & 0 & 0 & 0 \\ 0 & 1 & 0 & 1 & 0 & 0 & 0 \\ 0 & 0 & 2 & 0 & 0 & 3 & 0 \\ 0 & 1 & 0 & 0 & 0 & 1 & 0 \\ 0 & 0 & 1 & 0 & 2 & 0 & 0 \\ 0 & 1 & 0 & 0 & 2 & 0 & 0 \\ 0 & 2 & 0 & 0 & 0 & 0 & 1 \end{bmatrix}$$

The rank of this matrix is found by reducing it to echelon form by a series of row operations. The resultant echelon matrix is

$$\begin{bmatrix} 1 & 0 & 0 & 0 & 0 & 0 & 0 \\ 0 & 1 & 0 & 0 & 0 & 0 & 0 \\ 0 & 0 & 1 & 0 & 0 & 0 & 0 \\ 0 & 0 & 0 & 1 & 0 & 0 & 0 \\ 0 & 0 & 0 & 0 & 1 & 0 & 0 \\ 0 & 0 & 0 & 0 & 0 & 1 & 0 \\ 0 & 0 & 0 & 0 & 0 & 0 & 1 \\ 0 & 0 & 0 & 0 & 0 & 0 & 0 \\ 0 & 0 & 0 & 0 & 0 & 0 & 0 \\ 0 & 0 & 0 & 0 & 0 & 0 & 0 \\ 0 & 0 & 0 & 0 & 0 & 0 & 0 \\ 0 & 0 & 0 & 0 & 0 & 0 & 0 \end{bmatrix}; \text{Rank} = 7$$

This means that seven species among twelve are required to synthesize the total system. The seven species select are CO,CO_2 ,SO_2 ,FeS , Cu_2S ,Ni_3S_2 and SiO_2. The rank of the atom matrix determines the minimum number of independent reactions, in this case seven, required to describe the system.

C.1.2. Number of independent reactions in a chemical system [RAO, 1985:67] can be determined by the rank of stoichiometric coefficient matrix.

In the system composed of N species, there occur several reactions, involving some or all of the species present. Suppose that R is the number of possible reactions, not all of which can be linearly independent. Conversion of reactants to products can be written as follows:

$$\Sigma \nu_{ki} \overset{N}{\underset{i=1}{A_i}} = 0 \, (k = 1,2,\ldots,\text{R})$$

where ν_{ki} is the stoichiometric coefficient of the *i*th species in the *k*th reaction.
An R x N stoichiometric coefficient matrix for the system can be construct where each row vector in this matrix represents a possible reaction.
The linearly independent reactions are determined by the rank of the matrix.

Consider the Fe-Cu-Ni-Si-C-O-S system used in the thesis, twelve species are present: $Cu_2S_{(s)}$, $Cu_2O_{(s)}$, $FeS_{(s)}$, $FeO_{(s)}$, $Ni_3S_{2(s)}$, $NiO_{(s)}$, $SiO_{2(s)}$, CO, CO_2, SO_2, S_2, O_2.

The possible reactions can be written between these species:

$$CO + ½\ O_2 = CO_2$$

$$FeS + 3/2\ O_2 = FeO + SO_2$$

$$Cu_2S + 3/2O_2 = Cu_2O + SO_2$$

$$Ni_3S_2 + 7/2\ O_2 = 3NiO + 2SO_2$$

$$FeS + NiO = FeO + Ni_3S_2$$

$$Cu_2S + FeO = Cu_2O + FeS$$

$$FeS + 3/2\ O_2 = FeO + SO_2$$

$$½\ S_2 + O_2 = SO_2$$

$$2FeO + SiO_2 = 2FeO.SiO_2$$

$$Ni_3S_2 + O_2 = NiO + SO_2$$

$$CO + FeO + SO_2 = CO_2 + FeS + O_2$$

These equations rewrite are

$$CO + ½\ O_2 - CO_2 = 0$$

$$FeS + 3/2\ O_2 - FeO - SO_2 = 0$$

$$Cu_2S + 3/2O_2 - Cu_2O - SO_2 = 0$$

$$Ni_3S_2 + 7/2\ O_2 - 3NiO - 2SO_2 = 0$$

$$FeS + 3NiO + S_2 - FeO - Ni_3S_2 - SO_2 = 0$$

$$Cu_2S + FeO - Cu_2O - FeS = 0$$

$$½\ S_2 + O_2 - SO_2 = 0$$

$$2FeO + SiO_2 - 2FeO.SiO_2 = 0$$

$$CO + FeO + SO_2 - CO_2 - FeS - O_2 = 0$$

The stoichiometric-coefficient matrix is given by

CO	CO_2	SO_2	S_2	O_2	FeS	FeO	Cu_2S	Cu_2O	Ni_3S_2	NiO	SiO_2	Fe_2SiO_4
1	-1	0	0	½	0	0	0	0	0	0	0	0
0	0	-1	0	3/2	1	-1	0	0	0	0	0	0
0	0	-1	0	3/2	0	0	1	-1	0	0	0	0
0	0	-2	0	7/2	0	0	0	0	1	-3	0	0
0	0	-1	1	0	1	-1	0	0	-1	3	0	0
0	0	0	0	0	-1	1	1	-1	0	0	0	0
0	0	-1	1/2	1	0	0	0	0	0	0	0	0
0	0	0	0	0	0	2	0	0	0	0	1	1
1	-1	1	0	-1	-1	1	0	0	0	0	0	0

The rank of the matrix is six obtained using an echelon matrix.

$$\begin{bmatrix} 1 & -1 & 0 & 0 & 0 & 0 & 0 & 2 & -2 & -1 & 3 & 0 & 0 \\ 0 & 0 & 1 & 0 & 0 & 0 & 0 & -7 & 7 & 3 & -9 & 0 & 0 \\ 0 & 0 & 0 & 1 & 0 & 0 & 0 & -6 & 6 & 2 & -6 & 0 & 0 \\ 0 & 0 & 0 & 0 & 1 & 0 & 0 & -4 & 4 & 2 & -6 & 0 & 0 \\ 0 & 0 & 0 & 0 & 0 & 1 & 0 & -1 & 1 & 0 & 0 & 0.5 & 0.5 \\ 0 & 0 & 0 & 0 & 0 & 0 & 1 & 0 & 0 & 0 & 0 & 0.5 & 0.5 \\ 0 & 0 & 0 & 0 & 0 & 0 & 0 & 0 & 0 & 0 & 0 & 0 & 0 \\ 0 & 0 & 0 & 0 & 0 & 0 & 0 & 0 & 0 & 0 & 0 & 0 & 0 \\ 0 & 0 & 0 & 0 & 0 & 0 & 0 & 0 & 0 & 0 & 0 & 0 & 0 \end{bmatrix}$$

That means there are six independent reactions in this system.

APPENDIX - D

FURNACE ASSEMBLY COMPONENTS

			Dimensions		
Part	**Materials**	**Supplier**	I.D. (cm)	O.D. (cm)	Lt (cm)
Crucible	Silica	Lenton	4.3	4.5	3.9
Furnace tube	Mullite	C.C. Imelmann	6.4	7.3	52
Gas inlet tube	Silica	Lenton	4	6	48
Sampling tube	Silica	Lenton	4	6	60
Thermocouple protection	Mullite	Lenton	4	6	46

Table D-1. Dimensions of furnace assembly components

APPENDIX -E

CHEMICAL ANALYSIS AND SUPPLIERS OF MATERIALS

Pure gases.

Gas	Supplier	Analysis
CO	Afrox	99.97%
CO_2	Afrox	99.995%
Ar	Afrox	99.999%

Liquid charge

Liquid	Supplier	Analysis
SO_2	Chemical Initiatives	99.9%

Solid charge

Solid	Supplier	Analysis
Ni_3S_2 powder	Sigma-Aldrich	99.7%
Cu_2S powder	Sigma-Aldrich	
FeS grained	Saarchem	
SiO_2 powder	Saarchem	

Cr powder	Industrial Analytical	99%
Si		0.014%
C		0.016%
Fe		0.11%
Al		0.0062%
S		0.028%
O		0.74%
N		0.036%
Cr_2O_3 powder	Merck	99%
Ag crystals	Aldrich Chemicals Co.	99.99 +%
Fe electrolytic	BDH Chemicals Ltd.	
Iron (III) oxide [Fe_2O_3]:		99.98%
CO		13.2 ppm
Na		12.1 ppm
Cu		9.7 ppm
Ca		3.6 ppm
Mn		2.3 ppm
Mg		1.2 ppm
Iron (II) oxalate dihydrate [$C_2FeO_4.2H_2O$]:	Sigma-Aldrich	99%
Heavy metals (as Pb)		Max 0.01%
Chloride (Cl)		Max 0.005%
Sulfate (SO_4)		Max 0.1%

Fe wire	Industrial Analytical	99+%
C		0.06%
Mn		0.39%
P		0.007%
S		0.003%
Si		0.1%
Cr		0.0%
V		0.0%
Cu		0.0%
Ni		0.0%
Pt wire	Temperature Control	99.999%

APPENDIX –F

PREPARATION OF LABORATORY IRON OXIDE

Among all the components used in the experiment, FeO was obtained from an Iron (II) oxalate dihydrate [$C_2FeO_4.2H_2O$]. The principle consisted of obtaining FeO from $FeC_2O_4.2H_2O$ by using a muffle furnace at 1000^oC according to the reaction:

$$FeC_2O_4.2H_2O_{[S]} \xrightarrow{Ar} FeO_{[S]} + CO_{[g]} + CO_{2\,[g]} + 2H_2O_{[g]}$$

Each test was run at constant argon potential of 1atm.

The charge usually weighed around 10mg depending on the capacity of the iron crucible and was made from commercially produced $FeC_2O_4.2H_2O$.

The furnace was preflushed with argon gas for 20 minutes to ensure that all the air and impurities had been expelled. The iron crucible was placed in the furnace along with the iron (II) oxalate dihydrate for 20 minutes and quenched in the argon atmosphere for 20 minutes. The FeO obtained weighed approximately 4mg.

XRD tests of $FeC_2O_4.2H_2O$, Fe_sSiO_4, FeO are shown in the figures F-1, F-2 and F-3.

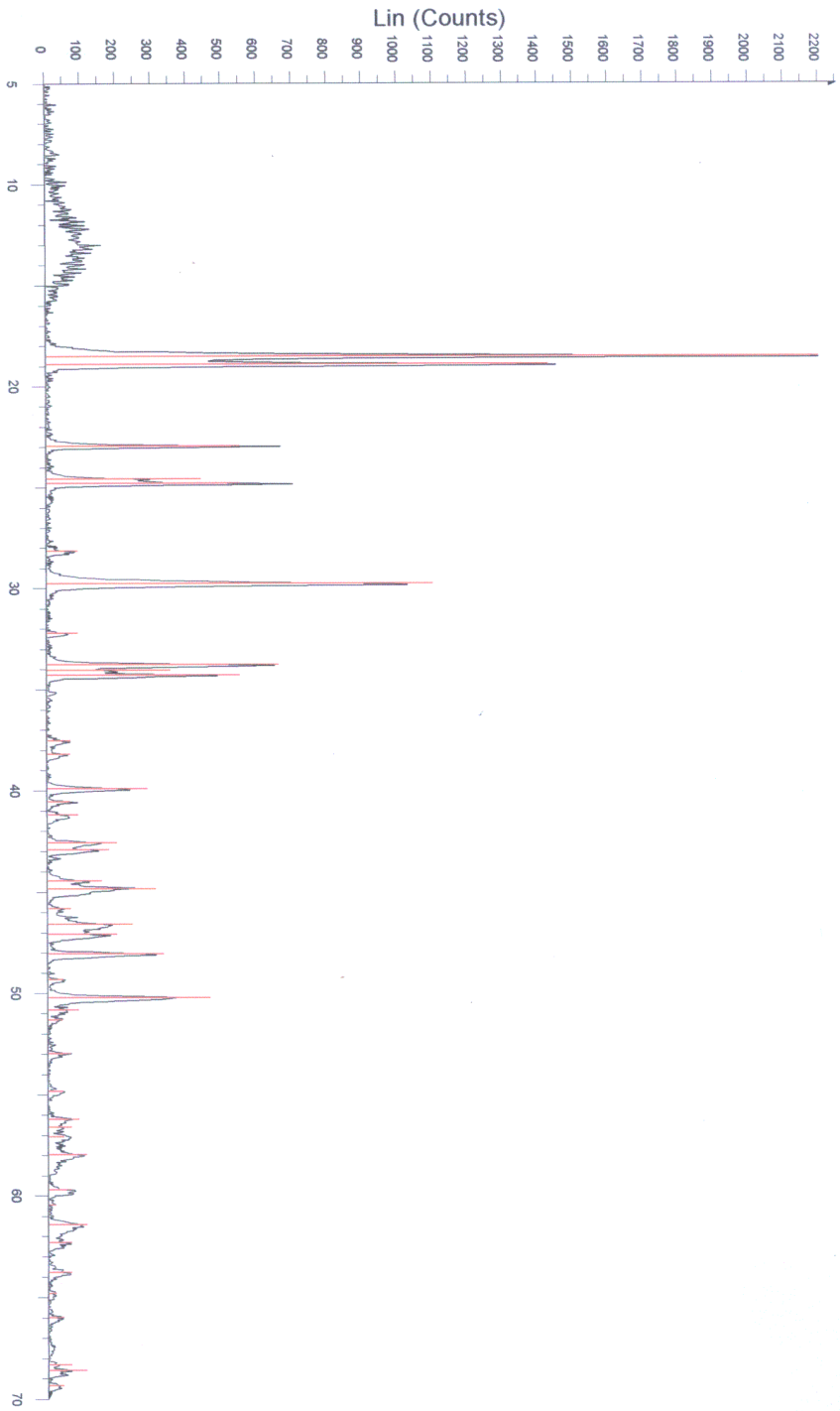

t

Figure F-1. XRD of $FeC_2O_4.2H_2O$

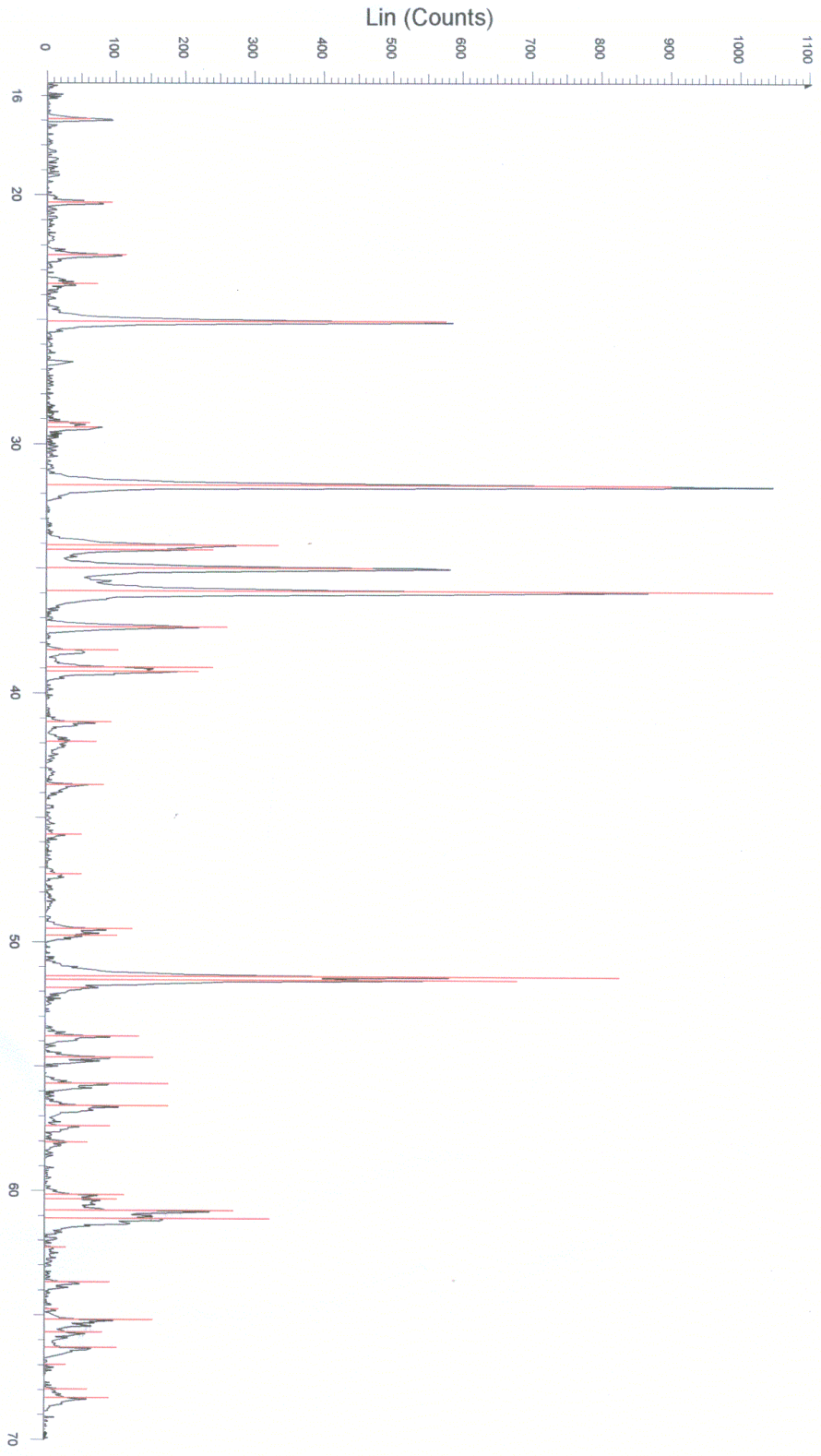

Figure F-2. XRD of Fe_2SiO_4

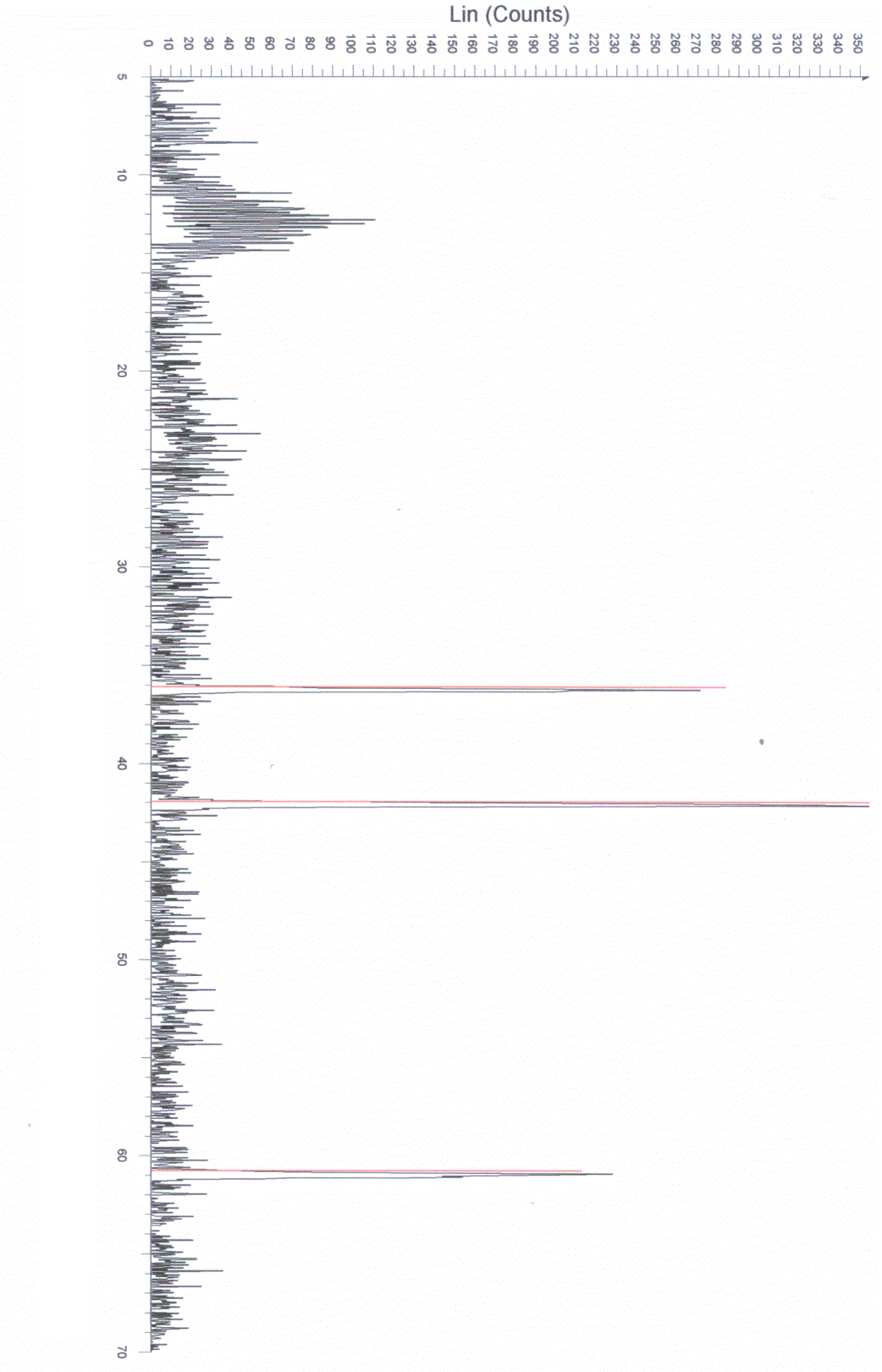

Figure F-3. XRD of FeO

APPENDIX -G

SPECIFICITY OF DIGITAL READOUT AND CONTROL SYSTEM E-7000.

-Gas flow

The Bronkhorst High-Tech B.V. series mass flow meter for gases is an accurate device for measuring gas flows up to 700 bar depending on body rating, virtually independent of pressure and temperature changes. The digital readout can measure and control gas flows from 3 ml_N/h up to several thousand m^3_N /h.

-Liquid flow

The Bronkhorst High-Tech B.V. series mass flow meter for liquids is an accurate device for measuring gas flows up to 400 bars, virtually independent of pressure and temperature changes. The system can be completed with a control valve to measure and control liquid flows from less than a gram per hour up to 20 kg/h.

-Pressure

The Bronkhorst High-Tech B.V. pressure meter measures pressures from 100 mbar up to 400 bar depending on body rating, either absolute pressure or gauge pressure and in the range 0 to 15-bar differential pressure too. The flow going through the pressure controller depends on up and downstream pressures, the orifice diameter of the valve and kind of fluid.

The gas mixing system shown below represents a

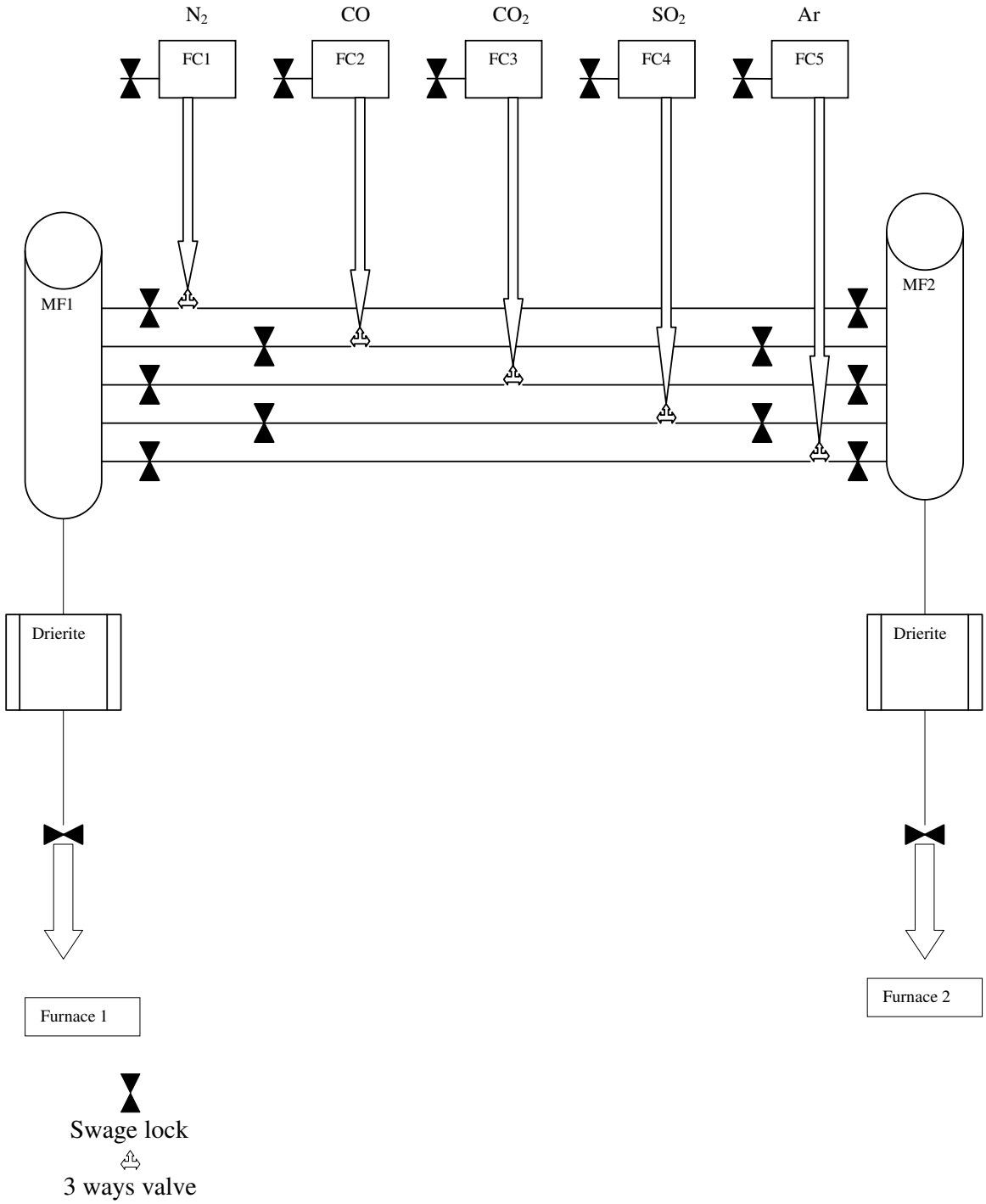

Figure G-1. Schematic representation of the gas mixing system

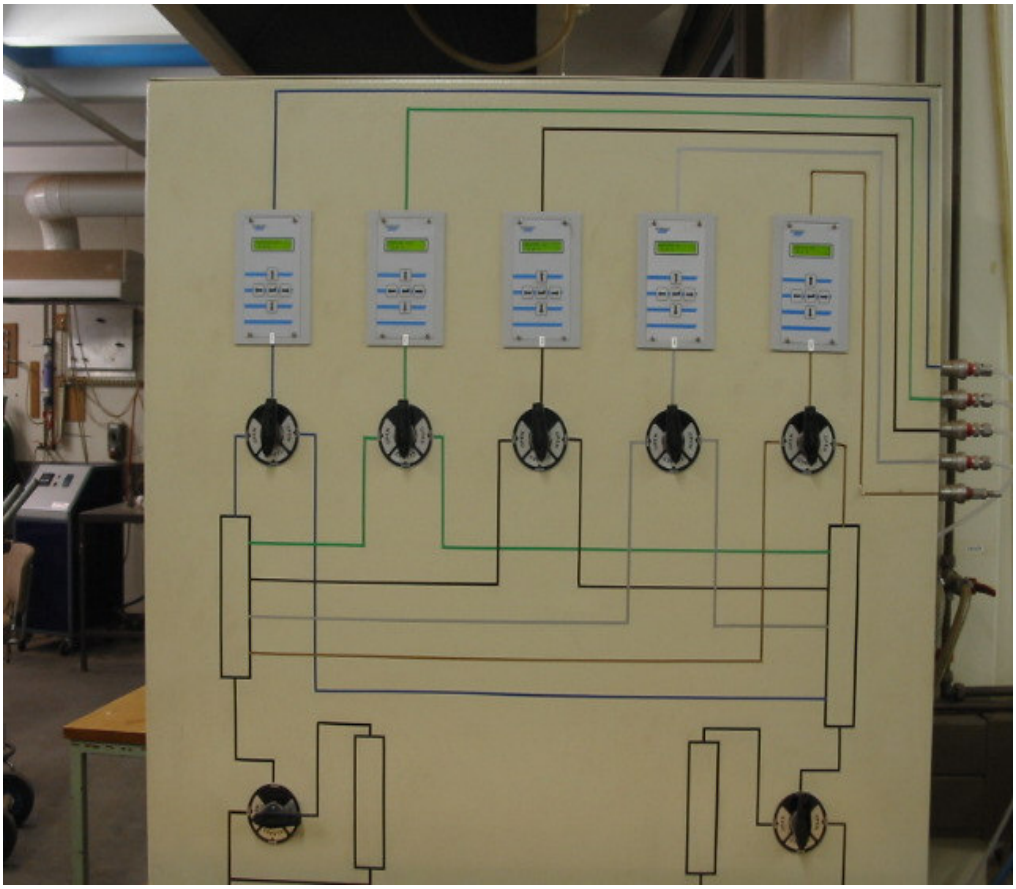

Figure G-2. Picture of gas mixing system used in these experiments.

APPENDIX-H

SPECTRO AND TABLES WITH ELECTRON PROBE MICROANALYSER.

This chapter presents the analyses presented as spectra obtained with the electron probe microanalyser CAMECA SX 100.

H.1. Spectra

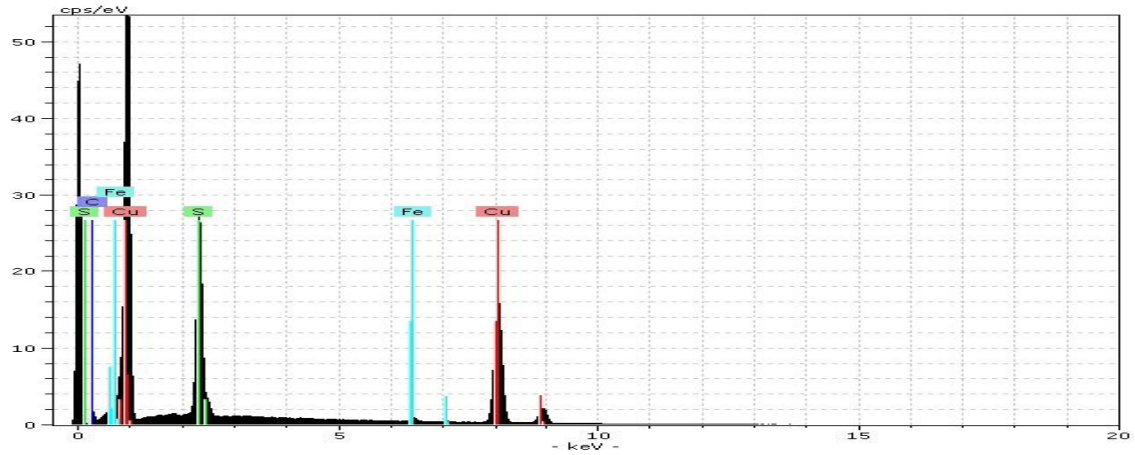

Cu-sulphide-Cr_2O_3-test2

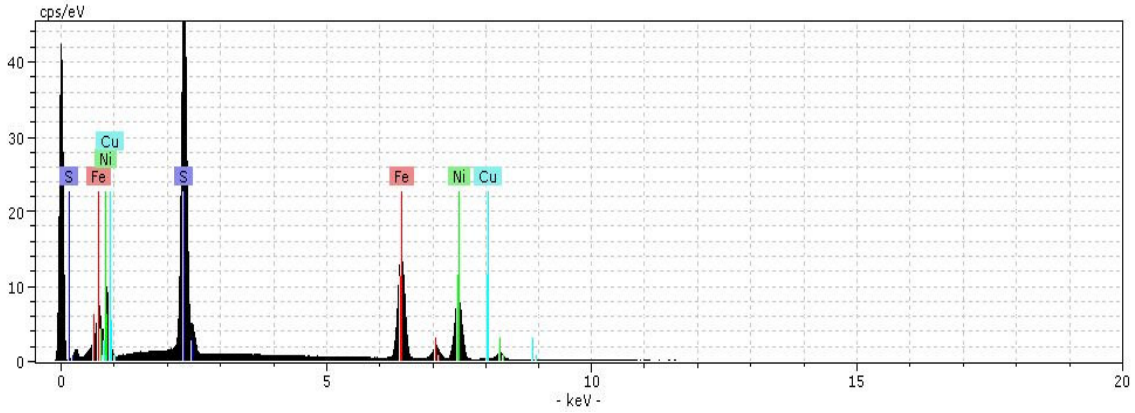

NiFe-sulphide-Fe_2O_3-test14

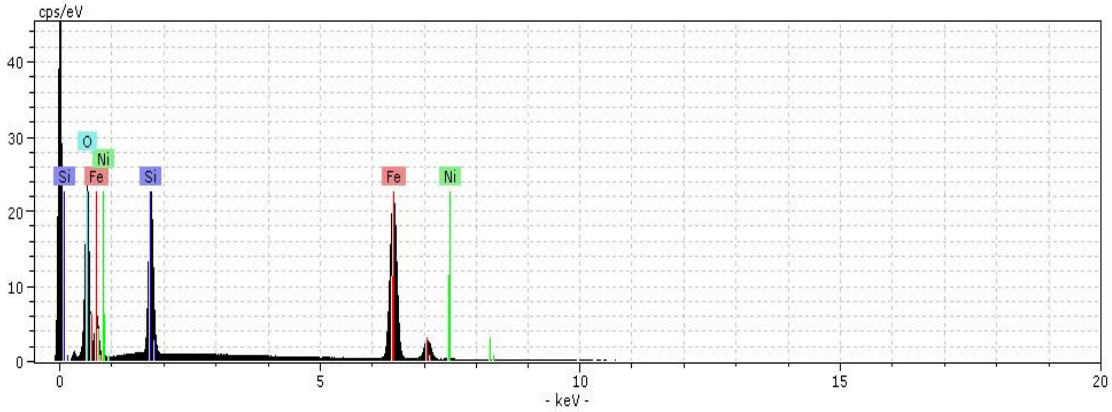

Fe_silicate-Fe_2O_3-test14

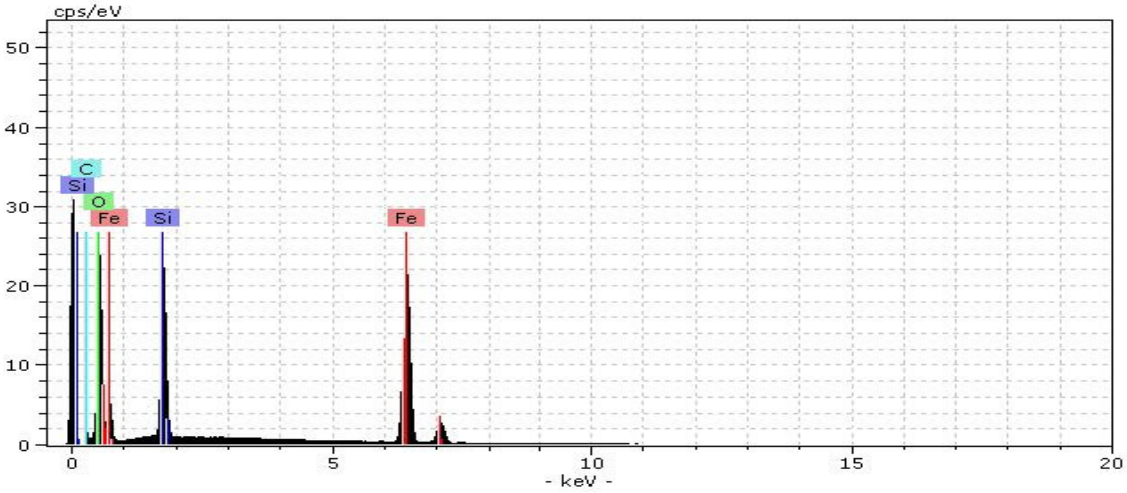

Fe_silicate-Fe_2O_3-test5

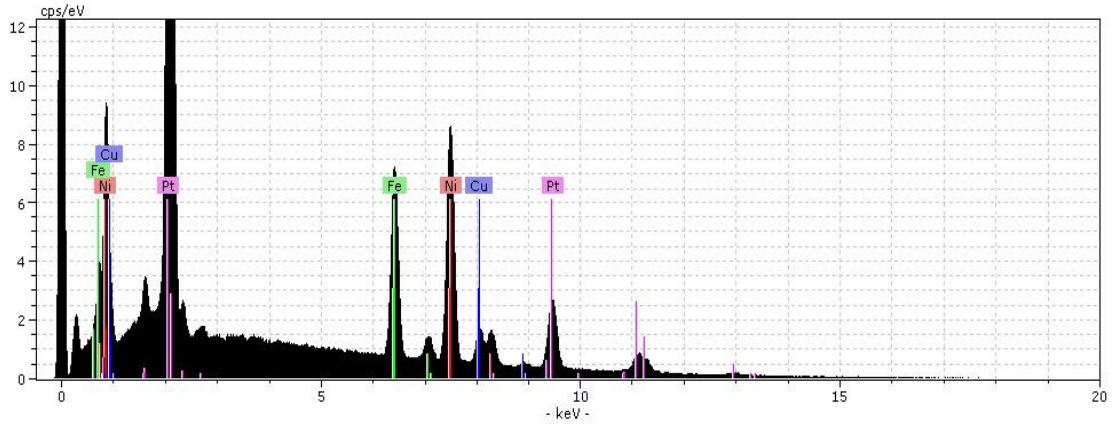

Alloy 1+Pt-Cr_2O_3-test2

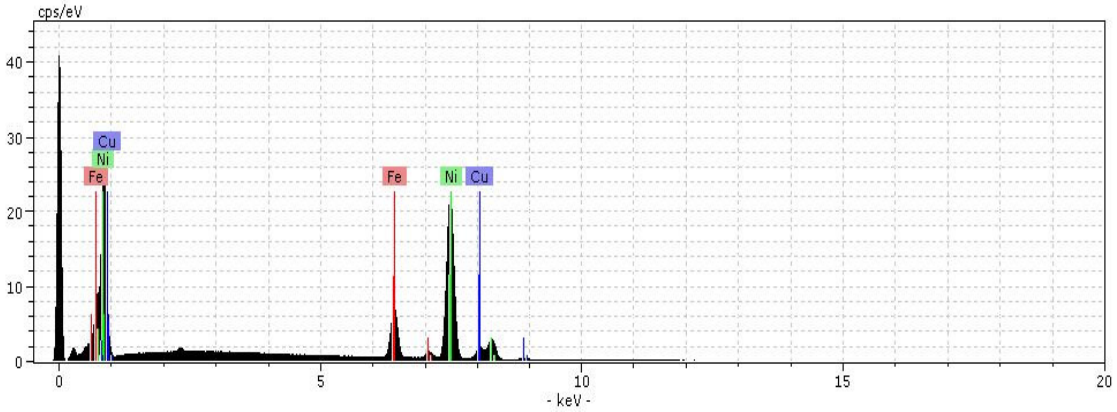

Alloy FeNiCu-Fe_2O_3-test14

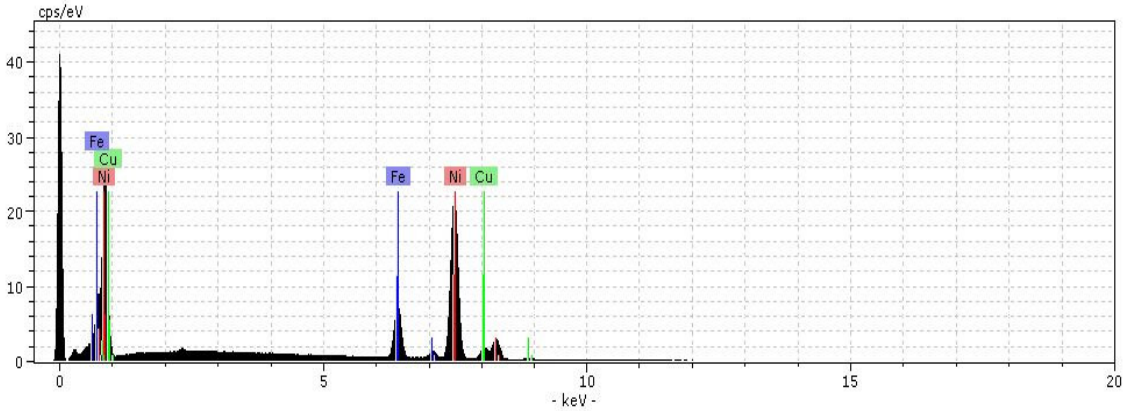

NiFeCu-alloy-Fe_2O_3-test12

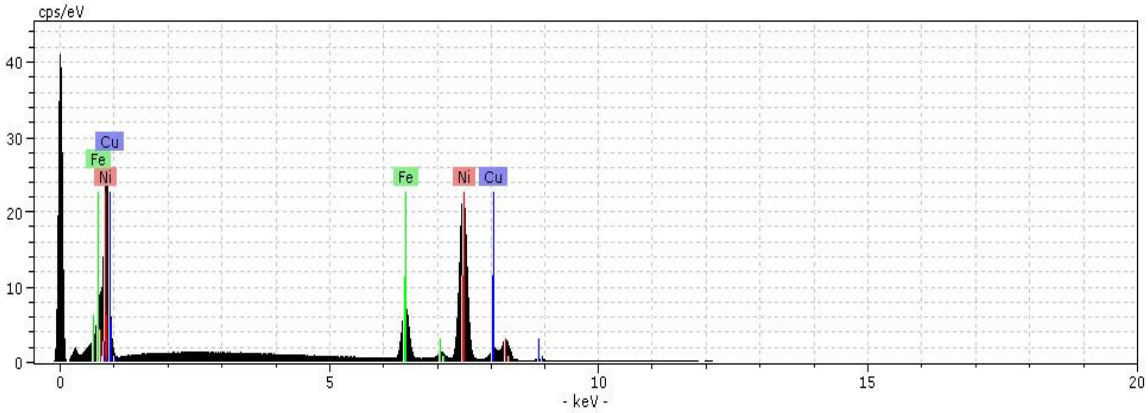

NiFeCu-alloy-Fe_2O_3-test13

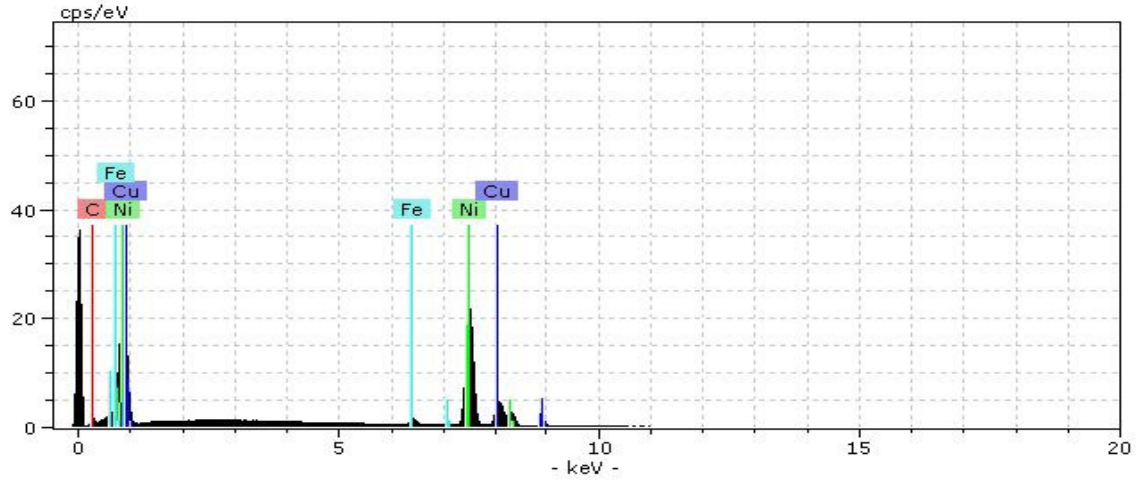

NiCuFe_alloy-Fe_2O_3-test10

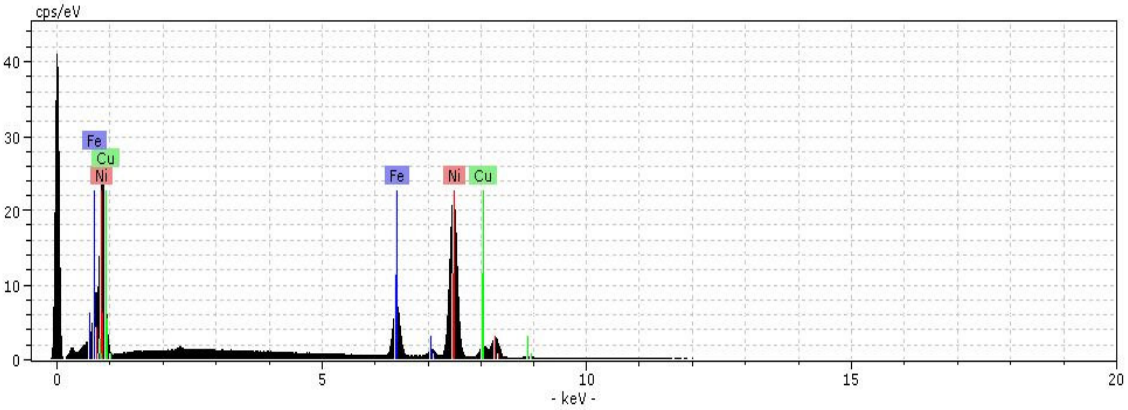

NiCuFe_alloy-Fe_2O_3-test12

Tables.

SiO_2-Cr_2O_3-test1

Element	**Silicon**	**Oxygen**	**Iron**	
Series	K series	K series	K series	
Net	301993	71781	1487	
unnor. wt. %	48.09	63.23	0.76	
norm. wt. %	42.90	56.42	0.68	100.00
at. %	30.15	69.61	0.24	100.00

Fe-Silicate-Cr_2O_3-test3

Element	**Silicon**	**Oxygen**	**Iron**	
Series	K series	K series	K series	
Net	67583	66020	114189	
unnor. wt. %	12.64	33.18	54.51	
norm. wt. %	12.59	33.07	54.33	100.00
at. %	12.85	59.26	27.89	100.00

Fe_2SiO_4-FeO-test5					
Element	***Carbon***	***Iron***	***Oxygen***	***Silicon***	
Series	K series	K series	K series	K series	
Net	9635	224216	127118	131900	
unnor. wt. %	3.407111	52.81801	33.10996	12.29493	
norm. wt. %	3.352465	51.97088	32.57892	12.09774	100
at. %	7.591456	25.31047	55.38255	11.71553	100

Fe_2SiO_4-FeO-test7b

Element	***Carbon***	***Iron***	***Oxygen***	***Silicon***	***Nickel***	
Series	K series	K series	K series	K series	K series	
Net	8868	222337	131316	134382	8458	
unnor. wt. %	3.039019	51.27874	32.85132	12.19988	3.081481	
norm. wt. %	2.96633	50.05224	32.06557	11.90808	3.007777	100
at. %	6.817382	24.74007	55.32387	11.70407	1.4146	100

Fe_2SiO_4-Fe_2O_3-test12

Element	*Iron*	*Oxygen*	*Silicon*	*Nickel*	
Series	K series	K series	K series	K series	
Net	225557	133853	132135	3843	
unnor. wt. %	54.30947	33.26472	12.38302	1.479027	
norm. wt. %	53.5405	32.79373	12.20769	1.458086	100
at. %	27.64505	59.10469	12.5339	0.716356	100

Fe_2SiO_4-Fe_2O_3-test13b

Element	*Iron*	*Oxygen*	*Silicon*	*Nickel*	
Series	K series	K series	K series	K series	
Net	227866	133106	133063	3197	
unnor. wt. %	55.62319	32.94222	12.66261	1.231222	
norm. wt. %	54.28811	32.15154	12.35868	1.20167	100
at. %	28.24072	58.38065	12.78383	0.594794	100

Cu-sulphide-Cr_2O_3-test2

Element	*Sulfur*	*Copper*	*Iron*	
Series	K series	K series	K series	
Net	125043	78916	20352	
unnor. wt. %	21.54133	63.92146	7.08732	
norm. wt. %	23.27531	69.06687	7.6578195	100
at. %	37.22613	55.74149	7.0323802	100

Cu-sulphide-Cr_2O_3-test1

Element	*Sulfur*	*Copper*	*Iron*	
Series	K series	K series	K series	
Net	101539	93927	3028	
unnor. wt. %	18.17155	75.25997	0.9443648	
norm. wt. %	19.25444	79.74492	1.0006421	100
at. %	32.0538	66.98973	0.9564721	100

Ni-sulphide-Cr_2O_3-test3

Element	*Nickel*	*Sulfur*	*Iron*	
Series	K series	K series	K series	
Net	41083	52588	738	
unnor. wt. %	75.66	24.26	0.60	
norm. wt. %	75.26	24.14	0.60	100.00
at. %	62.68	36.79	0.52	100.00

FeNi-sulphide-Cr_2O_3-test3

Element	*Carbon*	*Nickel*	*Sulfur*	*Copper*	*Iron*	
Series	K series	K series	K series	K series	K series	
Net	6797	46695	183326	1219	71342	
unnor. wt. %	6.15	31.78	29.49	0.99	29.30	
norm. wt. %	6.30	32.53	30.18	1.02	29.98	100.00
at. %	20.38	21.54	36.58	0.62	20.87	100.00

Cu-sulphide-FeO-test8

Element	*Carbon*	*Nickel*	*Sulfur*	*Copper*	*Iron*	
Series	K series	K series	K series	K series	K series	
Net	14364	4506	200214	187665	4677	
unnor. wt. %	7.245635	1.211249	16.91023	69.77298	0.6814194	
norm. wt. %	7.561594	1.264068	17.64764	72.81557	0.711134	100
at. %	26.67551	0.912557	23.31956	48.55283	0.539548	100

Cu-sulphide-FeO-test5

Element	*Carbon*	*Sulfur*	*Copper*	*Iron*	*Oxygen*	
Series	K series	K series	K series	K series	K series	
Net	12832	200942	182457	7655	13735	
unnor. wt. %	6.061333	16.87425	70.64997	1.1563649	5.2766149	
norm. wt. %	6.06021	16.87112	70.63688	1.1561506	5.2756371	100
at. %	20.24114	21.10695	44.5933	0.8305024	13.228103	100

FeNi sulphide-FeO-test6c

Element	*Carbon*	*Nickel*	*Sulfur*	*Copper*	*Iron*	
Series	K series	K series	K series	K series	K series	
Net	14160	61534	335878	38965	137635	
unnor. wt. %	6.025214	20.39458	27.2543	15.62146	27.760996	
norm. wt. %	6.207941	21.01309	28.08085	16.09522	28.602905	100
at. %	20.54239	14.22929	34.80551	10.06679	20.35602	100

Cu-sulphide-FeO-test8

Element	*Carbon*	*Nickel*	*Sulfur*	*Copper*	*Iron*	
Series	K series	K series	K series	K series	K series	
Net	15200	214006	271599	3882	9637	
unnor. wt. %	6.441028	69.94797	22.80767	1.53399	1.4349162	
norm. wt. %	6.304499	68.46531	22.32422	1.501475	1.4045007	100
at. %	21.5442	47.87847	28.57528	0.969815	1.0322409	100

Cu-sulphide-FeO-test5

Element	*Carbon*	*Sulfur*	*Copper*	*Iron*	*Oxygen*	
Series	K series	K series	K series	K series	K series	
Net	12122	237040	162243	31105	12973	
unnor. wt. %	5.914864	19.52303	62.2656	5.0478409	5.1325189	
norm. wt. %	6.042737	19.9451	63.61171	5.1569699	5.2434785	100
at. %	19.75881	24.42856	39.31473	3.6266121	12.871292	100

Cu-sulphide-FeO-test10

Element	*Carbon*	*Nickel*	*Sulfur*	*Copper*	*Iron*	
Series	K series	K series	K series	K series	K series	
Net	11818	2696	201236	190218	3107	
unnor. wt. %	6.021697	0.734389	17.27395	72.26865	0.4584873	
norm. wt. %	6.223514	0.759002	17.85289	74.69074	0.4738536	100
at. %	22.80893	0.569248	24.50824	51.74007	0.3735018	100

Ni sulphide-Fe_2O_3-test12

Element	*Nickel*	*Sulfur*	*Iron*	
Series	K series	K series	K series	
Net	216170	272644	1236	
unnor. wt. %	73.03065	23.94372	0.1857524	
norm. wt. %	75.16525	24.64356	0.1911817	100
at. %	62.39147	37.44175	0.1667799	100

Ni sulphide-Fe_2O_3-test10

Element	*Carbon*	*Nickel*	*Sulfur*	
Series	K series	K series	K series	
Net	12497	218211	279479	
unnor. wt. %	5.630103	69.89387	23.1157	
norm. wt. %	5.707747	70.85777	23.43448	100
at. %	19.69143	50.02533	30.28324	100

FeNi sulphide-Fe_2O_3-test12

Element	*Nickel*	*Sulfur*	*Copper*	*Iron*	
Series	K series	K series	K series	K series	
Net	92839	360065	3284	140425	
unnor. wt. %	33.63138	30.45018	1.428904	30.400615	
norm. wt. %	35.06517	31.74834	1.489822	31.696668	100
at. %	27.42351	45.44777	1.076174	26.052544	100

Cu-sulphide-Fe_2O_3-test12

Element	*Nickel*	*Sulfur*	*Copper*	*Iron*	
Series	K series	K series	K series	K series	
Net	1945	200364	186309	5561	
unnor. wt. %	0.55292	17.98237	73.75973	0.8592595	
norm. wt. %	0.593553	19.30385	79.18019	0.9224048	100
at. %	0.539445	32.11265	66.46686	0.881046	

Cu-sulphide-Fe_2O_3-test10

Element	*Carbon*	*Sulfur*	*Copper*	
Series	K series	K series	K series	
Net	10760	203512	191180	
unnor. wt. %	5.692978	17.01654	72.3323	
norm. wt. %	5.989972	17.90427	76.10576	100
at. %	22.11844	24.76399	53.11757	100

Ni sulphide-FeO-test9

Element	*Carbon*	*Nickel*	*Sulfur*	*Copper*	*Iron*	
Series	K series	K series	K series	K series	K series	
Net	13909	214008	268736	5274	2311	
unnor. wt. %	6.102027	69.74933	22.17335	2.085459	0.3331947	
norm. wt. %	6.075093	69.44145	22.07548	2.076254	0.331724	100
at. %	20.93546	48.97093	28.49536	1.352387	0.2458588	100

Ni sulphide-FeO-test5

Element	*Carbon*	*Nickel*	*Sulfur*	
Series	K series	K series	K series	
Net	14567	213793	271927	
unnor. wt. %	6.52962	70.83415	22.88699	
norm. wt. %	6.513287	70.65697	22.82974	100
at. %	22.06109	48.97468	28.96423	100

Ni sulphide-FeO-test8

Element	*Carbon*	*Nickel*	*Copper*	*Iron*	
Series	K series	K series	K series	K series	
Net	19574	236991	58113	11471	
unnor. wt. %	7.123416	70.97782	21.27806	1.3831352	
norm. wt. %	7.069516	70.44076	21.11705	1.3726696	100
at. %	27.43195	55.93465	15.48786	1.1455454	100

FeNi sulphide-FeO-test6a

Element	*Carbon*	*Nickel*	*Sulfur*	*Copper*	*Iron*	
Series	K series	K series	K series	K series	K series	
Net	12892	28527	415105	5444	217788	
unnor. wt. %	5.711504	10.08586	32.84074	2.296138	48.637991	
norm. wt. %	5.736041	10.12919	32.98182	2.306002	48.846946	100
at. %	18.44132	6.664143	39.71814	1.401298	33.775095	100

Ni sulphide-Fe_2O_3-test11

Element	*Carbon*	*Nickel*	*Sulfur*	*Iron*	
Series	K series	K series	K series	K series	
Net	12220	217473	275852	1295	
unnor. wt. %	5.610731	68.12894	22.69177	0.181969	
norm. wt. %	5.807405	70.51707	23.48718	0.1883476	100
at. %	19.9731	49.63038	30.2572	0.1393166	100

NiFe sulphide-Fe_2O_3-test14

Element	*Nickel*	*Sulfur*	*Copper*	*Iron*	
Series	K series	K series	K series	K series	
Net	92261	358891	2544	144277	
unnor. wt. %	33.30998	30.44098	1.101625	31.26799	
norm. wt. %	34.65437	31.66958	1.146086	32.529965	100
at. %	27.10153	45.33385	0.827855	26.736764	100

NiCu sulphide-Fe_2O_3-test10

Element	*Carbon*	*Nickel*	*Sulfur*	*Copper*	*Iron*
Series	K series	K series	K series	K series	K series
Net	14791	5475	197619	190095	1391
unnor. wt. %	7.430626	1.459024	16.19815	70.5752	0.197098
norm. wt. %	7.751532	1.522035	16.8977	73.62312	0.20561
at. %	27.34003	1.098566	22.32407	49.08136	0.1559678

Ni sulphide-Fe_2O_3-test14

Element	*Nickel*	*Sulfur*	*Iron*	
Series	K series	K series	K series	
Net	215553	272712	1399	
unnor. wt. %	73.48194	23.65563	0.2108884	
norm. wt. %	75.48342	24.29995	0.2166325	100
at. %	62.80364	37.00693	0.1894289	100

SiO_2-Fe_2O_3-test14a

Element		*Iron*	*Oxygen*	*Silicon*	*Nickel*	
Series		K series	K series	K series	K series	
Net		3443	138755	597397	898	
unnor. wt. %		0.938052	62.85777	49.82189	0.352879	
norm. wt. %		0.823065	55.15263	43.71469	0.309623	100
at. %		0.293368	68.61856	30.98306	0.105008	100

SiO_2-Fe_2O_3-test13a

Element		*Iron*	*Oxygen*	*Silicon*	
Series		K series	K series	K series	
Net		3108	143200	599482	
unnor. wt. %		0.827867	64.90356	53.3052	
norm. wt. %		0.695473	54.52403	44.7805	100
at. %		0.24833	67.95688	31.79479	100

$FeNiSiO_2$-Fe_2O_3-test10

Element	*Carbon*	*Iron*	*Oxygen*	*Silicon*	**Nickel**	
Series	K series	K series	K series	K series	K series	
Net	7778	192567	129519	132269	29438	
unnor. wt. %	2.689208	43.59758	32.46247	12.26465	10.53772	
norm. wt. %	2.648119	42.93145	31.96647	12.07725	10.37671	100
at. %	6.134516	21.38935	55.59208	11.96487	4.919179	100

Fe_2SiO_4-Fe_2O_3-test14b

Element	*Iron*	*Oxygen*	*Silicon*	*Nickel*	
Series	K series	K series	K series	K series	
Net	224430	131861	132996	3369	
unnor. wt. %	52.78615	33.1882	12.30762	1.250117	
norm. wt. %	53.03431	33.34422	12.36548	1.255994	100
at. %	27.1681	59.62373	12.59595	0.61221	100

SiO_2-FeO-test5a

Element	*Carbon*	*Iron*	*Oxygen*	*Silicon*	*Aluminium*	*Potassium*	*Sodium*	*Titanium*
Series	K series	K series	K series	K series	K series	K series	K series	K series
Net	396	30553	102787	374329	52291	24193	4164	3447
unnor. wt. %	0.289263	8.325343	53.89242	37.05329	5.3835465	2.9759491	0.792364	0.502114
norm. wt. %	0.258596	7.442691	48.17875	33.1249	4.8127837	2.6604394	0.708358	0.44888
at. %	0.46221	2.861059	64.64703	25.32032	3.8293613	1.4608049	0.661477	0.201267

SiO_2-FeO-test7

Element	*Carbon*	*Iron*	*Oxygen*	*Silicon*
Series	K series	K series	K series	K series
Net	4153	3847	155524	605161
unnor. wt. %	2.43688	0.972912	63.82991	42.96969
norm. wt. %	2.211136	0.882785	57.91694	38.98914
at. %	3.534753	0.303513	69.50639	26.65534

SiO_2-FeO-test5b

Element	Carbon	*Iron*	*Oxygen*	*Silicon*
Series		K series	K series	K series
Net	2770	144596	596083	
unnor. wt. %	0.70676	62.4732	43.86304	
norm. wt. %	0.660258	58.36272	40.97703	100
at. %	0.230972	71.26516	28.50387	100

Fe_2SiO_4-FeO-test7a

Element	*Carbon*	*Iron*	*Oxygen*	*Silicon*	*Nickel*	
Series	K series	K series	K series	K series	K series	
Net	8404	233795	131924	133967	1043	
unnor. wt. %	2.88576	55.55626	32.90566	12.08489	0.396013	
norm. wt. %	2.77935	53.50768	31.69229	11.63927	0.38141	100
at. %	6.443404	26.67887	55.15707	11.53971	0.180948	100

Pt-alloy-FeO-test5

Element	*Carbon*	*Iron*	*Copper*	*Nickel*	*Platinum*	
Series	K series	K series	K series	K series	M series	
Net	20776	45958	24539	104517	269367	
unnor. wt. %	14.79939	8.882061	8.227377	29.3223	38.93146	
norm. wt. %	14.77537	8.867643	8.214022	29.27471	38.86826	100
at. %	55.50694	7.164676	5.832514	22.50564	8.990225	100

Pt-alloy2-FeO-test5

Element	*Carbon*	*Iron*	*Copper*	*Nickel*	*Platinum*	
Series	K series	K series	K series	K series	M series	
Net	20329	53670	18604	141231	197306	
unnor. wt. %	7.972933	10.92009	6.747346	42.7086	31.234	
norm. wt. %	8.006321	10.96582	6.775603	42.88746	31.3648	100
at. %	35.81765	10.55078	5.729318	39.26307	8.639188	100

Ni-alloy-FeO-test5

Element	*Carbon*	*Iron*	*Copper*	*Nickel*	
Series	K series	K series	K series	K series	
Net	19117	62329	19771	243292	
unnor. wt. %	7.101207	8.989218	7.596674	77.14862	
norm. wt. %	7.042353	8.914716	7.533714	76.50922	100
at. %	27.04392	7.362727	5.468295	60.12506	100

FeNiCu-alloy-FeO-test9

Element	*Iron*	*Copper*	*Nickel*	
Series	K series	K series	K series	
Net	30968	40217	248351	
unnor. wt. %	4.244951	15.95614	80.69308	
norm. wt. %	4.20733	15.81473	79.97794	100
at. %	4.466128	14.7536	80.78027	100

NiCuFe-alloy-Fe_2O_3-test14

Element	*Iron*	*Copper*	*Nickel*	
Series	K series	K series	K series	
Net	71244	20248	243143	
unnor. wt. %	11.33568	8.146723	81.72458	
norm. wt. %	11.20049	8.049566	80.74994	100
at. %	11.77651	7.438133	80.78535	100

NiCuFe-alloy-Fe_2O_3-test13

Element	*Iron*	*Copper*	*Nickel*	
Series	K series	K series	K series	
Net	75739	19555	244179	
unnor. wt. %	11.92795	7.96426	82.12681	
norm. wt. %	11.69189	7.806642	80.50147	100
at. %	12.28783	7.210516	80.50165	100

NiCuFe-alloy-Fe_2O_3-test12

Element	*Iron*	*Copper*	*Nickel*	
Series	K series	K series	K series	
Net	75948	18702	241238	
unnor. wt. %	12.27783	7.637082	82.31995	
norm. wt. %	12.00944	7.470134	80.52043	100
at. %	12.61628	6.896815	80.4869	100

NiCu-alloy-Fe_2O_3-test10a

Element	*Carbon*	*Copper*	*Nickel*	
Series	K series	K series	K series	
Net	16119	146193	132696	
unnor. wt. %	6.671596	51.90846	37.53212	
norm. wt. %	6.941468	54.0082	39.05033	100
at. %	27.61021	40.60401	31.78578	100

NiCu-alloy-Fe_2O_3-test10b

Element	*Carbon*	*Copper*	*Nickel*	
Series	K series	K series	K series	
Net	14526	213590	49651	
unnor. wt. %	6.19427	73.03698	12.93144	
norm. wt. %	6.721017	79.24789	14.0311	100
at. %	27.35324	60.96105	11.68571	100

NiCuFe-alloy-Fe_2O_3-test13

Element	*Iron*	*Copper*	*Nickel*	*Platinum*	*Tin*	
Series	K series	K series	K series	M series	L series	
Net	55771	27075	223594	16638	23132	
unnor. wt. %	9.835246	10.30965	70.92565	2.756923	3.449148	
norm. wt. %	10.1106	10.59828	72.9113	2.834107	3.545711	100
at. %	11.07651	10.20407	76.00314	0.888852	1.827435	100

NiCuFe-alloy-Fe_2O_3-test11a

Element	*Carbon*	*Iron*	*Copper*	*Nickel*	
Series	K series	K series	K series	K series	
Net	16941	65813	21402	250088	
unnor. wt. %	5.80366	9.460456	8.197295	79.28179	
norm. wt. %	5.648704	9.207865	7.978431	77.165	100
at. %	22.66	7.944186	6.0495	63.34631	100

NiCuFe-alloy-Fe_2O_3-test11b

Element	*Carbon*	*Iron*	*Copper*	*Nickel*	
Series	K series	K series	K series	K series	
Net	16595	74534	18151	245244	
unnor. wt. %	5.783948	10.94176	6.922409	77.38512	
norm. wt. %	5.724797	10.82986	6.851615	76.59373	100
at. %	22.87802	9.308089	5.17538	62.63851	100

APPENDIX -I

XRD AND XRF OF ZIRCONIA PROBE

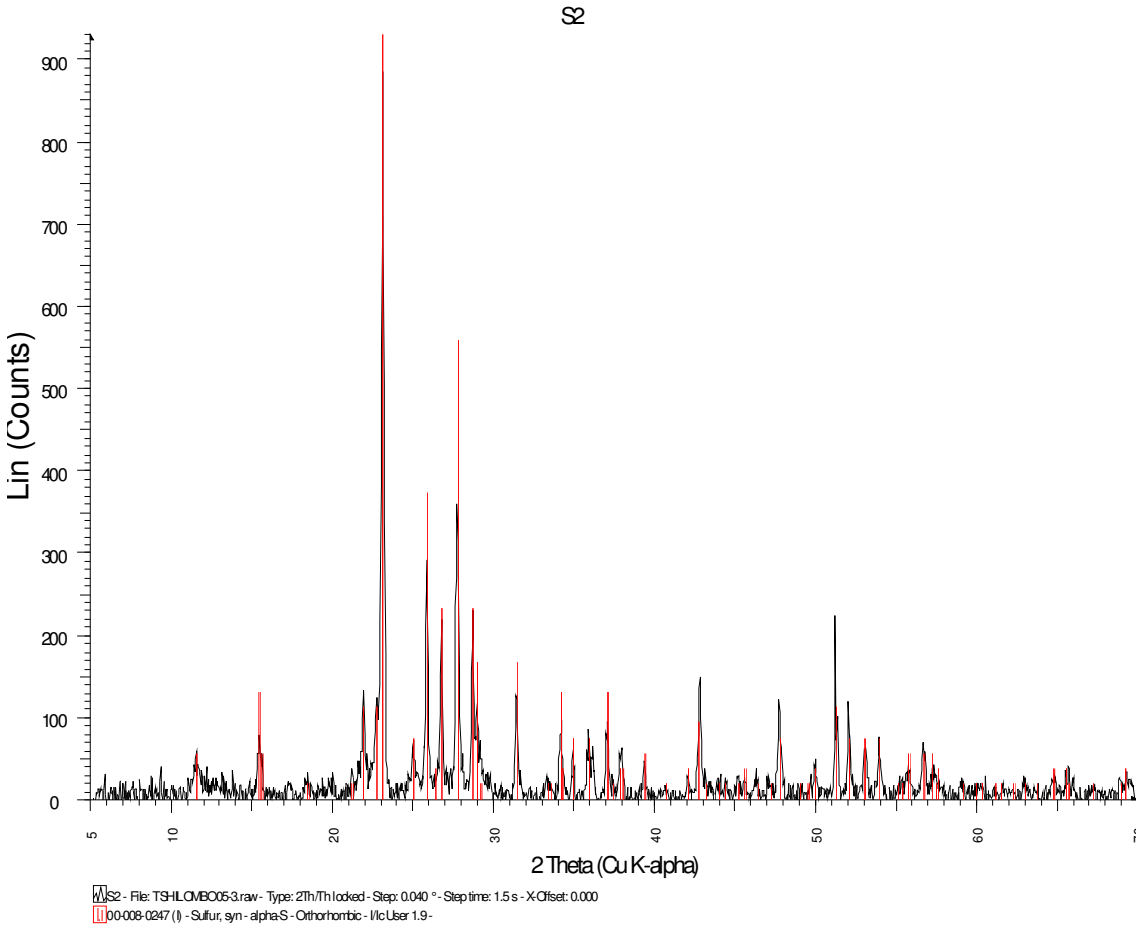

Figure I-1. XRD of sulphur content obtained in the upper level of the furnace

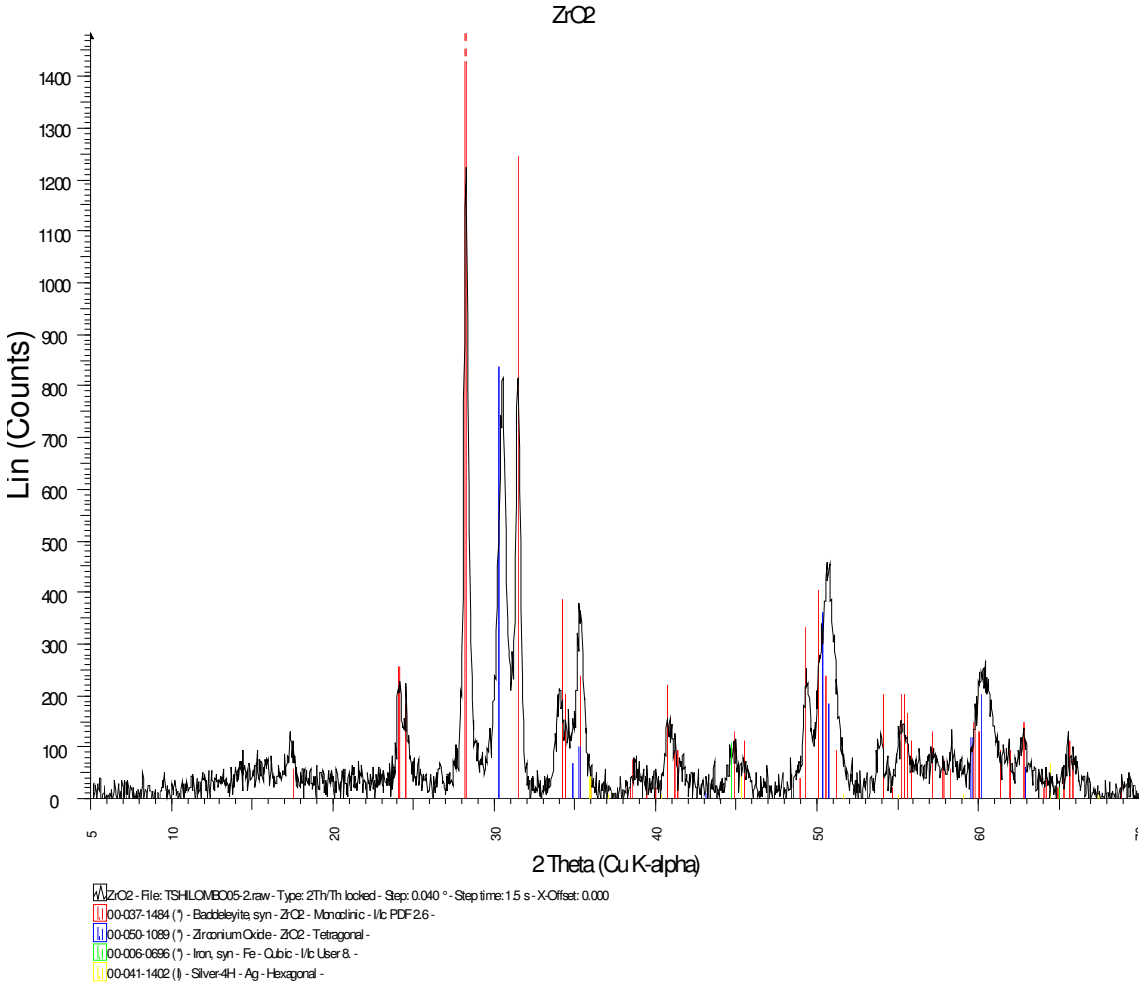

Figure I-2. XRD of zirconia probe

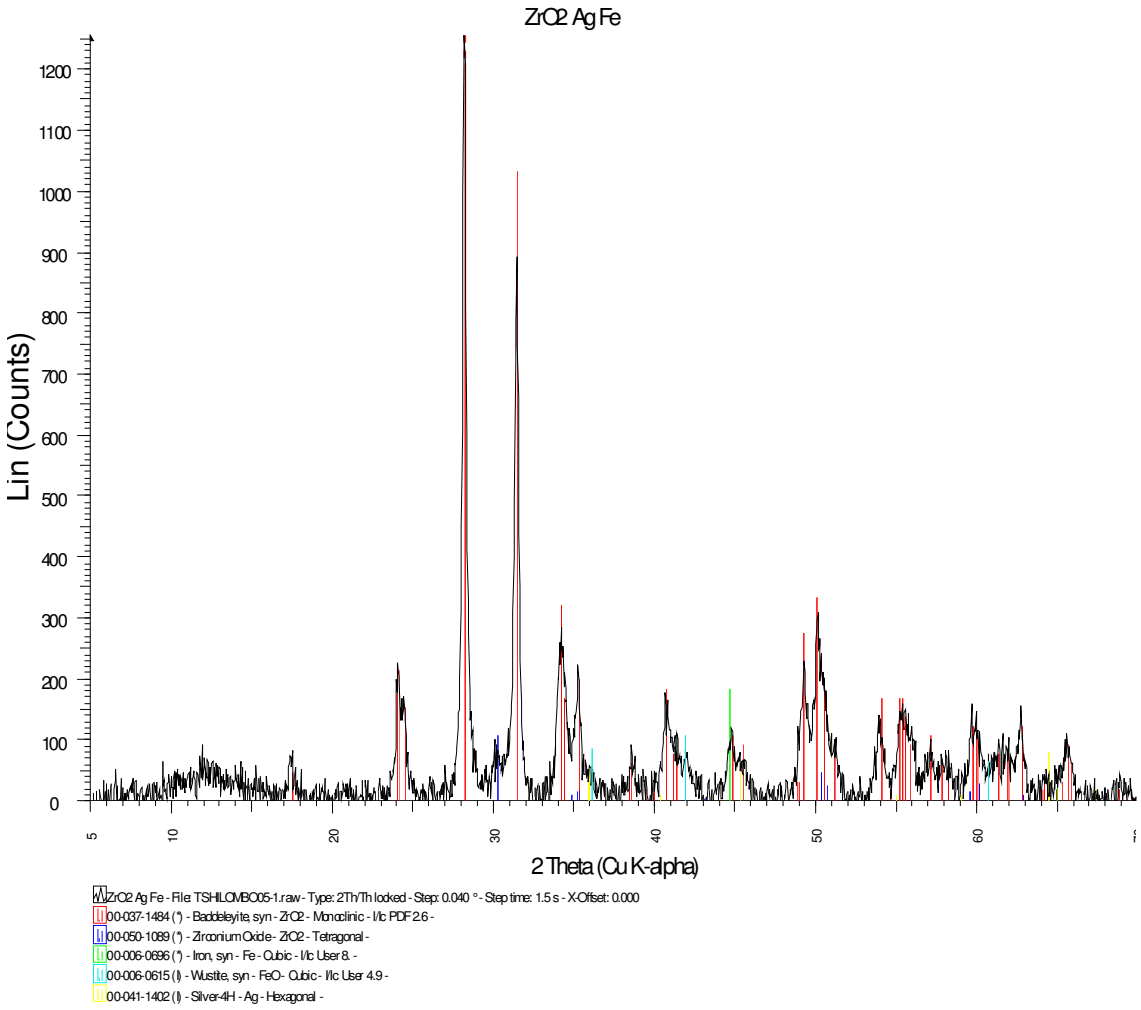

Figure I-3. XRD of zirconia probe with iron oxide, lead as part of the solid electrolyte

%	ZrO2+Ag+Fe	ZrO2
SiO_2	1.40	1.83
TiO_2	0.07	0.12
Al_2O_3	1.09	1.54
Fe_2O_3	25.74	0.50
MnO	0.031	0.015
MgO	2.975	3.372
CaO	0.30	0.31
Na_2O	1.336	1.341
K_2O		
P_2O_5		
Cr_2O_3	0.14	0.06
NiO	0.013	0.009
V_2O_5	0.02	
ZrO_2	62.94	89.22
ZnO	0.043	0.018
Nb_2O_5	0.08	0.13
CuO	0.026	0.011
Ag_2O	2.102	
HfO_2	1.153	1.296
SO_3	0.484	0.199
ThO_2	0.026	0.017
Ta_2O_5	0.020	0.027
PbO	0.019	

%	S2
S	82.90
Cu	0.907
Si	0.358
Mg	0.146
Zn	0.109
Sn	0.101
Fe	610 ppm
Pb	310 ppm
Al	200 ppm
Ni	93 ppm
Zr	72 ppm

Table I-1. XRF results of sulphur content in the upper level of the furnace, of zirconia probe and zirconia probe added with iron oxide and lead.

APPENDIX-J.

XRD RESULTS OF A MATTE SAMPLE